

**INVESTIGATION OF TRIBOLOGICAL  
PERFORMANCE OF B<sub>4</sub>C REINFORCED  
ALUMINIUM MATRIX COMPOSITES**

**A Thesis Submitted to  
the Graduate School of Engineering and Sciences of  
İzmir Institute of Technology  
in Partial Fulfillment of the Requirements for the Degree of**

**MASTER OF SCIENCE**

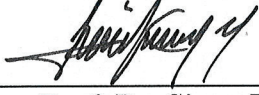
**in Materials Science and Engineering**

**by  
Sevgi SERKİR**

**June 2019  
İZMİR**


We approve the thesis of **Sevgi SERKİR**

**Examining Committee Members:**



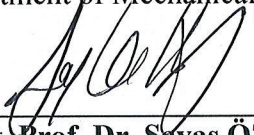
**Assoc. Prof. Dr. Sinan KANDEMİR**

Department of Mechanical Engineering, İzmir Institute of Technology



**Assist. Prof. Dr. M. Fatih TOKSOY**

Department of Mechanical Engineering, İzmir Institute of Technology



**Assist. Prof. Dr. Savaş ÖZTÜRK**

Department of Metallurgical and Materials Engineering, Manisa Celal Bayar University

**21 June 2019**



**Assoc. Prof. Dr. Sinan KANDEMİR**

Supervisor

Department of Mechanical

Engineering

İzmir Institute of Technology



**Assoc. Prof. Dr. Yaşar AKDOĞAN**

Co-Supervisor

Department of Material Science and

Engineering

İzmir Institute of Technology



**Assoc. Prof. Dr. Haldun SEVİNÇLİ**

Head of the Department of

Material Science and Engineering

**Prof. Dr. Aysun SOFUOĞLU**

Dean of the Graduate School of

Engineering and Sciences



## ACKNOWLEDGMENTS

First of all, I would like to thank my advisor Assoc. Prof. Dr. Sinan Kandemir for his knowledge and access to laboratory facilities that he provided me during my research. I would like to thank my supervisor Assoc. Prof. Dr. Yaşar Akdoğan for his kindness and help. I am also grateful to the other members of my thesis defence committee, Assist. Prof. Dr. M. Fatih Toksoy, Assist. Prof. Dr. Savaş Öztürk for their suggestions.

I would like to express my sincere thanks to my fellow lab mates Neslihan Böber and Seçkin Martin for their knowledge, cooperation and their precious support in every step throughout my research. They have always been willing to help me solve any problems which I have faced throughout my research.

I would like to thank the research scientists at the Centre for Materials Research (IZTECH) for their help on the SEM analysis and XRD measurements.

My deepest gratitude goes foremost to my father Selim Serkir who has given his unconditional love and endless encouragement to me. He has always been understanding and supportive all over my education life and I can tell from the bottom of my heart that he has definitely deserved the thesis to be dedicated to him. Also, I warmly thank my mother Nilüfer Ceylan, my brother Emin Serkir and my sister Duygu Serkir for being there for me all the time.

I would like to express my gratitude to Faruk Tuna for his continuous support, guidance and valuable friendship. We have always spent enjoyable coffee breaks together which made me feel myself more and more confident and cheerful. He has always encouraged me to do my best. I could not have imagined having a better mentor.

Most importantly, I would like to express my appreciation to Benal Nerad and Mukaddes Kalayci who have always caressed me. I will eternally be grateful since they have opened their home and heart to me without any expectations.

I would like to sincerely thank İlknur Beyaz and Serkan Kangal for their great contribution and their friendship while writing my thesis. I would like to thank Hatice İlhan, Gülçin Dönmez and Tuğçe Demirtay for their precious friendship and all the fun we have had all the time. They have always motivated me to conduct my research and write my thesis. I am deeply grateful to Onurcan Çakır for all the memories which have motivated me spiritually throughout this thesis. Lastly, I am also thankful to Raşit Demir, Yasemin Keskin and Kıvanç Işıklı for all their help.

## ABSTRACT

### INVESTIGATION OF TRIBOLOGICAL PERFORMANCE OF B<sub>4</sub>C REINFORCED ALUMINIUM MATRIX COMPOSITES

Aluminium, on account of its easy accessibility and superior metallic characteristics, has a wide variety of applications. Increasing demand on the use of aluminium in areas such as automobile, aviation and space industries which requires high performance has led to development of aluminium metal matrix composites. For this purpose, the ceramic reinforcing particles are mostly preferred to provide better mechanical and tribological properties than their conventional counterparts.

In this study, aluminium metal matrix composite (AMC) reinforced with 5 wt.%, 10 wt.% and 15wt.% of B<sub>4</sub>C were fabricated using the powder metallurgy method. In order to obtain the optimum processing parameters necessary for efficient fabrication, several trials, at first place, were studied under different conditions by changing milling parameters such as milling time, milling medium, milling speed and process control agent, and sintering process parameters such as sintering time, sintering temperature. The production of composite powders was carried out using a planetary ball mill in a wet medium for 7 hours with 0.05 wt.% of stearic acid process control agent which helps to avoid contamination and cold welding of ductile Al particle. The milled powders were pressed at 314 MPa at RT and composite samples with a diameter of 30 mm and height of 4 mm were obtained. The samples were sintered at 550, 575, 600 and 625°C for one hour under argon atmosphere. The micro-structures of samples were analysed by scanning electron microscopy and the X-ray diffraction techniques. The wear behaviour of sintered composite samples with ball-on-disc dry wear tester and the mechanical behaviour of the samples with Vickers hardness test were investigated.

**Keywords:** *particle reinforced metal matrix composite, powder metallurgy, ball milling, mechanical alloying method, tribological property, mechanical property*

## ÖZET

### B<sub>4</sub>C TAKVİYELİ ALÜMİNYUM MATRİSLİ KOMPOZİTLERİN AŞINMA PERFORMANSININ İNCELENMESİ

Alüminyum kolay ulaşılabilirliği ve üstün metalik özellikleri ile birçok alanda yaygın kullanıma sahiptir. Yüksek performans gerektiren otomotiv, havacılık ve uzay sanayi gibi alanlarda alüminyum kullanımına olan talebin artması, alüminyum metal matrisli kompozitlerin üretilmesine ve geliştirilmesine olanak sağlamıştır. Bu amaçla, geleneksel rakiplerinden daha iyi mekanik ve aşınma özelliklerine sahip alüminyum matrisli kompozit malzeme üretimi için çoğunlukla seramik takviye elemanı tercih edilir.

Bu çalışmada, ağırlıkça %5, 10 ve 15 oranında bor karbür takviyeli alüminyum matrisli kompozit malzemeler toz metalurjisi yöntemiyle üretilmiştir. İlk etapta gerekli olan optimum üretim parametrelerini belirlemek için; öğütme parametreleri (öğütme süresi, öğütme ortamı, öğütme hızı ve proses kontrol ajanı) ve sinterleme parametreleri (sinterleme süresi, sinterleme sıcaklığı) değiştirilerek farklı koşullarda çalışılmıştır. Kompozit tozların üretimi, gevrek Al tozları arasındaki kaynaşmayı ve kontaminasyonu azaltmak için kullanılan ağırlıkça %0.05 oranında stearik asit proses kontrol ajanı ile, 7 saat boyunca gezegen tipi bilyalı öğütücü kullanılarak ıslak bir ortamda gerçekleştirilmiştir. Öğütme işleminin ardından kompozit tozlar 30 mm çapında olan sıkıştırma kabında 314 MPa basınçta oda sıcaklığında sıkıştırılmıştır. Presleme sonrası çapı 30 mm ve yüksekliği 4 mm olan numuneler elde edilmiştir. Üretim süresince belirlenen optimum parametreler ile hazırlanan kompozit numuneler, oksidasyonu azaltmak için argon gazı ortamında, atmosfer kontrollü sinterleme fırınında 550, 575, 600 and 625 °C sıcaklık değerlerinde 60 dakika boyunca sinterleme prosesine tabii tutulmuştur. Üretilen numunelerin mikro-yapıları taramalı elektron mikroskobu ve X ışınları kırınımı ile analiz edilmiştir. Sinterlenen kompozit numunelerin ball-on-disk aşınma test cihazı ile aşınma davranışları ve Vickers sertlik testleri ile mekanik davranışları incelenmiştir.

**Anahtar kelimeler:** *partikül takviyeli metal matrisli kompozitler, toz metalurjisi, bilyeli öğütme, mekanik alaşımlama metodu, tribolojik özellik, mekanik özellik.*

# TABLE OF CONTENTS

LIST OF FIGURES .....	viii
LIST OF TABLES .....	xii
CHAPTER 1 INTRODUCTION .....	1
CHAPTER 2 BACKGROUND AND LITERATURE REVIEW .....	3
2.1. Metal Matrix Composites .....	3
2.1.1. The Al-B <sub>4</sub> C Interface .....	8
2.1.2. The Wettability.....	10
2.2. Fabrication Methods of MMCs .....	11
2.2.1. Powder Metallurgy .....	12
2.2.2. Sintering Process .....	19
2.3. Wear Performance of MMCs .....	20
2.3.1. The Tribological Behaviour of AMCs .....	21
2.4. Application Areas of Aluminium Metal Matrix Materials.....	23
CHAPTER 3 METHODOLOGY .....	24
3.1. Materials .....	24
3.2. Experimental Procedure .....	26
3.2.1. Sample Preparation .....	27
3.2.2. Ball Milling Process.....	29
3.2.3. Compaction Process .....	32
3.2.4. Sintering Process .....	33
3.2.5. Metallographic Specimen Preparation .....	34
3.3. Characterization of the Materials .....	35
3.3.1. Optical Microscopy .....	35
3.3.2. X-Ray Diffraction .....	36
3.3.3. Scanning Electron Microscopy .....	37
3.3.4. Particle Size Analyzer .....	37
3.3.5. Ball-on-disc Dry Sliding Test .....	38
3.3.6. Vickers Hardness Test.....	39
CHAPTER 4 RESULTS AND DISCUSSION.....	40
4.1. Ball Milling Process .....	40
4.2. Sintering Process .....	48
4.3. The Mechanical and Tribological Behaviours of AMCs .....	56

CHAPTER 5 CONCLUSION .....	65
REFERENCES .....	67

## LIST OF FIGURES

<b><u>Figure</u></b>	<b><u>Page</u></b>
Figure 2.1. The classification of reinforcement based on its form .....	5
Figure 2.2. Types of reinforcement based on its form.....	6
Figure 2.3. The formation of potential phases at interface between Al-B depending on process temperature . .....	9
Figure 2.4. The wettability of water droplet. ....	10
Figure 2.5. The fabrication methods of MMCs. ....	11
Figure 2.6. Schematic representation of process stages in PM.....	13
Figure 2.7. Mechanical alloy process by ball milling. ....	15
Figure 2.8. The three stages during ball milling.....	16
Figure 2.9. B <sub>4</sub> C powders are embedded into Al powders by MA .....	17
Figure 2.10. The particles are welding to each other during sintering process. ....	19
Figure 3.1. SEM images of Al powders at 1000x and 2500x magnifications. ....	25
Figure 3.2. SEM images of B <sub>4</sub> C powders at 1000x and 2500x magnifications. ....	25
Figure 3.3. The cumulative particle size distribution of B <sub>4</sub> C powders.....	25
Figure 3.4. The fabrication and characterization steps of composite samples. ....	26
Figure 3.5. Contamination of milling tools by the cold-welded Al particles during milling in the absence of any PCA. ....	27
Figure 3.6. Agate milling balls covered by Al powder and cleaned with NaOH solution. ....	28
Figure 3.7. The planetary ball mill utilized in the study.....	29
Figure 3.8. The elemental mapping of 5 wt. % B <sub>4</sub> C reinforced Al matrix composite powder milled in dry milling medium. ....	30
Figure 3.9. The presence of Fe, Cr and Ni elements in 5 wt. % B <sub>4</sub> C reinforced Al matrixcomposite powder due to the milling process by the EDS analysis. ....	31
Figure 3.10. Carver hydraulic unit model uniaxial press.....	32
Figure 3.11. The pressed samples with a diameter of 30 mm. ....	33
Figure 3.12. Tube sintering furnace used in the sintering process. ....	34
Figure 3.13. Automatic grinding and polishing machine. ....	34
Figure 3.14. The components of the optical microscope.....	35

<b><u>Figure</u></b>	<b><u>Page</u></b>
Figure 3.15. Schematic representation of Bragg diffraction.....	36
Figure 3.16. A schematic diagram of the ball-on-disc wear test. ....	39
Figure 3.17. The indentation areas after applying 9 kN and 19 kN loads. ....	39
Figure 4.1. The backscattered SEM image of a) as-received pure Al powders b) B <sub>4</sub> C powders at 1000x magnification.....	41
Figure 4.2. The backscattered SEM images of cold welding of 5 wt.% of B <sub>4</sub> C reinforced Al matrix composite powders after the mechanical alloying process for one hour at 420 rpm with a) 100x b) 250x magnifications.....	41
Figure 4.3. The backscattered SEM images of a) as-received Al powder b) milled 5 wt.% of B <sub>4</sub> C reinforced Al matrix composite powders for 3 hours in dry milling medium without the PCA at 2500x magnification. ....	41
Figure 4.4. The backscattered SEM images of milled 10 wt.% of B <sub>4</sub> C reinforced Al matrix composite powder for 5 hours a) without the PCA in dry medium b) without the PCA in wet medium at 250x magnification.....	42
Figure 4.5. The backscattered SEM images of milled 10 wt.% of B <sub>4</sub> C reinforced Al matrix composite powder for 5 hours a) in wet medium with the 0.05 wt.% of PCA b) in wet medium without the 0.05 wt.% of PCA at 250x magnification.....	43
Figure 4.6. The Backscattered SEM image of 10 wt.% B <sub>4</sub> C reinforced Al matrix composite powders fabricated by ball milling process for 5 hours in wet milling medium with the 0.05 wt.% of PCA at 2500x magnification.....	43
Figure 4.7. SEM images of 10 wt.% of B <sub>4</sub> C reinforced Al composite powders milled with 0.05 wt.% of PCA in wet medium for 7 hours at a) 350 rpm b) 450 rpm at 2500x magnification.....	44
Figure 4.8. SEM images of 10 wt.% of B <sub>4</sub> C reinforced Al composite powders milled with 0.05 wt.% of PCA in wet medium for different milling time a) 3 b) 5 hours at 1000x magnification. ....	45
Figure 4.9. SEM images of 5 wt.% of B <sub>4</sub> C reinforced Al composite powders milled with 0.05 wt.% of PCA in wet medium for different milling time a) 7 b) 9 hours at 1000x magnification. ....	45
Figure 4.10. The variation of the average particle size as a function of the milling time.....	46

<b><u>Figure</u></b>	<b><u>Page</u></b>
Figure 4.11. The dispersion of elements found in Al matrix composite powder reinforced 5 wt. % of B <sub>4</sub> C by EDS analysis.....	47
Figure 4.12 The dispersion of elements found in Al matrix composite powder reinforced 10 wt. % of B <sub>4</sub> C by EDS analysis.....	47
Figure 4.13. The dispersion of elements found in Al matrix composite powder reinforced 15 wt. % of B <sub>4</sub> C by EDS analysis.....	48
Figure 4.14. SEM images of 10 wt.% of B <sub>4</sub> C reinforced Al matrix composite sample sintered at a) 550 °C, b) 575 °C, c)600 °C and d) 625 °C at 500x magnification.....	49
Figure 4.15. Optical microscope images of 10 wt.% of B <sub>4</sub> C reinforced Al matrix composite sample sintered at a) 550 °C and b) 625 °C.....	49
Figure 4.16. Backscattered SEM image of 10 wt.% of B <sub>4</sub> C reinforced Al matrix composite sintered at 550 °C. ....	50
Figure 4.17. EDS element mapping of 10 wt.% of B <sub>4</sub> C particle reinforced Al matrix composite sample sintered at 550°C. ....	50
Figure 4.18. EDS line analysis of 10 wt.% of B <sub>4</sub> C particle reinforced Al matrix composite sample sintered at 550 °C.....	51
Figure 4.19. EDS analysis of 10 wt.% of B <sub>4</sub> C reinforced Al matrix composite sample sintered at 625°C. ....	51
Figure 4.20. X-ray diffraction patterns of as- received Al and B <sub>4</sub> C powders.....	52
Figure 4.21. X-ray diffraction pattern of B <sub>4</sub> C particle reinforced Al -MMC sample sintered at 625 °C.....	53
Figure 4.22. The graphs of X-ray diffraction patterns of Al matrix composites with 5, 10 and 15 wt.% B <sub>4</sub> C contents sintered at RT, 550, 575, 600 and 625 °C.....	54
Figure 4.23. The graphs of X-ray diffraction patterns of Al matrix composites with 5, 10 and 15 wt.% B <sub>4</sub> C contents sintered at 550, 575, 600 and 625°C.....	55
Figure 4.24. The variation of density as a function of the sintering temperature and the content of B <sub>4</sub> C.....	56
Figure 4.25. Porosity values of B <sub>4</sub> C reinforced Al matrix composites sintered at 575°C as a function of B <sub>4</sub> C content using BET (Brunaues- Emmett-Teller) density analysis.....	57



Figure 4.26. Variation of hardness with varying the content of B <sub>4</sub> C and the sintering temperature. ....	58
Figure 4.27. Variation of the coefficient of friction with varying content of the B <sub>4</sub> C for the Al composites sintered at 575 °C. ....	59
Figure 4.28. The variation of the wear rate with varying the content of B <sub>4</sub> C for the Al composites sintered at 575 °C. ....	60
Figure 4.29. The wear tracks of 5, 10 and 15 wt.% B <sub>4</sub> C reinforced Al matrix composites sintered at 575 °C. ....	61
Figure 4.30. The optical microscope images of wear tracks of 5, 10 and 15 wt.% B <sub>4</sub> C reinforced Al matrix composites sintered at 575 °C. ....	62
Figure 4.31. Hardened steel balls used for ball-on disc dry sliding wear test. ....	62
Figure 4.32. The SEM images of worn surface of 10 wt.% of B <sub>4</sub> C reinforced Al matrix composite sample sintered at 575°C a) 174x b) 442 x magnifications. ....	63
Figure 4.33. EDS analysis of worn surface of 10 wt. % B <sub>4</sub> C reinforced Al matrix composite sample sintered at 575 °C. ....	64

## LIST OF TABLES

<b><u>Table</u></b>	<b><u>Page</u></b>
Table 2.1. Mechanical properties of different types reinforcement on their forms .....	7
Table 2.2. Properties of ceramic reinforcements used in AMCs .....	8
Table 3.1. Physical and chemical properties of the materials.....	24
Table 3.2. Different composite powder preparation with ball milling .....	27
Table 3.3. The optimized ball milling parameters.....	32
Table 3.4. The sintering parameters of the samples for the analyses of microstructure and mechanical properties.....	33

# CHAPTER 1

## INTRODUCTION

Rapid developments in the technological field resulted in requirement of new materials with superior properties than conventional ones. Therefore, scientists have conducted numerous researches to produce new substance that have superior properties than conventional materials. In this way, new materials have been produced under the name of “composite materials” with improved properties than other substances.

Composite materials represent a type of advanced technological materials. These materials are the one of the materials that human beings developed to protect themselves from external influences and their usage areas are increasing in almost every phase of our lives in this century. Research on composite materials is increasing due to their advantages including cost, lightness and excellent mechanical-thermal properties.

Aluminium matrix composites (Al-MMC) have an important place in the automotive, space and energy industries on account of their improved mechanical and tribological properties. Hard ceramic particle reinforced Al-MMCs, especially in automotive industry applications, have been used due to low weight, high strength and high wear resistance. Ceramics such as SiC, Al<sub>2</sub>O<sub>3</sub>, TiC and B<sub>4</sub>C are among the reinforcements used to improve the mechanical properties of aluminium matrix composites. Among these ceramics, B<sub>4</sub>C has outstanding due to its superior physical and chemical properties such as its low density, high strength, high hardness, high wear resistance and good ability to bond with aluminium. The rich boron resources that our country makes B<sub>4</sub>C preferred reinforcing material. Studies on B<sub>4</sub>C reinforced Al-MMCs have started to increase, although these are still new and in fact researches about boron carbide has remained limited because of the high costs compared to other ceramic reinforcing elements.

An economic fabrication method that will provide advanced physical and mechanical properties has not been standardized yet. Various techniques have been used for fabrication of B<sub>4</sub>C reinforced Al-MMC, which are roughly classified as liquid phase routes and solid phase routes. The infiltration method, which is the one of the liquid state fabrication methods of Al-MMC, has the difficulty in application and fabrication

conditions due to the lowest rate of wetness. The casting technique, which is mostly preferred liquid state method, using a mechanical mixer is also an advantageous technique with the applicability of the mass production to produce B<sub>4</sub>C reinforced Al- MMCs. However, due to the difference in density and poor wetting between aluminium and boron carbide, composite material production is difficult by mixing particles in the liquid phase. As a result of the non-homogenous dispersion of the reinforcement element in molten matrices element and the addition of them together, the production of composite materials is not improved in mechanical and tribological properties of composite materials may not be improved. Consequently, the main and common problem in the production of these composites by liquid state fabrication methods is the low wetting between the Al matrix and the B<sub>4</sub>C reinforcement. However, the control of surface kinetics can be achieved theoretically by powder metallurgy (PM) method, which is one of the solid-state routes. Therefore, studies with PM have been concentrated on the homogeneity of particle distribution by eliminating the issues related to the low wettability of ceramics by molten metal. The production of composite materials with mechanical alloying process, which is a PM method used in the industry, is an easy and cost-effective method due to particle size reduction and homogeneous reinforcement distribution into the matrix. With the mechanical alloying process, Al and B<sub>4</sub>C powder are welded together, and a high-strength metal matrix composite material with homogeneous microstructure could be produced. For this reason, it is possible to produce more homogeneous composite material by mechanical alloying process which does not accommodate the wettability and particle agglomeration problems.

In this study, it is aimed to examine the mechanical and tribological properties of boron carbide reinforced aluminium matrix composites which were produced by the mechanical alloying process, and to investigate their microstructures detailed in following chapters.

## CHAPTER 2

### BACKGROUND AND LITERATURE REVIEW

#### 2.1. Metal Matrix Composites

Studies on metal matrix composites (MMCs) started in the late 1950s with the aim of protecting the superior characteristics of metallic materials and for developing their structural performance. High fabrication costs of MMC materials caused its applications to be limited to the aerospace industry at first. Thanks to later studies aiming to reduce their fabrication costs for the materials to be used in commercial applications, MMC started to be developed and used in various areas including mainly the automotive, aircraft and aerospace industries. The interest related to MMC materials was focused on properties such as rigidity, strength, fatigue resistance, wear resistance and coefficient of thermal expansion. Mechanical properties of metal matrices are enhanced via incorporation with reinforcement material, which made the material centre of attention in many areas. Various matrix and reinforcement combinations can be used in MMC systems.

Composite materials are formed by combining a minimum of two or more materials which have individual physical and chemical characteristics. A newly created composite material can show new and advanced characteristics that cannot be provided by any constituents forming the composite. Advantages of composite materials can be listed as high rigidity, strength, fatigue resistance, specific elasticity, low weight, corrosion resistance, wear resistance, good thermal and heat conductivity.

Composite materials consist of matrix and reinforcement constituents. Reinforcement is embedded into the matrix constituents to create a composite material. The role of matrix in composite materials can be listed as follows protecting the mostly brittle reinforcement materials from the external and environmental conditions, transferring the load on the composite material to reinforcement materials and holding the entire composite structure together. Morphology of the reinforcement used in composite materials is an important parameter affecting the characteristics of composite material. Reinforcement material strengthens and stiffens the composite by bearing the

loads, preventing mechanical restraint from matrix deformation and providing thermal and electrical conductivity depending on the type of reinforcement material used. Composite materials can be classified as polymer matrix composites (PMC), ceramic matrix composites (CMC) and metal matrix composites (MMC) based on the type of matrix material.

Among composites, PMCs are the most commonly used composite type in several applications. The reason beyond this, PMCs are much easier to manufacture the most complex and big parts than MMC and CMC due to relatively low processing temperatures required to fabricate them with lower cost. Also, polymer phase increases the elastic modulus, creep resistance, yield and tensile strength.

Ceramic matrix such as glass-ceramics, borides, carbides, graphite, nitrides and silicates reinforced with ceramic particles, whiskers and fibers provide enhanced strength and toughness even at high temperatures. Monolithic ceramics usually have considerable high strength and stiffness, but they are brittle with low toughness. One of the main reasons for producing CMCs is to increase toughness. Their low density, ability to work at high temperatures, high strength, high hardness and chemical inertness properties are the greatest factors for choosing them as the matrix materials. However, their brittle structure makes them so vulnerable against impacts. Apart from their brittleness, low mechanical and thermal shock resistance and shear strength are among their other important disadvantages. While metal matrix composites are preferred instead of polymer matrix composites in application at elevated temperatures, ceramic matrix composites emerge as a good alternative to metal matrix composites due to their lightness and high oxidation resistance.

MMCs are metals reinforced with other metal, ceramic or organic compounds. Main reasons of selecting metals as the matrix material are their ability to work at high temperatures, high compressive/shear/tensile strength, overall well toughness and high resistance/density, fatigue resistance, high electrical and thermal conductivity and thermal expansion characteristics. Various metal matrices are used in MMC systems. The most commonly used matrices are aluminium, titanium, copper and magnesium. Among these metal matrix composites, aluminium matrix composites (AMCs) are widely used in advanced applications such as automobile, aerospace, and transportation which require high performance. Aluminium has low density ( $2.7 \text{ g/cm}^3$ ) as compared to their counterparts which is about one third of materials such as steel ( $7.83 \text{ g/cm}^3$ ), copper ( $8.93 \text{ g/cm}^3$ ) and brass ( $8.53 \text{ g/cm}^3$ ). Also, aluminium is one of the most commonly found

elements on earth, which is one of the reasons that makes it the most preferred matrix material due to ease of accessibility.<sup>1-8</sup> Other prompted properties of AMCs compared to monolithic (un-reinforced) aluminium alloys are,

- ✓ Greater strength
- ✓ Excellent stiffness
- ✓ Better corrosion and wear resistance
- ✓ Better toughness value
- ✓ Improved high temperature properties
- ✓ Controlled thermal expansion coefficient
- ✓ High thermal and electrical conductivity
- ✓ Ease in machinability

AMCs can be classified based on the form of reinforcements as particles, continuous fiber, non-continuous fiber (whisker or short fiber) composites and they can be reinforced with several oxides, carbides, nitrides and borides in layer form.

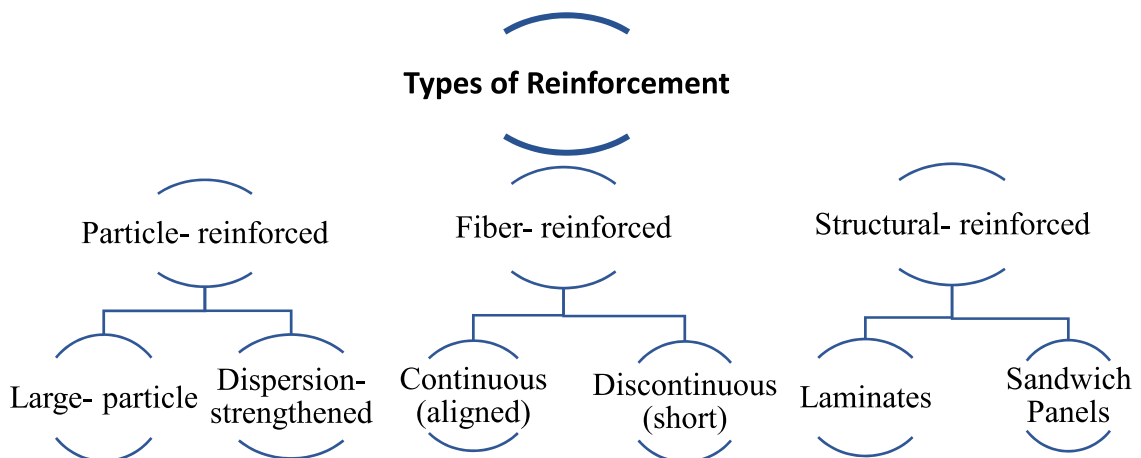


Figure 2.1. The classification of reinforcement based on its form

Metal carbides (SiC, TaC, WC, B<sub>4</sub>C), metal nitrides (TaN, ZrN, Si<sub>3</sub>N<sub>4</sub>, TiN), metal borides (TaB<sub>2</sub>, ZrB<sub>2</sub>, TiB<sub>2</sub>, WB) and metal oxides (ZrO<sub>2</sub>, Al<sub>2</sub>O<sub>3</sub>, ThO<sub>2</sub>) are the reinforcing particles. In general, continuous fibers show the best characteristics in terms of fiber alignment but they constitute the highest cost group. Short fibers or whiskers are weaker in their fiber alignment as compared to continuous fibers. High cost of whiskers that are commonly preferred has led the interest towards particle reinforced AMC materials. By

using particle reinforcements, both strength and rigidity values close to non-continuous reinforced MMC materials can be obtained and low-cost fabrication methods that are easy to apply can be used. Therefore, particle reinforced metal matrix composites and in particular aluminium matrix composites have already been shown as candidates for industrial applications.

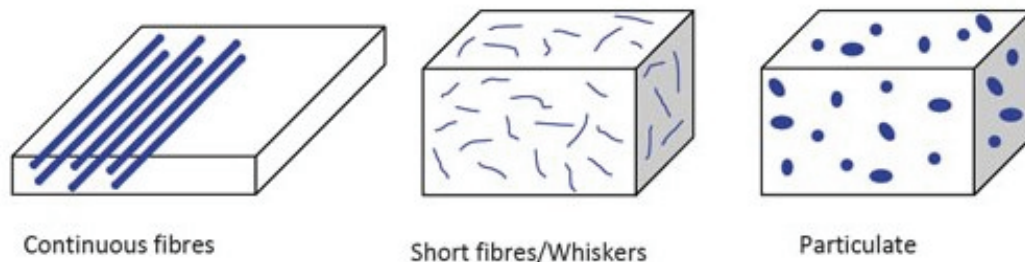


Figure 2.2. Types of reinforcement based on its form.  
(Source: (9))

Producing tough and durable material is a challenge for Al metal matrix composites (AMC), that is necessary for improving static and dynamic characteristics of the material and reducing the crack formation. Mechanical behaviours such as fracture toughness and ductility in MMCs should be developed by considering processing conditions (contents and characteristics of reinforcement). Ceramic reinforcement materials generally create a good combination with a matrix element in terms of rigidity, strength and density values. AMCs are used in combining ceramic reinforcement elements such as SiC, Al<sub>2</sub>O<sub>3</sub>, B<sub>4</sub>C, TiC, MgO, TiO<sub>2</sub> and BN. While graphite or boron fibers are generally used in AMC materials as continuous fibers, SiC, B<sub>4</sub>C or Al<sub>2</sub>O<sub>3</sub> particles or whiskers are often preferred for non-continuous reinforcement elements.

It is known that the combination of B<sub>4</sub>C with a metal can decrease the problems related to brittleness, which makes B<sub>4</sub>C a promising reinforcement material for AMCs so that mechanical properties such as fracture toughness and wear resistance can be improved.

B<sub>4</sub>C (HV = 30 GPa) has a little hardness less than that of diamond and boron nitride, excellent chemical inertness, thermal stability, high strength, high wear resistance, high melting point and high abrasive capacity. It is a robust material which is used for manufacturing bullet proof vests, armor tanks, etc. Furthermore, due to the high



neutron absorption capacity of B<sub>4</sub>C, it is a valuable material for nuclear applications. Aluminium matrix reinforced with B<sub>4</sub>C particles has been the focus of research due to its potential for significant improvement in mechanical and thermal properties of Al. The potential lies in good bonding characteristics of B<sub>4</sub>C with Al and its alloys as compared to other ceramic reinforcement elements. Particle B<sub>4</sub>C reinforced AMCs have a unique combination of high specific strength, high elastic modulus, low coefficient of thermal expansion value, good wear resistance and good thermal stability as compared to the corresponding non-reinforced matrix alloy systems.

Table 2.1. Mechanical properties of different types reinforcement on their forms

<b>Materials</b>	<b>Reinforcement</b>	<b>Modulus of Elasticity (GPa)</b>	<b>Density (g/cm<sup>3</sup>)</b>	<b>Thermal Conductivity (W/mK)</b>	<b>Thermal Expansion Coefficient (x10<sup>-6</sup>/K)</b>
SiC	Particulate	448	3.21	120	3.4
SiC	Short Fiber	400-700	3.21	32	3.4
SiC	Fiber	450	3.46	-	-
Al <sub>2</sub> O <sub>3</sub>	Particulate	410	3.9	25	8.3
B <sub>4</sub> C	Particulate	450	2.52	29	5.0-6.0
TiB <sub>2</sub>	Particulate	370	4.5	27	7.4
TiC	Particulate	320	4.93	29	7.4
BN	Particulate	90	2.25	25	3.8
Al <sub>2</sub> O <sub>3</sub>	Short Fiber	300	3.29	-	-

B<sub>4</sub>C has become more attractive as a reinforcement than SiC and Al<sub>2</sub>O<sub>3</sub> in AMCs applications because it is as hard as SiC (2800 KH) and harder than Al<sub>2</sub>O<sub>3</sub> (2100 KH), and lighter (2.52 g/cm<sup>3</sup>) than both reinforcements (3.20 and 3.96 g/cm<sup>3</sup>, respectively) and even aluminium alloy (2.70 g/cm<sup>3</sup>). However, many researchers have studied on the most widely used SiC and Al<sub>2</sub>O<sub>3</sub> as reinforcing materials<sup>10-15</sup>, but very limited research has been conducted on B<sub>4</sub>C as a reinforcement because of its high raw material cost and poor wettability complications arising during the fabrication of composites. However, there are several studies mainly focused on the problem of wettability and chemical reaction between aluminium and B<sub>4</sub>C at higher processing temperature. Few attempts have been made so far to fabricate B<sub>4</sub>C particle reinforced Al matrix composites and mainly focused

on the synthesis and characterization of Al– B<sub>4</sub>C composite powders and the fabrication problem due to higher processing temperature in using liquid state routes. To the best of our knowledge, very limited studies were conducted on the mechanical and tribological characteristics of bulk B<sub>4</sub>C particle reinforced aluminium matrix composites fabricated by solid state routes.

Table 2.2. Properties of ceramic reinforcements used in AMCs

<b>Reinforcement</b>	<b>Density (10<sup>3</sup> kg m<sup>-3</sup>)</b>	<b>Thermal Expansion Coefficient (10<sup>-6</sup> C<sup>-1</sup>)</b>	<b>Melting Temperature (°C)</b>	<b>Strength (MPa)</b>	<b>Modulus of Elasticity (GPa)</b>
Al <sub>2</sub> O <sub>3</sub>	3.98	7.92	2100	-	379 (1090 °C)
SiC	3.21	5.40	2750	-	324 (1090 °C)
SiO <sub>2</sub>	2.66	<1.08	1710	-	73
B <sub>4</sub> C	2.52	6.08	2420	2759 (24 °C)	448 (24 °C)

Composite materials cannot be obtained only by combining matrix and reinforcement materials at certain ratios and under suitable conditions. Along with matrix and reinforcement, several additional materials such as lubricants and process control agents, etc. are added in order to increase the performance and, quality of the products.

### 2.1.1. The Al-B<sub>4</sub>C Interface

Interface refers to the area where the matrix and the reinforcement meet. Diffusion and chemical reactions may occur at the interface between the matrix and the reinforcement. The amount of the interfacial reactions and type of reaction products depend on the factors such as process temperature, pressure, time, atmosphere, matrix composition and surface chemistry of reinforcement. The interaction between liquid metal and reinforcement at high temperatures can cause chemical reactions. Diffusion and reaction kinetics are more rapid at high temperatures. Bonding, physical or chemical reactions in MMC materials are related to the interface between the matrix and the

reinforcement, and bonds formed between Al, B and C elements on this interface can be metallic, ionic or covalent. In the literature, different types of binary and ternary compounds such as  $\text{Al}_3\text{BC}$ ,  $\text{Al}_4\text{BC}$ ,  $\text{AlB}_{24}\text{C}_4$ ,  $\text{AlB}_2$ ,  $\text{AlB}_{12}$  and  $\text{AlB}_{12}\text{C}_2$  can be formed at interface between Al- $\text{B}_4\text{C}$  at elevated process temperature.<sup>13,16–19</sup> Figure 2.3 presents the formation of potential phases at the interface between Al- $\text{B}_4\text{C}$  depending on process temperature in Al-B binary phase diagram. The characteristics of these interfacial bonds and interfacial reaction products have a significant effect on the physical, mechanical and tribological properties of composite. Potential reactions might be preferred for MMCs depending on the requirement. For instance, the interface where a metallic bond is located becomes more ductile as compared to other bonds and might be preferred in MMC materials. Also, a strong interface is significant to enable properly transferring of load from reinforcement to matrix, and hence improving mechanical properties.

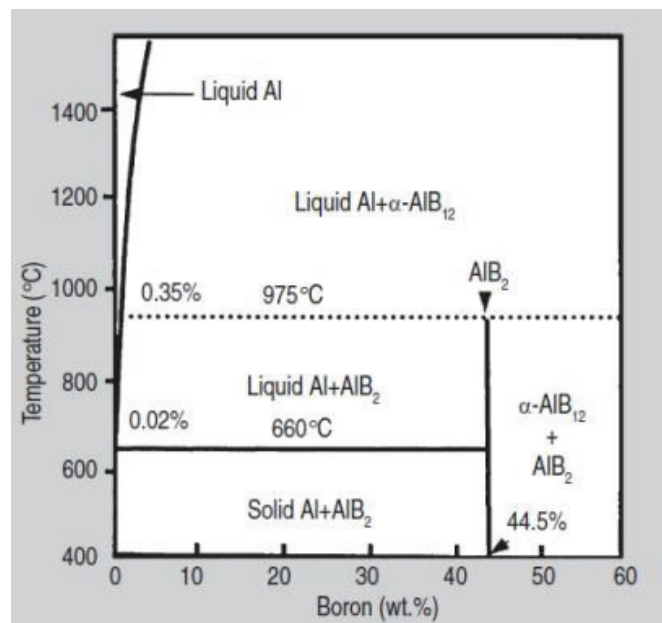


Figure 2.3. The formation of potential phases at interface between Al-B depending on process temperature (Source: (20)).

On the other hand, any chemical reaction products which occur at matrix-reinforcement interface can affect composite properties negatively leading to decrease in the mechanical and tribological performance of composites. Therefore, understanding the thermodynamics and kinetics of interface reactions is critical to control the process and obtain composites with improved properties.

### 2.1.2. The Wettability

Wettability is defined as the ability of a liquid to disperse on the solid surface. Contact angle of a liquid drop on a solid with the solid surface ( $\Theta$ ) is a physical measure of wettability. Contact angle can be determined using test methods such as sessile drop. Accordingly, Figure 2.4 shows the wettability of materials based on the contact angle.

The first requirement for the contact between matrix and reinforcement materials is to enable the wettability of reinforcement by molten metal matrix. Wettability depends on many parameters such as stoichiometry, interface chemical reactions, process temperature, time, atmosphere, porosity and roughness of reinforcement, and can be affected by many factors.<sup>21-23</sup> Oxide layer formed on the molten metal surface affects wetting negatively by preventing the penetration of particle reinforcements into the liquid metal. Furthermore, ceramic particle surfaces are generally covered with gas and this gas layer causes the wettability to decrease by preventing the contact of molten matrix material with ceramic surface. Particle surface characteristic is another factor that affects wetting. The impurities absorbed on the particle surface can reduce wettability.

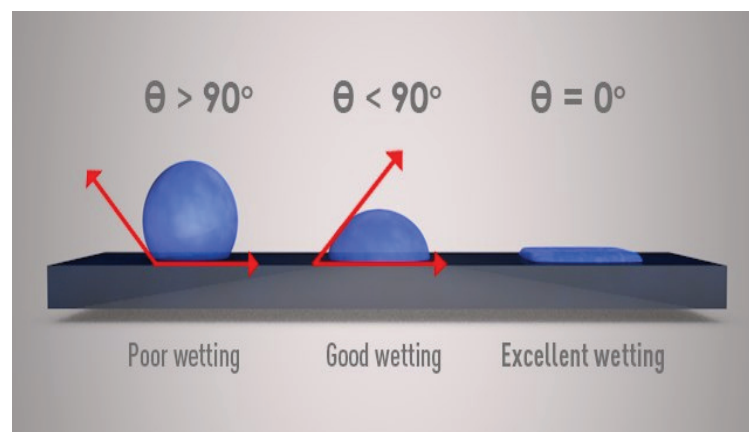


Figure 2.4. The wettability of water droplet.  
(Source: (24))

The first requirement for the contact between matrix and reinforcement materials is to enable the wettability of reinforcement by molten metal matrix. Wettability depends on many parameters such as stoichiometry, interface chemical reactions, process temperature, time, atmosphere, porosity and roughness of reinforcement, and can be affected by many factors.<sup>21-23</sup> Oxide layer formed on the molten metal surface affects

wetting negatively by preventing the penetration of particle reinforcements into the liquid metal. Furthermore, ceramic particle surfaces are generally covered with gas and this gas layer causes the wettability to decrease by preventing the contact of molten matrix material with ceramic surface. Particle surface characteristic is another factor that affects wetting. The impurities absorbed on the particle surface can reduce wettability.

An increase of the surface energy of solid, a decrease of the surface tension of liquid alloy or a decrease of the liquid-solid interface energy on the interface improve wettability. The addition of alloying elements into the matrix alloy, coating of ceramic particles by a readily wettable agent and processes applied on ceramic particles are main solutions used to improve wettability.

## 2.2. Fabrication Methods of MMCs

The use of different matrix and reinforcement materials has led to the development of different fabrication methods for MMCs. The fabrication methods of MMC can be roughly grouped as liquid state fabrication<sup>6,21,22,25-32</sup> and solid-state fabrication<sup>10,18,33-39</sup> techniques based on the phase of matrices. The methods commonly used in the fabrication of MMCs are shown in the Figure 2.5.

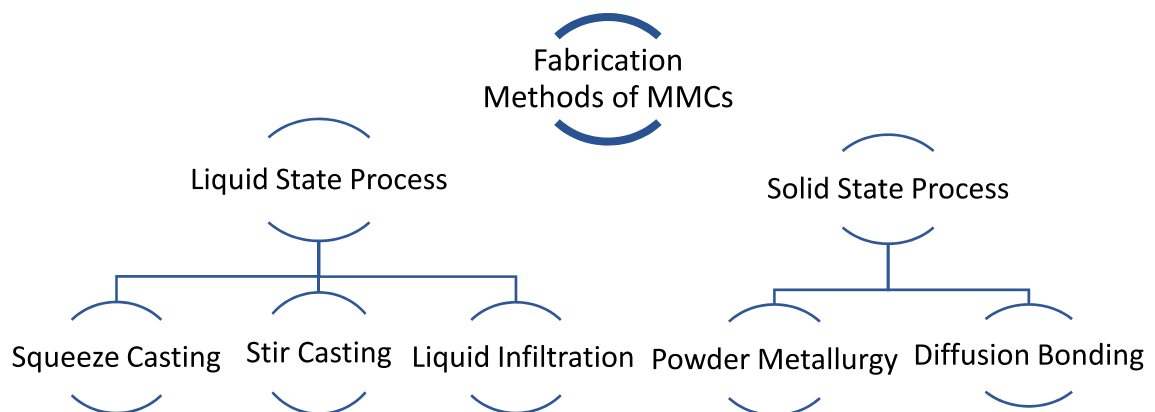


Figure 2.5. The fabrication methods of MMCs.

Characteristics and wettability of the reinforcement to be chosen in the fabrication of metal matrix composites are important issues. The PRAMCs are usually produced by powder metallurgy and casting route.<sup>16</sup> In the liquid phase fabrication methods of MMC materials, wettability must occur in order to create contact and strong bonding between the matrix and reinforcement during fabrication processes. Reinforcements are generally exposed to a pre-treatment in liquid phase fabrication methods to enhance wettability of reinforcement since many reinforcement materials are not wetted sufficiently by the molten metal. Undesired phases occur on the matrix and reinforcement interface due to the chemical interaction. Additionally, casting problems, which are regarded as the disadvantages of liquid phase fabrication methods, such as insufficient level of bonding, porosity and reinforcement segregations occur during solidification. Liquid phase fabrication methods are quite appealing in terms of their simplicity and low cost as well as the ease of fabrication of complex 3D parts.

Solid phase fabrication techniques offer some advantages including significant decrease in the formation of undesired matrix and reinforcement interfacial chemical reaction products due to low process temperature, absence of casting problems such as porosity, segregation and non-uniform distribution of the reinforcement phase in general. The most common solid phase fabrication method is the powder metallurgy method. Therefore, as the topic of this thesis, this method is focused in detail in the following section.

### **2.2.1. Powder Metallurgy**

Some problems emerging in fabrication of MMCs using liquid state routes do not arise when using powder metallurgy method. This advantage over liquid state routes encouraged broadly use of Powder Metallurgy method and made it the first developed method among solid state routes. It was observed that blending powder mixture significantly provides a homogeneous distribution of reinforcement without any evidence of reinforcement powder agglomerated into the matrix.<sup>1,16,40</sup> Processing using PM method considerably avoids the formation of undesirable interfacial chemical compound due to the low manufacturing temperature.<sup>5,41-44</sup> The issues related to the wettability of B<sub>4</sub>C- Al matrix and the segregation typical of casting are eliminated using PM method. Therefore,

clean interfaces and strong bonding between reinforcement/matrix improve the mechanical and tribological properties of Al-MMCs.

Powder metallurgy (PM) method is used widely to fabricate aluminium matrix composites.<sup>40</sup> PM method consists of a series of steps based on the mixing or blending and mechanical alloying of matrix/reinforcement powders and further compaction processes such as cold or hot pressing, isostatic pressing followed by sintering, extrusion, forging, injection casting and hot rolling processes as shown in Figure 2.6.

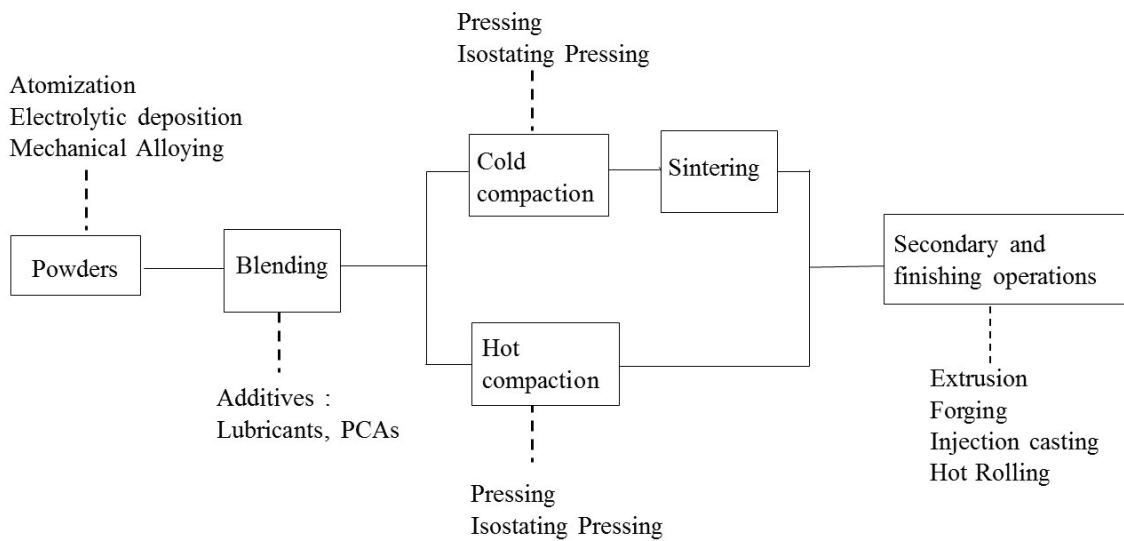


Figure 2.6. Schematic representation of process stages in PM.  
(Source: (45))

Electrolytic deposition, chemical methods, atomization and mechanical alloy methods are the main methods used to produce composite powders. The microstructures of powders such as geometrical shape and surface of powder and the chemical/mechanical properties of powders vary depending on these production of composite powder methods.

### ***Mechanical Alloying Methods***

Mechanical alloy (MA), on account of its applicability and simplicity, is the most utilized method of PM processes to produce composite powder with hard particles and soft metal matrices.<sup>18,46,47</sup> MA mechanism follows a repeated series of processes which are deformations, cold welding, fracture and rewelding of powders. This mechanism

allows reinforcing powders to be well incorporated into metal matrix powders. It also provides to obtain composites with homogeneous particle reinforcement distribution into the matrix material.

The MA process is performed by a wide range of mills used such as horizontal, vertical, planetary, industrial ball mills. Planetary type ball milling is utilized to achieve mechanical alloying of Al-B<sub>4</sub>C composite powder mixtures in this study. The milling method is based on the mechanical forces acted upon particle such as shear, impact, compressive forces. The main objectives of mechanical alloying are as follows,

- ✓ Mechanical or solid-state mixing
- ✓ Solid state alloying
- ✓ Particle size reduction
- ✓ Particle size growth
- ✓ Homogeneous particle distribution
- ✓ Modification of material property

### ***Mechanical Alloying Mechanism by Ball Milling***

Powders that are to be mixed by planetary ball milling are loaded into the milling jar together with milling balls. Centrifugal force created by the jars that rotate around their own axis together with the additional force created by the rotating support disc affects the milled material and milling balls in the jars.

These forces lead to the collisions between ball-ball, ball-wall. As shown in Figure 2.7, some impact energy is loaded to the powder remaining between such collisions and leads to elastic, plastic and shear deformations of the particles and work hardening followed by recovery phenomena. Mechanical alloying results from two opposite process which are cold welding and fracturing of powder. Due to the loaded impact energy, powder particles form layers, weld with each other, break and weld again. Initially ductile metal powder particles become flakes due to cold welding. This leads to formation of layered composite particles that includes various combinations of the initial content. More brittle particles prevent the formation of particle welding and they are easily embedded into the matrix.

During this process, powder particles flatten in cycles, break with cold welding and weld again. Size of these composite particles changes significantly. As the milling continues, cold welding and breaking processes continue as well leading to recovery of



the microstructure. Due to the increase in the amount of cold deformation, particle failures, porosity and number of grain boundaries increase over time through short cycle diffusion. Effect of ball-ball, ball-powder and ball-wall collisions leads to an increase in the temperature of powder and eases diffusion. Some impact energy is loaded to the powder remaining during such collisions. Mechanical alloying is formed due to the mixture of such effects. At this stage, microstructure recovery continues, and oxide distribution is more uniform. Efficiency of breaking and welding processes mostly depends on the deformation characteristics of the initial powder.

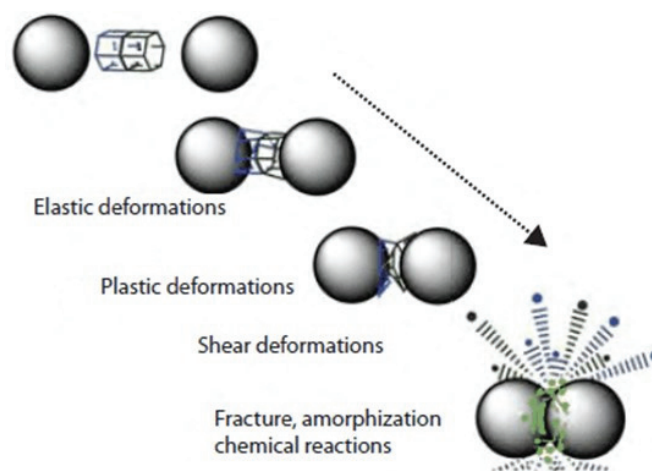


Figure 2.7. Mechanical alloy process by ball milling.  
(Source: (48)).

Ductile Al powders have a high tendency to weld with each other, which causes an increase in powder aggregate size. Those welded Al powders become flake form due to the collision. The particle size increases indicating formation of a large amount of laminates due to cold welding of particles. At the initial stage (Figure 2.8), average particle size becomes bigger and might exceed the initial size of particle due to formation of a large amount of flake forms. Process Control Agents (PCA) are added in order to control this situation. Composite particles have a layered structure that involves various combinations of initial powder mixtures at this stage of milling. Along with the ongoing deformations, hardening continues through a fatigue mechanism or re-breaking of the brittle layered powder particles. In the absence of agglomeration, size of the powder particles created by this mechanism keeps reducing. Due to the ongoing impact effect of milling balls, structure of the particles becomes stable, and homogenous in terms of initial

composition. Ductile powders become flake while brittle powders break due to ball-powder collisions. Broken brittle powders embed into the ductile component. Brittle components locate along the gaps between layers (Figure 2.9). As a result of the later milling processes, powders are exposed to deformation hardening, layers multiply and their sizes are reduced. Breaking occurs more and system achieves the coaxial morphology at earlier times in systems with brittle particles.

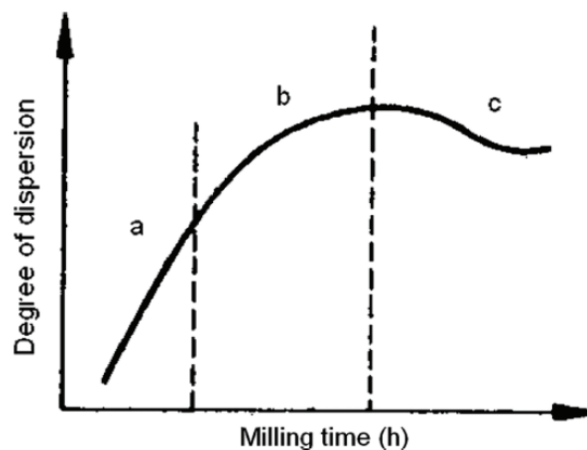


Figure 2.8. The three stages during ball milling (Source: (20)).

Volume of the balls that will be placed in the jar and amount of the material to be milled are quite important for a homogenous mixture. Milling type, milling jar, milling energy/speed, milling time, ball/powder ratio, process control agents and milling temperature are parameters with important effects in the ball milling process.

**Milling Jar:** Contamination occurs if the materials to be milled corrode the inner walls of milling jar. Material of the milling jar is very important to avoid such a situation. Milling jar corrosion might contaminate or change the chemistry of powder.<sup>49</sup>

**Milling speed:** One of the most important factors in mechanical alloying is the milling speed. Excessive plastic deformation that the particles are exposed to, with the ball collisions enables the particles to form cold welding with each other and break. As the rotation speed increases, the energy transferred to powder increases and thus there will be more and stronger ball collisions. However, if the temperature of jar increases significantly at higher speeds, temperature may contaminate the powder. In order to avoid

excessive temperature , gas or liquid can be used as the cooling fluid depending on the type of system.<sup>49</sup>

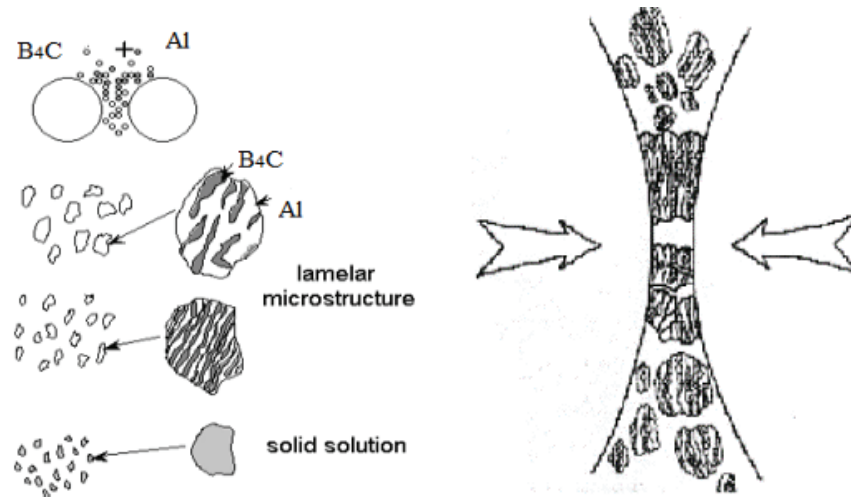


Figure 2.9. B<sub>4</sub>C powders are embedded into Al powders by MA (Source: (50)).

**Milling speed:** One of the most important factors in mechanical alloying is the milling speed. Excessive plastic deformation that the particles are exposed to, with the ball collisions enables the particles to form cold welding with each other and break. As the rotation speed increases, the energy transferred to powder increases and thus there will be more and stronger ball collisions. However, if the temperature of jar increases significantly at higher speeds, temperature may contaminate the powder. In order to avoid excessive temperature , gas or liquid can be used as the cooling fluid depending on the type of system.<sup>49</sup>

**Milling Time:** Milling time is one of the most crucial parameters for the efficiency of the milling process. The optimum milling time is arranged to enable a balance between deformation, cold welding and fracturing mechanisms of powder particles. There are many studies reported in the literature on the effect of milling time on microstructure of composite powder. Milling time significantly affects the particle size of powders and the distribution of reinforcement on the matrix. An increase in milling time provides smaller composite powders with homogeneous powder distribution.<sup>40</sup> Time depends on various factors such as the type of mill used, milling speed, ball/powder ratio, characteristics of powders etc.<sup>49</sup>

**Powder/Ball weight ratio:** Ratio of powder weight to the weight of balls (PBR) is occasionally named as volume ratio. This parameter is an important variable in milling process. A wide range of parameters from low values such as 1:1 to high ones such as 1:220 have been used by many researchers. In general, (PBR) 1:10 is the most commonly used ratio in milling of the powder in low capacity mills. But if the milling is performed in a high capacity attritor-like mill, a high ball-powder ratio such as 1:50 or a higher one like 1:100 can be used. Increase in this rate decreases the alloying time based on the total energy obtained while it may also accelerate negative effects such as contamination of powder. At a high powder-ball ratio, number of collisions at unit of time increases, and thus more energy is transferred to powder particles.<sup>49</sup>

**Jar volume ratio:** Sufficient space is necessary for the balls and powder to collide in the mill jar. Therefore, jar volume range is important for powder and balls. If the amount of balls and powder is low, fabrication amount will also be low. In other words, if the amount is high, there won't be sufficient space for the movement of balls and collision energy will be lower. As a result, no alloying may occur or even if it occurs, it takes longer than necessary. Therefore, care must be taken not to fill the jar too much. Volume of balls must be nearly half of the volume of jar, and amount of the material to be milled must be about 25% of jar's volume for dry milling process. 75% of the jar must be filled in wet milling process.<sup>49</sup>

**Process control agent (PCA):** Cold welding occurs between the powder particles. If the powder particles are ductile, sometimes too much cold welding occurs due to high plastic deformation during milling. PCA is added to the powder mixture throughout the milling process in order to decrease the excessive cold-welding effect. PCAs may be solid, liquid or gas. PCA is absorbed by the surfaces of powder particles minimizing the cold welding between powder particles and thus preventing agglomeration. The most important PCAs are stearic acid, hexane methanol and ethanol. These compounds have low melting and evaporation temperature. Therefore, they melt and evaporate as the temperature rises during milling.<sup>4,5,35,37,42,46,47,51</sup>

## 2.2.2. Sintering Process

Sintering can be defined as the process of providing density and it is applied in a controlled atmosphere under high temperature with the aim of providing strength to the shaped raw parts. In sintering process, powders are bonding together at elevated temperature to form a solid part.<sup>12,34,52-54</sup> Atom mobility increases due to the increased diffusion along with the increased temperature during sintering process, and the size of pores between are reduced as seen in Figure 2.10. Therefore, the strength and hardness are provided by the metallic bonds created between powders in the sintering process.

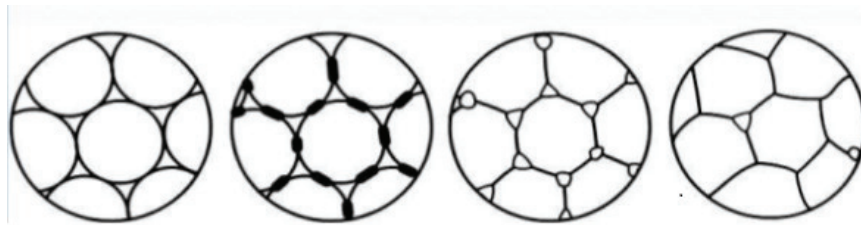


Figure 2.10. The particles are welding to each other during sintering process.  
(Source: (55))

Sintering process may be divided into two groups: as solid phase sintering and liquid state sintering. During welding, the bond between the particles increases gradually with the movement of atoms in a solid or liquid state. Solid state sintering occurs when the bonds between the particles are formed with the movement of atoms. While solid state sintering occurs at a complete solid phase sintering temperature, liquid state sintering occurs when powders come together in the liquid phase. Solid state sintering is the sintering process performed at a temperature below the melting point of metal or alloy.<sup>8,36,56-58</sup> Liquid state sintering is applied on alloys and composites that melt at a specific temperature range. Normally, solid granules can dissolve in liquid. During liquid phase sintering, liquid phase and a solid powder group are present simultaneously. Generally, liquid phase sintering significantly increases the bond generation between particles and sintering speed.<sup>12</sup>

### 2.3. Wear Performance of MMCs

Wear is considered the phenomenon of moving a material away from a surface that is interacting with a bonding surface.<sup>21</sup> Wear occurs due to the physical removal of material caused by micro cracking through chemical degradation or melting on the contact interface. Many parameters are observed to be effective on the wear behaviours of MMC materials.<sup>7,21,59</sup> These parameters can be listed under the titles of material characteristics and experiment conditions.

*Material characteristics:* Characteristics of the matrix material, thermal process condition of matrix; volume ratio, type, size, shape, distribution and interface characteristics of reinforcements into the matrix.

*Experiment conditions:* Applied load, contact type, sliding speed, sliding distance, temperature and characteristics of the other material such as impurities, additives, lubricants and PCAs.

Sliding speed, roughness of worn surface and shape of worn particle provide important information about the characterization of wear. The main wear types occurs in MMC materials are as follows:

**Adhesive wear:** Adhesive wear occurs with material transfer from one surface to another as a result of cold welding or regional bonding on surfaces that are in movement. Adhesive wear takes place when the pressure on the surfaces that slide on each other reaches up to a point sufficient for regional plastic deformation. In adhesive wear, sliding speed, applied load and material hardness are significant parameters.<sup>31,60</sup>

**Abrasive wear:** As another important wear type, abrasive wear occurs during the sliding movement of a material that has hard particles or protrusions on another material. Material loss takes place when the hard protrusion on the material “scratches” the relatively softer surface of the other material. It occurs during the moving contact of a material with another one that is hard and abrasive. Abrasive wear is defined as two-body wear whereas entrapment of hard ceramic particles in the abrasion surface during wear is referred to as three-body wear. The parameters that are effective at the abrasive stage of MMC materials are the applied load, sliding speed, size of reinforcement, volume ratio and interface bond strength. Composites with high volume ratio and large particles are said to be more resistant to abrasive wear in general.<sup>57,60–63</sup>

**Friction oxidation:** The presence of an oscillation movement between surfaces with little roughness that contact each other drives friction oxidation. If the surfaces are dry, a dark reddish layer is formed on the surface as a result of the small amplitude oscillation movements of surface pairs that are not mounted tightly enough. Over time, such layers thicken leading to large deformations on the surface, cracks and breaks accordingly.<sup>64,65</sup>

**Fatigue wear:** It occurs between mating surfaces with point or linear contact. Material particles flake off the surface over time on very small contact points under the effect of a variable load, leaving small pits behind.<sup>66,67</sup>

**Erosive wear:** It is the same as abrasive wear in its general structure. The difference is that main material is exposed to a repeated impact load by small particles that are harder than the main material itself. Gases and liquids compressed in an enclosed volume also lead to the same effect at certain speeds. Temperature, speed, size of the particle, shape of the particle and its hardness are the factors that affect erosive wear.

Another important characteristic considered in determination of the wear behaviours of MMC materials other than the wear resistance is the friction coefficient. In the most general sense, friction coefficient is defined as the ratio of friction force to load. Main factors affecting friction under dry sliding conditions in MMC materials are adhesion of flat areas on the rubbing surfaces, scratching carried out by the abrasive particles and hard surface roughness, and deformation of the surface roughness.<sup>7,11,21,31,59–61,64,68,69</sup> The effect of such elements on the friction coefficient value depends on the friction conditions and environment.

### **2.3.1. The Tribological Behaviour of AMCs**

Many approaches have been studied to comprehend the tribological behaviour of B<sub>4</sub>C reinforced AMCs.<sup>7,22,23,54,57,61,70</sup> From the studies conducted on the mechanical properties of ceramic reinforced AMCs, it is well known that hard reinforcing material provides AMCs with enhanced mechanical properties. The hardness of AMCs precisely increases with the incorporation of hard and stiff ceramic particles, and also those ceramic particles successfully deal with bearing the load transferred from soft Al metal

matrix.<sup>62,63,71,72</sup> Therefore, the contribution of ceramic reinforcing particles to the matrix make AMCs strengthened compared to unreinforced matrices.

The investigations reveal that the tribological properties of AMCs such as wear rate, wear resistance, friction of coefficient, are correlated with the hardness and strengthening mechanism. Shorowordi et. al. fabricated AMCs with B<sub>4</sub>C and SiC reinforcing particles using the liquid state route (stir casting method) with the same process parameters.<sup>13,15,31,68</sup> Their results show that both hard B<sub>4</sub>C and SiC ceramic particles enhanced the hardness of AMCs, and the wear rate for the reinforced AMCs is considerably less than that of unreinforced material, and the coefficient of friction and wear rate of Al-SiC composites were higher than those of Al-B<sub>4</sub>C composites.<sup>13,15,68,73</sup>

Other research on ceramic particle reinforced AMCs fabricated by the solid state route showed the similar results with the liquid state routes.<sup>56,61,74,75</sup> The wear rate of AMCs decreases with the presence of B<sub>4</sub>C particles for all load conditions compared to unreinforced aluminium. However, the study on the tribological behaviour of B<sub>4</sub>C particles reinforced AMCs indicated that the wear rate increased up to 8 wt.% addition of micron and nano-sized B<sub>4</sub>C particles.

The increase in wear rate is due to the agglomeration of particles which cause the presence of micro-porosity resulting in a decrease of hardness value.<sup>64</sup>micro The wear rate of micron-sized B<sub>4</sub>C reinforced composites are higher than that of nano-sized B<sub>4</sub>C for less than 8 wt.% particle content because the nano-sized particles tend to be agglomerated more than the micro-sized particles and the large amount agglomeration leads to increase the wear rate of nano-sized B<sub>4</sub>C for more than 8 wt.% particle content, which is dominant at high concentration of nano-sized B<sub>4</sub>C particles. Some researches reveal that the coefficient of friction is higher for micron particle reinforced composites than nano reinforced AMCs due to the easily sliding nano particles between mating metal surfaces.<sup>28,66,76</sup> The phenomenon associated with the wear rate, the coefficient of friction and the hardness of B<sub>4</sub>C reinforced Al-MMCs have still not clear yet due to insufficient researches conducted.



## 2.4. Application Areas of Aluminium Metal Matrix Materials

AMC materials have uses in different areas of the industry due to the aforementioned superiority. The most common sectors for the use and application of AMC materials are aviation, space and automotive industries.

*Application to the automotive industry:* The use of aluminium in vehicles has been an increasing trend since the mid-century. The importance of aluminium in the automotive industry is a growing trend because of the increasing energy costs and efforts made towards reducing emission values. High hardness, high abrasive resistance and fatigue resistance properties are expected from parts used in the automotive industry. While weight gain is rather important in the automotive industry, costs can be less tolerable than the aviation industry. Therefore, AMC materials are used in the applications where properties and costs are combined at the desired levels. Major uses of AMC materials in the automotive industry are brake discs and cylinders, which is expected to have high abrasion resistance. Therefore, AMCs are used for applications such as pistons, engine blocks, drive shafts. AMC materials are also used as brake discs in another important transportation vehicle: high-speed trains.

*Application to the aviation-space industries:* Unlike the automotive industry, performance is more important than the final cost in the aviation-space industries. Thermal expansion, high strength, ductility and corrosion resistance are preferred with low density. Fan guide vanes in commercial jet aircraft, propeller shafts in helicopters, frequency sensors in space telescope antennas, are examples of usage areas in aviation-space industries of AMCs.

*Other application areas:* Due to its properties such as high thermal conductivity, low thermal expansion, and low intensity, AMC materials are used in the electrical and electronic fields such as electronic packaging and high voltage electrical transmission lines. Al-B<sub>4</sub>C composites are used in nuclear shields due to the neutron absorption property of boron carbide. AMCs have also different usage areas like sport applications, and drilling equipment in the mining industry.

## CHAPTER 3

### METHODOLOGY

The material and experimental procedure for fabrication of the composite materials and characterization methods employed for the microstructure analysis are presented in this section.

#### 3.1. Materials

Pure aluminium with a purity of 99.5% and <44  $\mu\text{m}$  particle size was used as the matrix. The boron carbide ( $\text{B}_4\text{C}$ ) with 700 nm particle size was selected as the reinforcement to fabricate the composite samples. Stearic acid was used as a process control agent.

The physical and chemical properties of the materials used which are Al,  $\text{B}_4\text{C}$  and stearic acid are shown in Table 3.1. Particle size and particle shape of as-received powders were analysed using scanning electron microscopy. Figure 3.1 and Figure 3.2 represent the backscattered SEM images of as-received Al and  $\text{B}_4\text{C}$  particles, respectively.

Table 3.1. Physical and chemical properties of the materials.

Materials	Density (g/cm <sup>3</sup> )	Melting Point (°C)	Boiling Point (°C)	Physical State at Room Temperature
Pure Aluminium Al	2.70	660.32	2467	Solid
Boron Carbide $\text{B}_4\text{C}$	2.52	2763	3500	Solid
Stearic Acid $\text{C}_{18}\text{H}_{30}\text{O}_2$	0.94 at 20 °C 0.85 at 70 °C	69.3	361	Waxy Solid

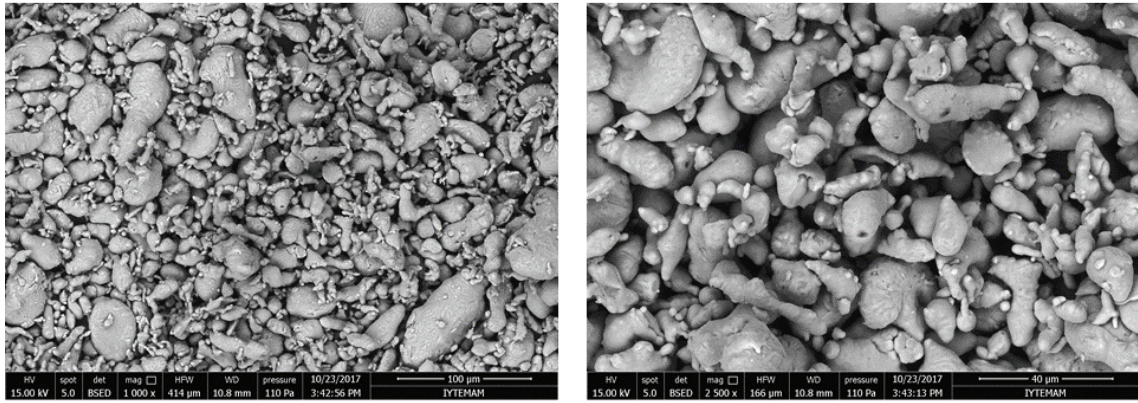


Figure 3.1. SEM images of Al powders at 1000x and 2500x magnifications.

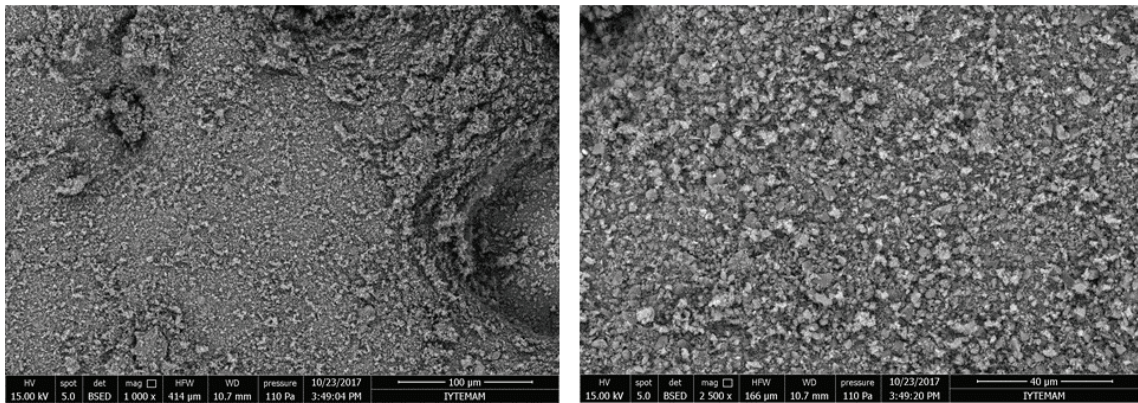


Figure 3.2. SEM images of B<sub>4</sub>C powders at 1000x and 2500x magnifications.

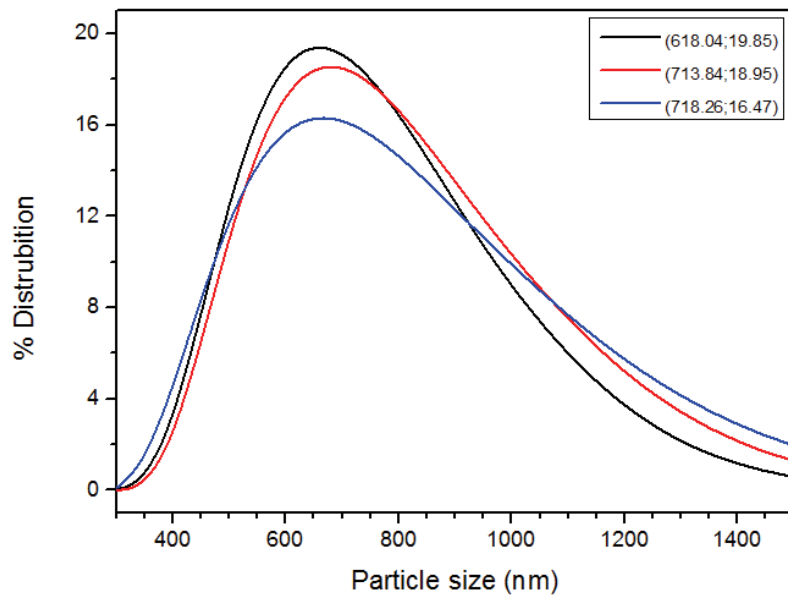


Figure 3.3. The cumulative particle size distribution of B<sub>4</sub>C powders.

As can be seen, as-received Al powders had a random morphology. The average particle size was about 1  $\mu\text{m}$ . The average size of  $\text{B}_4\text{C}$  nanoparticles was determined to be about 700 nm as shown in Figure 3.3 by means of dynamic scattering light technique.

### 3.2. Experimental Procedure

The processes used to fabricate the composites using powder metallurgy methods will be detailed in this section as illustrated in Figure 3.4.

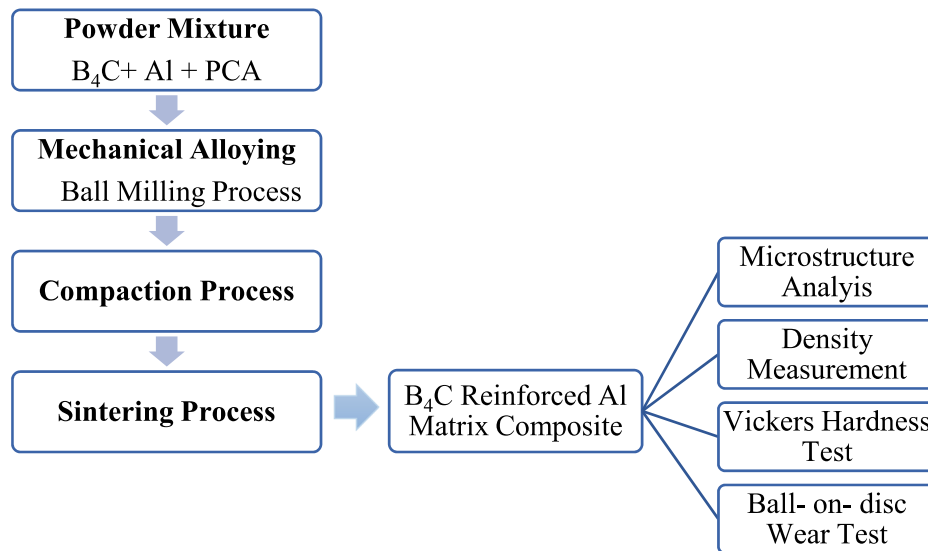


Figure 3.4. The fabrication and characterization steps of composite samples.

In order to fabricate composite powder, Al,  $\text{B}_4\text{C}$  and PCA powders were mixed in pre-determined proportion and the powder mixture was milled by ball milling process, in which mechanical alloying mechanism was employed. This provides  $\text{B}_4\text{C}$  being embedded into Al powders, which resulted in the fabrication of composite powder by ball milling process. Followed by milling process, the composite powder was compacted. The samples of each content with 5, 10 and 15 wt. % of  $\text{B}_4\text{C}$  were sintered. Finally, the composite samples were fabricated by PM methods, and they were prepared for the investigation of microstructures and the mechanical, tribological tests.

### 3.2.1. Sample Preparation

The experimental samples were produced from Al powders reinforced with 5 wt.%, 10 wt.% and 15wt.% B<sub>4</sub>C powders using the PM method. Several trials were made to obtain the optimum parameters for efficient ball milling as shown in Table 3.2.

Table 3.2. Different composite powder preparation with ball milling

<b>Trials</b>	<b>Material</b>	<b>Medium</b>	<b>PCA</b>
1	Al + B <sub>4</sub> C	Dry	–
2	Al + B <sub>4</sub> C	Dry	Stearic Acid
3	Al + B <sub>4</sub> C	Wet	–
4	Al + B <sub>4</sub> C	Wet	Stearic Acid

i) Firstly, only Al and B<sub>4</sub>C powders were ball milled together without using any process control agent or lubricant in order to avoid the undesirable matter like impurity in the composite sample; however, it was observed that cold welding occurred between the metal powders. Ductile aluminium particles tend to agglomerate due to cold welding and thus small Al particles formed onto larger particles with a rough surface. Also, many Al particles were found to stick to the vial surface after ball milling as seen in Figure 3.5.



Figure 3.5. Contamination of milling tools by the cold-welded Al particles during milling in the absence of any PCA.



As a result, cold welding of Al powders led to a decrease in mechanical alloying efficiency. In order to remove the cold-welded particles from the vial surface, sodium hydroxide (NaOH) was used by using distilled pure water, thus the milling tools were thoroughly cleaned with the solution as seen in Figure 3.6.



Figure 3.6. Agate milling balls covered by Al powder and cleaned with NaOH solution.

ii) Secondly, stearic acid in powder form as process control agent (PCA) was added to the composite powders to minimize the cold welding which was encountered in the previous trial. This PCA content was determined as 0.05 wt.% based on the widely accepted values reported in the literature.<sup>46</sup> However, cold welding still remained a problem but relatively lower than the previous composite sample without PCA

iii) Thirdly, ethyl alcohol was also used along with stearic acid to obtain wet medium in order to minimize cold welding. The used alcohol amount was approximately 25 ml to cover the milling balls in the jar.<sup>77</sup> Forming large particles due to cold welding of powders was largely eliminated.

Finally, it was decided to employ stearic acid and ethyl alcohol as PCAs for the rest of the experiments. The total amount of composite powders without PCA was set to be 9.00 gram.

### 3.2.2. Ball Milling Process

Milling was performed by means of a planetary ball mill (Retsch PM 100) without a protective atmosphere. Different ball milling parameters such as milling time, milling medium, milling speed and milling tools were studied to optimize ball milling process, whereas the parameter of the ball-to-powder weight ratio was fixed at 10:1 during the whole milling process.



Figure 3.7. The planetary ball mill utilized in the study.

It was observed during the ball milling process that the powders were agglomerated and contaminated by the vial material which is hardened steel. At the beginning of the experiment, a hardened steel vial (250 ml) and twenty hardened steel balls with a diameter of 10 mm were used. As mentioned in the previous chapter, the vial must be densely filled with enough material up to %75 of its volume to ensure the effective milling process, so there would be more impacts between balls and powders inside the vial.<sup>8</sup> More free spaces in the vial which was used in the experiment resulted in ineffective ball milling process because the balls constantly kept rotating in the same path without collision between balls and powders. Another problem is regarding vial and ball material, because Al powders cold welded to the metal vial and balls. Cold welding between identical materials reached to an extreme level. This resulted in the fact that the powders stuck to the surface of the balls and vial were not completely removed. The excessive use of NaOH solution which help the stuck powders to be removed was likely

to damage the steel milling tools by a chemical reaction and caused the contamination. This is observed with the presence of Fe, Ni and Cr elements which shown in Figure 3.8 and Figure 3.9. The high level of cold welding between Al and steel substantially promoted the agglomeration problem. Therefore, in the second trial, it was decided to use non-metallic vial-balls.

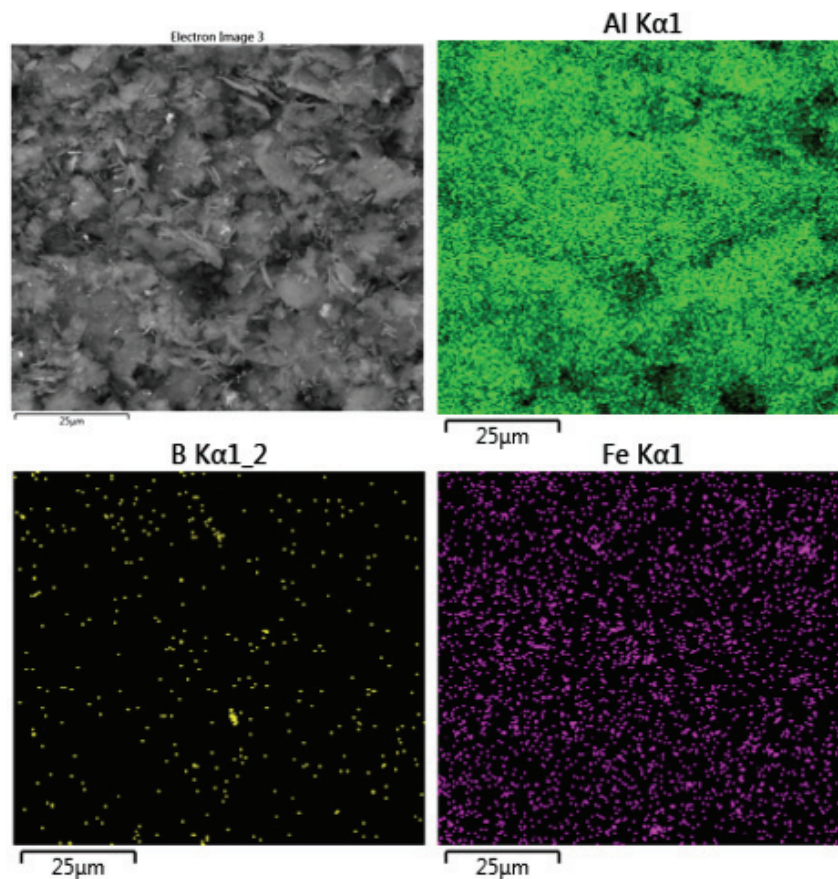


Figure 3.8. The elemental mapping of 5 wt. % B<sub>4</sub>C reinforced Al matrix composite powder milled in dry milling medium.

To solve the problems related to the contamination and agglomeration due to the cold welding, the agate vial (125ml) containing twenty agate (SiO<sub>2</sub>) balls were used instead of their metal counterparts during the experiments and wet medium was also used to avoid internal friction between the ball and powders. Ball milling was operated at 420 rpm and intermittent milling with intervals of 5 min by waiting 5 minutes for each interval was applied in order to keep the temperature low.

To solve the problems related to the contamination and agglomeration due to the cold welding, the agate vial (125ml) containing twenty agate (SiO<sub>2</sub>) balls were used



instead of their metal counterparts during the experiments and wet medium was also used to avoid internal friction between the ball and powders. Ball milling was operated at 420 rpm and intermittent milling with intervals of 5 min by waiting 5 minutes for each interval was applied in order to keep the temperature low.

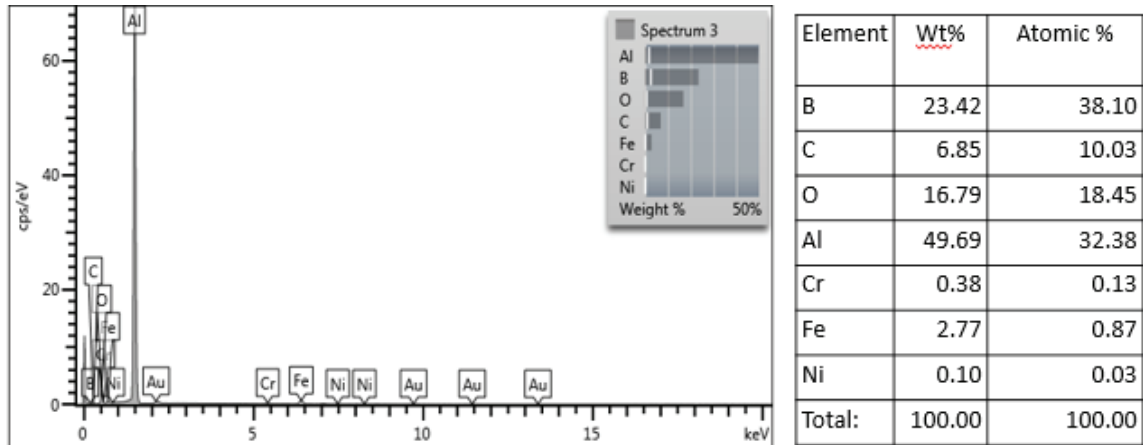


Figure 3.9. The presence of Fe, Cr and Ni elements in 5 wt. % B<sub>4</sub>C reinforced Al matrix composite powder due to the milling process by the EDS analysis.

To solve the problems related to the contamination and agglomeration due to the cold welding, the agate vial (125ml) containing twenty agate (SiO<sub>2</sub>) balls were used instead of their metal counterparts during the experiments and wet medium was also used to avoid internal friction between the ball and powders. Ball milling was operated at 420 rpm and intermittent milling with intervals of 5 min by waiting 5 minutes for each interval was applied in order to keep the temperature low.

The increasing in the temperature due to the kinetic energy of the rotating balls resulted in the evaporation of ethyl alcohol which increased the pressure inside the vial; therefore, the milling tools and composite powder could be damaged. In order to determine the optimum milling time, ball milling process for different milling time intervals was carried out from 0.5 to 9 hour. A very small quantity of sample powders was systematically taken from the vial per every 2 hours. These powder samples were characterized to evaluate the change of particle size and distribution using the scanning electron microscopy. The effect of milling time on particle size and distribution was discussed in detail in Chapter 4, optimum milling time was chosen as 7 hours. Table 3.3 clearly shows the final parameter chosen for milling process.

Table 3.3. The optimized ball milling parameters.

Composite Powder	Ball Material	Vial Material	Milling Medium	Ball to Powder Ratio	Time	Interval	Rpm
B <sub>4</sub> C + Al + PCA	Agate with diameter of 10 mm	Agate with volume of 125 ml	Wet	1:10	7 hours	5 minutes	420

### 3.2.3. Compaction Process

The milled powders were pressed to prepare the pellet samples whose weights were 6 gr for each one. The compaction was accomplished at 314 MPa using a hydraulic press which is Carver Hydraulic Unit Model. The hardened steel dies with an inner diameter of 30 mm were used for uniaxial press. The surface of dies was covered by a solid lubricant to avoid sticking between the dies and powders.



Figure 3.10. Carver hydraulic unit model uniaxial press.

After pressing process, the samples with a diameter of 30 mm and height of 4 mm were ready for sintering process as can be seen in Figure 3.11.



Figure 3.11. The pressed samples with a diameter of 30 mm.

### 3.2.4. Sintering Process

The samples were sintered in a tube sintering furnace (Protherm PTF16/50/450) under argon atmosphere with a gas flow rate of 0.2 dm<sup>3</sup>/lt.

Sintering experiments were carried out at different sintering temperature and time to obtain the optimum parameters and observe the structure and properties of the samples. The sintering temperature varied between 550 °C and 650 °C, and the sintering time ranged from 0.5 to 1.5 hours. The sintering parameters of the samples were shown in Table 3.4. The sintered samples for each variation were analysed to investigate the effect of sintering parameters on their microstructures.

Table 3.4. The sintering parameters of the samples for the analyses of microstructure and mechanical properties

The amount of wt.% Reinforcement	Temperature	Time	Increment
5 wt.% B <sub>4</sub> C	550°C	1 Hour	5°C per 1 minute
	575°C		
	600°C		
	625°C		
10 wt.% B <sub>4</sub> C	550°C	1 Hour	5°C per 1 minute
	575°C		
	600°C		
	625°C		
15 wt.% B <sub>4</sub> C	550°C	1 Hour	5°C per 1 minute
	575°C		
	600°C		
	625°C		



Figure 3.12. Tube sintering furnace used in the sintering process.

### 3.2.5. Metallographic Specimen Preparation

The sintered samples were prepared for metallography by cutting and molding with thermoset resin. The prepared samples were grinded by using 400 and 800 grid SiC sand paper by a grinding and polishing machine as seen in Figure 3.13. Then, the grinded samples were polished with diamond suspensions by using 6,3 and 1 microns. After polishing, an etching procedure is required to visualize the grains. The etching process is carried out by Keller's reagent ( $\text{HNO}_3$ ,  $\text{HCl}$ ,  $\text{HF}$ ) about 15 minutes.



Figure 3.13. Automatic grinding and polishing machine.

### 3.3. Characterization of the Materials

Several characterization methods and devices such as optical microscopy, x-ray diffractometer (XRD), scanning electron microscopy (SEM), dynamic light scattering (DLS) ball on disc dry sliding test, Vickers hardness test and Archimedes' method were employed for the composite samples to investigate their microstructures and mechanical properties.

#### 3.3.1. Optical Microscopy

Optical microscopy is widely used to examine metals, ceramics and polymers. Optical microscopes illuminate samples with visible or ultraviolet light. The principles of optical microscopes include image formation, magnification and resolution. They include the main components which are objective lens, ocular lens, lens tube, stage and reflector as shown in Figure 3.14.

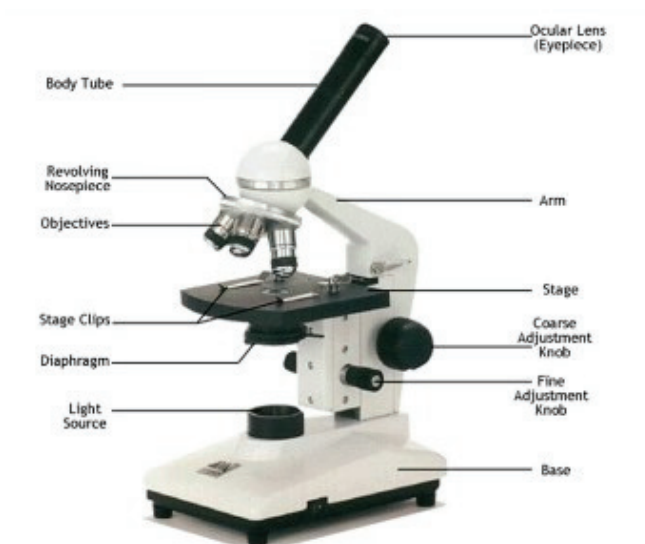


Figure 3.14. The components of the optical microscope.  
(Source: (78))

Two types of optical microscope which are based on the measurement of transmitted light from transparent materials and reflected light from opaque materials are

employed. Sample preparation methods such as polishing and grinding processes are applied to obtain better image information by decreasing the roughness of surface which cause the light scattering from surface.

### 3.3.2. X-Ray Diffraction

X-Ray diffraction (XRD) can define solid materials in atomic and molecular orders. This method is based on the distances between atoms in the crystals and the wavelength of the X-rays that are of the similar magnitude (1 Å or 100 pm).

Scattered rays by atoms are in phase if the path difference is equal to the whole number  $n$  of wavelength (Figure 3.15). Equation 3.1 is known as the Bragg's law where  $d$  is the interplanar distance,  $\lambda$  is the wavelength of the beam,  $n$  is an integer and  $\theta$  is the angle between incoming light and the surface.

$$n\lambda = 2d.\sin\theta \quad (3.1)$$

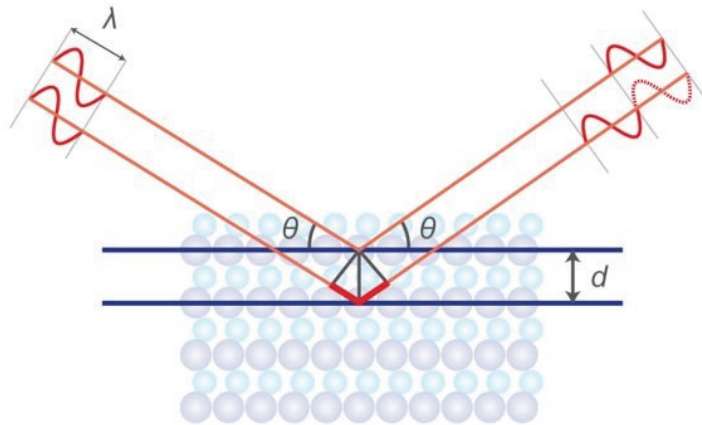


Figure 3.15. Schematic representation of Bragg diffraction.  
(Source: (79))

XRD was used to identify the compounds and impurities (if any) in the composite samples. XRD measurements were performed with a high-resolution X-ray diffractometer (Philips X'Pert Pro) supplied by the İzmir Institute of Technology (IZTECH) Material Research Center. X-ray diffraction patterns of the samples were collected with 0,1670 step size ( $^{\circ}2\theta$ ) between 10-90 degrees. The scan step time (s) value

is 152,4. The phase analyses of the X-ray diffraction patterns of samples were determined by using standard database, search and match process in High Score Plus commercial software program.

### **3.3.3. Scanning Electron Microscopy**

A scanning electron microscope (SEM) yields qualitative and quantitative information such as an image of a surface and concentrations of atoms. It is basically composed of an electron optical column, electronics and a vacuum system. The focused beam of the electrons with high energy is used to produce image of a sample. Imaging the surface topography and morphology, and determining chemical composition is based on the interaction between electrons and sample in a SEM. The beam produced in the vacuum moves to lenses through the electromagnetic fields and it is focused on the sample. Secondary electron (SE) which are emitted by the surface between 5-50 nm, back-scattered electrons (BSE) which some of primary electrons are reflected and X-ray which are emitted by sample emerge due to the interaction between electrons and sample. After a suitable detector collects the emitted electron and X-rays, it converts to signal. The secondary electrons are used for morphology and topography analysis. The backscattered electrons related to atomic number are used to see the contrast in multiphase samples. The X-rays emission due to electron relaxation from the higher energy levels to the lower energy levels is used for the composition information with the help of the Energy Dispersion Spectroscopy (EDS) detector. The SEM was used to determine the distribution of matrix and reinforcing powders, powder size, porosity of samples and presence of impurities. Both secondary electrons (SE) and backscattering electron (BSE) imaging were used for these purposes. Philips XL 30S FEG was utilized in this work for SEM analysis with EDS, and it was supplied by the IZTECH Material Research Centre.

### **3.3.4. Particle Size Analyzer**

Particle size analysis was performed by using dynamic light scattering (DLS) technique which is used to determine the average particle size with size distribution.

Particle size analysis can be used for solid material, suspensions and emulsions to investigate the particle size in addition to molecular mass, the transmittance and the refractive index particles in liquid dispersions. It works on the principle that when the light strikes to the particles, the light scatters in all directions, which is called as Rayleigh scattering, as a function of the particle size, and the size of the particles is inversely proportional to the angle of scattered light. If the scattered light undergoes destructive phases, the signal cancels out and there would be no detectable signal. The signal is read out for only the constructive phases and it carries the information related the fluctuation intensity of the scattered light as a function of the time. The intensity of scattered light by particles fluctuates over a time.

The particle size distribution of the B<sub>4</sub>C powders was determined by DLS measurements. To measure the particle size of the ceramic powder, the 1 mg of the powders was dissolved in 1.5 ml ethanol and ultrasonically disaggregated for 1 minutes. Al powders were not included in the average particle size distribution due to their agglomeration tendency in the solvent. Instead, their SEM images were compared with the average particle size data provided by the Al powder manufacturer. The measurement is performed by using the dynamic light scattering instrument (DLS; Zetasizer Nano ZS, Malvern Instruments, Worcestershire, UK) provided by IZTECH Material Science and Engineering department.

### **3.3.5. Ball-on-disc Dry Sliding Test**

The tribological tests were performed using ball-on-disc wear test under dry sliding conditions in the air with the applied load of 10 N, sliding velocity of 184 mm/s and a constant sliding distance of 800 m.

A schematic diagram of the ball-on-disc wear test is represented in Figure 3.16. All the specimens followed a single-track 20mm in diameter. Prior to the tests, the samples were subjected to metallographic specimen preparation. The mass loss of the samples was calculated before and after each wear test. Three separate tests were run for each specimen, and the average wear rates and coefficients of friction were recorded. The surface morphology and elemental distribution of the samples and the wear tracks were examined using SEM analysis with EDS.



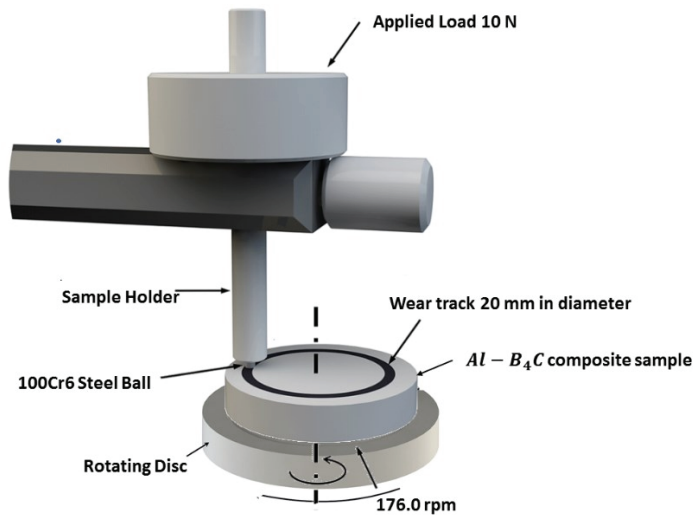


Figure 3.16. A schematic diagram of the ball-on-disc wear test.

(Source: (80))

### 3.3.6. Vickers Hardness Test

The hardness tests of 5, 10 and 15 wt.% of  $B_4C$  reinforced Al-MMC samples were carried out using Vickers Test which is Shimadzu DUH-W201S model. were applied to arrange an appropriate indentation area, and the load of 19kN was preferred in order to avoid disproportional contribution of reinforcing particles and micro-porosity inside the indentation area. The influence of indentation area in microscale on the hardness value is crucial for composite samples which highly have the possibility of the presence of porosity to get more precise information about mechanical properties of composite.

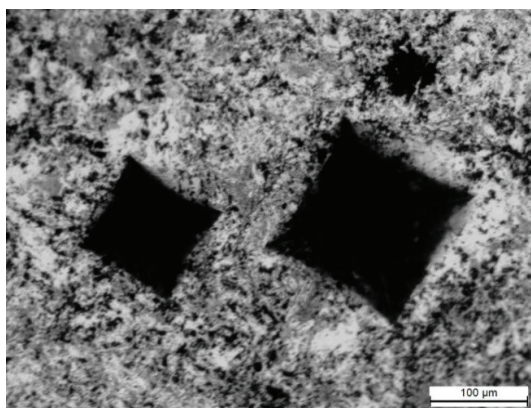


Figure 3.17. The indentation areas after applying 9 kN and 19 kN loads.

## CHAPTER 4

### RESULTS AND DISCUSSION

In this chapter, the results obtained during the study are presented as being divided into two groups. The former, based on experimental results for the fabrication of B<sub>4</sub>C reinforced Al-MMCs, the optimum process conditions, the effect of changing fabrication parameters on the microstructure using SEM with EDS and X-ray diffraction measurements are discussed. The later, based on the results of Vickers hardness test and ball-on-disc dry sliding wear test, is to investigate the effect of the content of B<sub>4</sub>C reinforcing particles on matrix along with the effect of sintering temperature on the mechanical and tribological behaviours of composites such as hardness, wear loss and coefficient of friction values of composite samples.

#### 4.1. Ball Milling Process

The efficiency of the ball milling process depends on the characteristics of powders and the system process conditions. The optimum parameters for the ball milling process are standardized by providing a balance between deformation, cold welding and fracturing mechanisms of powders. Al and B<sub>4</sub>C as received powders were imaged to observe the change of the morphology throughout the fabrication of composite powders using the ball milling process (Figure 4.1).

Ductile Al powders have a high tendency to weld with each other. During the ball milling process, the powders were extremely cold-welded as can be seen in Figure 4.2. The Al powders had almost spherical forms in the initial stage, but after milling for one hours the particle form started to considerably change into cold-welded powders with a rough surface, which resulted in the enlargement in the size of welded Al powders. The Figure 4.3 shows that average size of the particles increased even exceeded the initial size of Al powders, which may mean the failure of the particle size reduction by ball milling. It also caused the non-homogeneous distribution of B<sub>4</sub>C particles into the Al matrix.

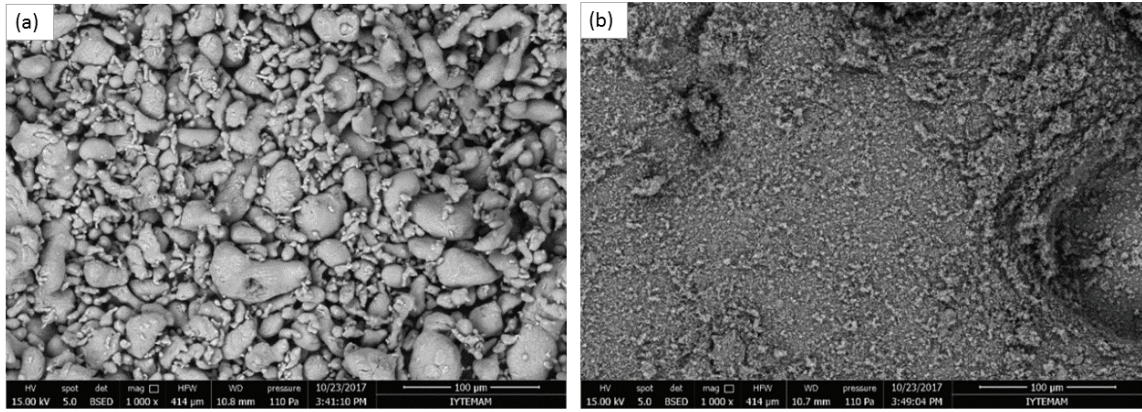


Figure 4.1. The backscattered SEM image of a) as-received pure Al powders b) B<sub>4</sub>C powders at 1000x magnification.

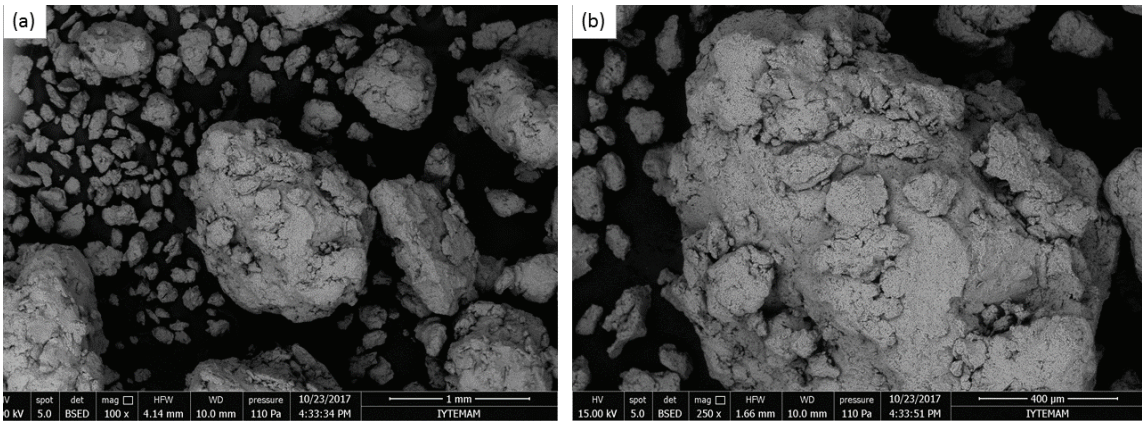


Figure 4.2. The backscattered SEM images of cold welding of 5 wt.% of B<sub>4</sub>C reinforced Al matrix composite powders after the mechanical alloying process for one hour at 420 rpm with a) 100x b) 250x magnifications.

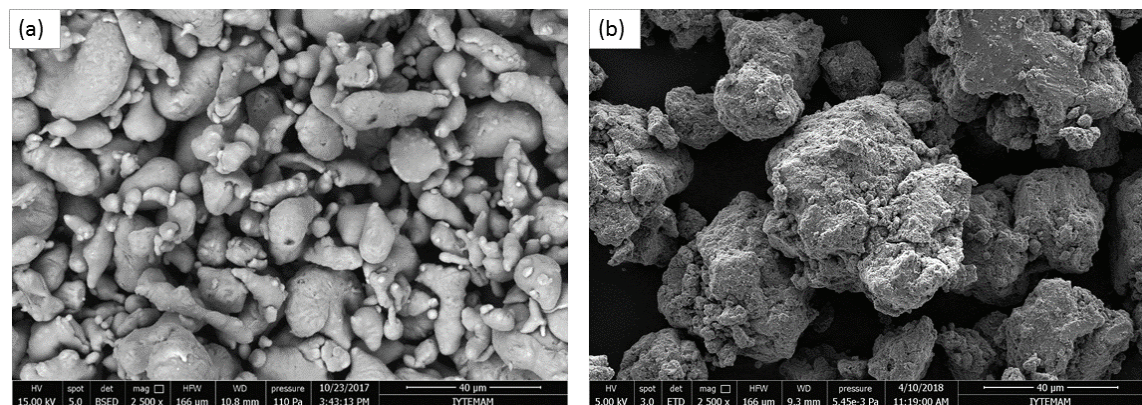


Figure 4.3. The backscattered SEM images of a) as-received Al powder b) milled 5 wt.% of B<sub>4</sub>C reinforced Al matrix composite powders for 3 hours in dry milling medium without the PCA at 2500x magnification.



Different milling medium with a process control agent was tried in order to overcome such problems such as the enlargement of the particle size the contamination of powder, which resulted from the cold welding. The results showed that the ball milling process in a wet medium with ethanol gave better results as compared to dry milling medium. Figure 4.4 indicates that the morphology of composite powders milled at dry medium turned into welded particles with a rough surface and they had irregular size distribution, on account of an increase in powder aggregate size, whereas powder milled at wet medium become flaky shape, which was resulted from the plastic deformation and fracture mechanism employed by minimizing excessive cold welding of ductile Al powders

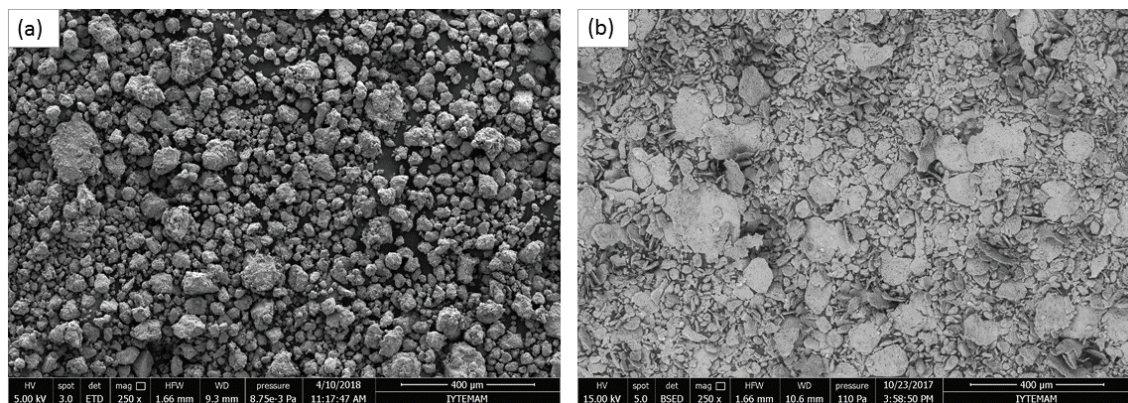


Figure 4.4. The backscattered SEM images of milled 10 wt.% of B<sub>4</sub>C reinforced Al matrix composite powder for 5 hours a) without the PCA in dry medium b) without the PCA in wet medium at 250x magnification.

The PCA was added into the powder mixture throughout the milling process to observe the effect of PCA on the microstructure of composite powders and the efficiency of ball milling process. The results based on the SEM analysis indicated that the presence of stearic acid as the PCA along with ethanol accelerated the ball milling process and made the milling faster, which provides a decrease in the time needed to reach steady state. The PCA which was absorbed by the surface of Al powders prevented the increase in the size and volume of agglomerated powders and avoided the excessive cold-welding. Therefore, the average size of powders milled with the PCA in a wet medium remarkably reduced, and these composite powders had smaller particle sizes compared to that of the powders milled in wet medium without the PCA (Figure 4.5). Also, the addition of the PCA minimized the degree of contamination and weight loss of milled powders.

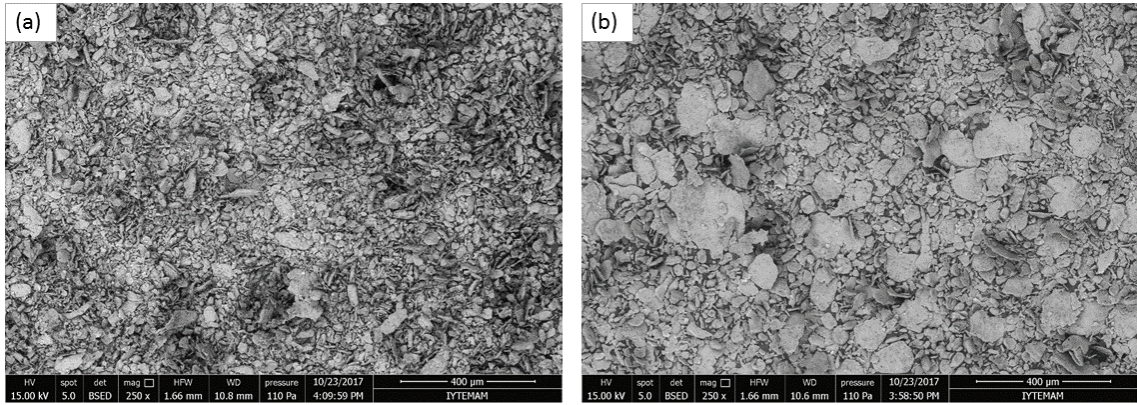


Figure 4.5. The backscattered SEM images of milled 10 wt.% of B<sub>4</sub>C reinforced Al matrix composite powder for 5 hours a) in wet medium with the 0.05 wt.% of PCA b) in wet medium without the 0.05 wt.% of PCA at 250x magnification.

The SEM images as shown in Figure 4.6 represents the microstructure of 10 wt.% of B<sub>4</sub>C reinforced Al matrix composite powders milled in the wet medium with the PCA. It shows that the fracture started with the edge of flake powders following by work hardening and plastic deformation mechanism; therefore, B<sub>4</sub>C reinforcing particles were well embedded into the Al matrix via ball milling process. Even the use of PCA avoided the cold welding and provided facilitation of the mechanical alloying mechanism; however, the average particle size of composite powder milled with the PCA still was bigger than as-received composite powder.

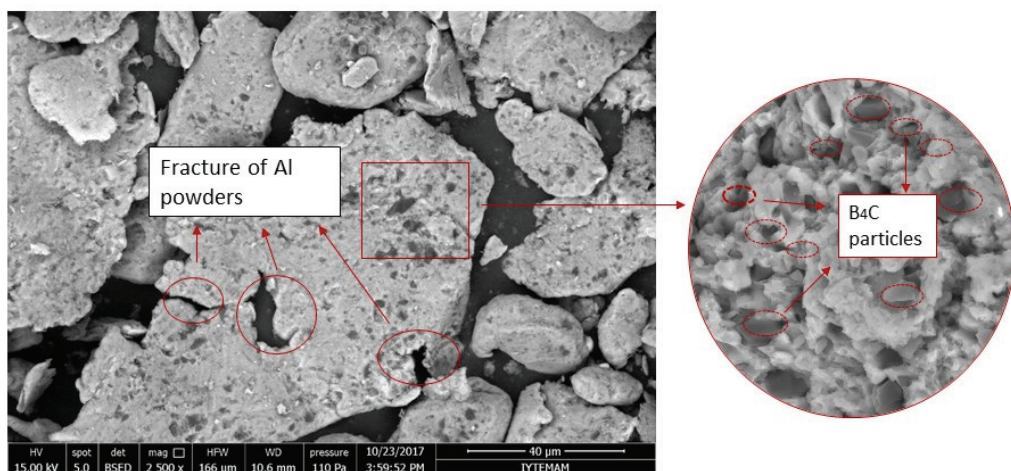


Figure 4.6. The Backscattered SEM image of 10 wt.% B<sub>4</sub>C reinforced Al matrix composite powders fabricated by ball milling process for 5 hours in wet milling medium with the 0.05 wt.% of PCA at 2500x magnification.



The other ball milling parameter investigated for the optimum process parameters is milling speed. It was seen that the lower milling speed reduce the kinetic energy of the milling balls into the jar, which is correlated with ball impact speed. As a result of the lower milling speed, the longer milling time is required to undergo the particle size reduction. The milling process at the higher milling speed provided the composite powders with a smaller particle size than that of milling at the lower milling speed as seen clearly in Figure 4.7.

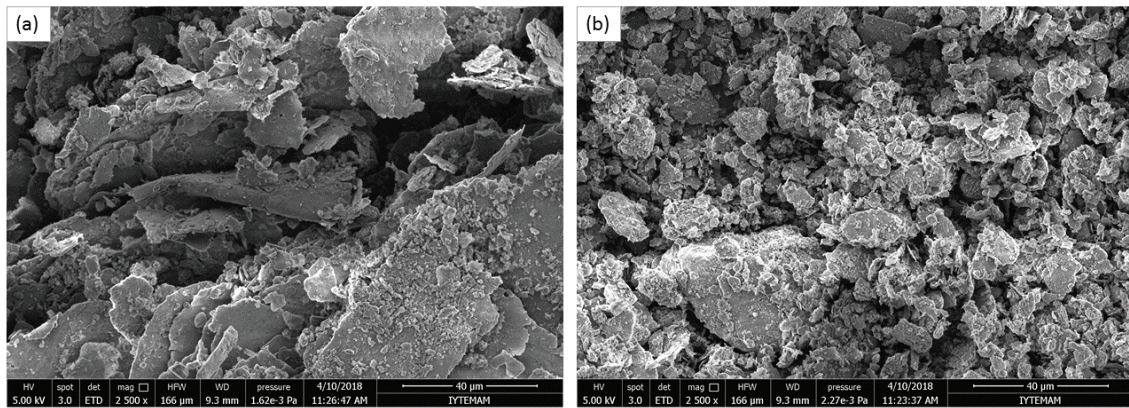


Figure 4.7. SEM images of 10 wt.% of  $B_4C$  reinforced Al composite powders milled with 0.05 wt.% of PCA in wet medium for 7 hours at a) 350 rpm b) 450 rpm at 2500x magnification.

Milling time is also one of the most important parameters for the efficiency of the ball milling process. The size and distribution of powders depend on the milling time. For this reason, different milling times were tried to examine the effect of the milling time on the particle size of composite powders and to determine the optimum milling time for the rest of experiments.

At the first stage of milling process, the ductile Al particles milled up for a certain time were deformed with the collision effect of balls and turned into flakes form on account of the activities of the plastic deformation and the cold-welding mechanisms, which led to enlargement in the particle size due to the formation of a large amount of flake forms. After 3 hours milling, and larger it was observed that larger flake particles were broken into smaller pieces by the activation of the fracture mechanism, and average particle size started to reduce. Up to 5 hours milling, the morphology of particle still remained unchanged as a flake form as seen from Figure 4.8, but the average particle size dramatically started to decrease with the increase of the milling time.

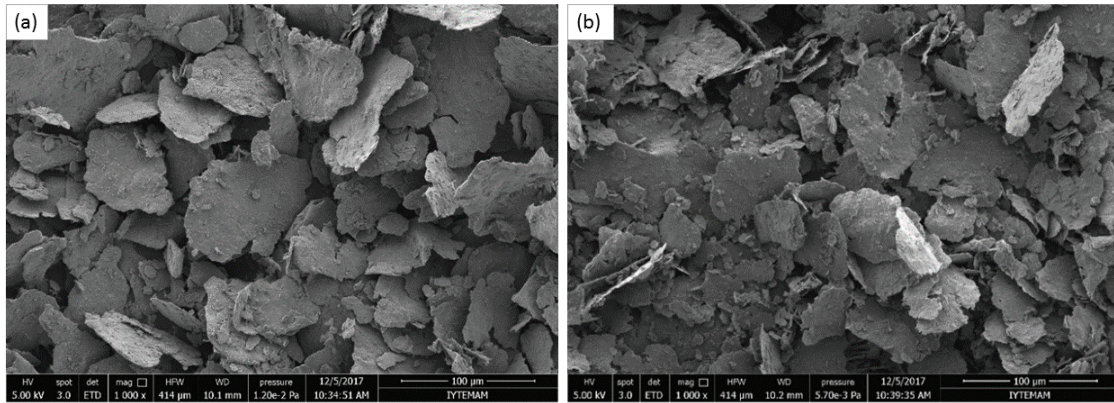


Figure 4.8. SEM images of 10 wt.% of B<sub>4</sub>C reinforced Al composite powders milled with 0.05 wt.% of PCA in wet medium for different milling time a) 3 b) 5 hours at 1000x magnification.

The average size of powders milled between 7 and 9 hours slightly decreased, and the particles had irregular and smaller flake shape. Figure 4.9. reveals that after milling for 9 hours, composite powders had a stable shape and narrow size distribution as seen in

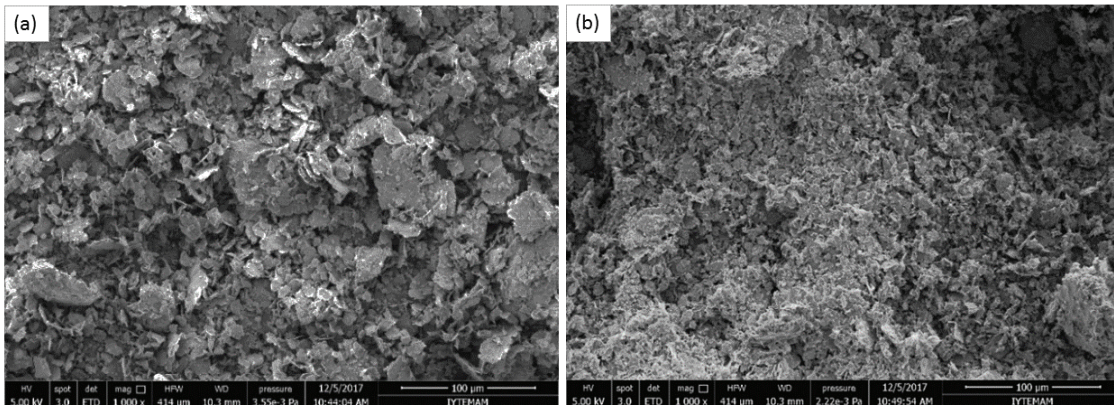


Figure 4.9. SEM images of 5 wt.% of B<sub>4</sub>C reinforced Al composite powders milled with 0.05 wt.% of PCA in wet medium for different milling time a) 7 b) 9 hours at 1000x magnification.

The graph shown in Figure 4.10 was obtained from the experimental results of 5 wt.% B<sub>4</sub>C reinforced Al matrix composite powders shows that the milling time considerably affected the particle size. The particle size reached at a constant value for 9 hours milling and remained stable for even longer milling time (11 hours). However, since there is no significant difference between 7 and 9 hours milling in terms of resulting average particle sizes, the suitable milling time was chosen as 7 hours, which will also

lead to saving time and energy. Also, in literature it was observed that the nanoparticle size led to the agglomeration of powders and the non-uniform distribution of reinforcing particles into matrix.<sup>2</sup>

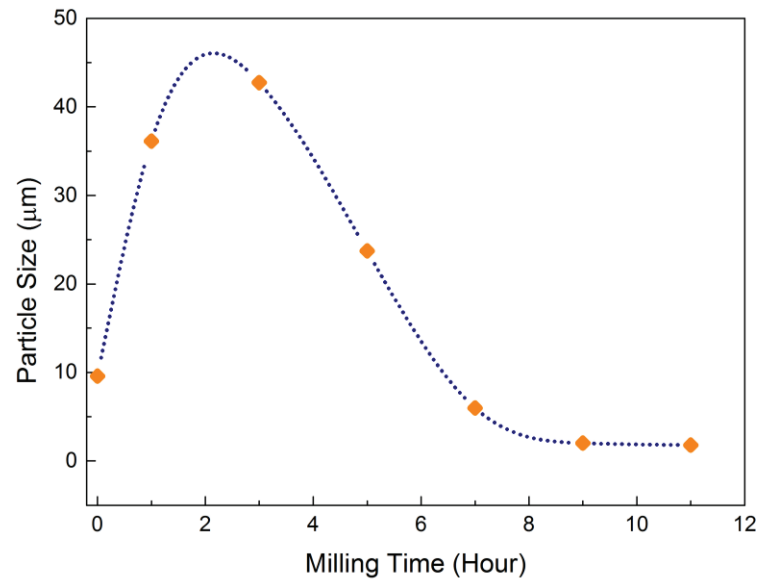


Figure 4.10. The variation of the average particle size as a function of the milling time.

As a result, the optimum parameters were obtained for the ball milling process as wet medium with stearic acid at 420 rpm for 7 hours. The composite powders with different contents, i.e. 5, 10 and 15 wt.% of B<sub>4</sub>C, which were milled using the optimum parameters were analysed by the EDS technique. It can be seen from Figure 4.11 to Figure 4.13 that the composite powders have relatively uniform distributions of reinforcing particles into the Al powders.

The experimental results of ball milling process indicated that particle size reduction and a homogeneous distribution of B<sub>4</sub>C reinforcing particles into the Al matrix were achieved, which proved that ball milling process was successfully performed to fabricate B<sub>4</sub>C reinforced Al matrix composites.



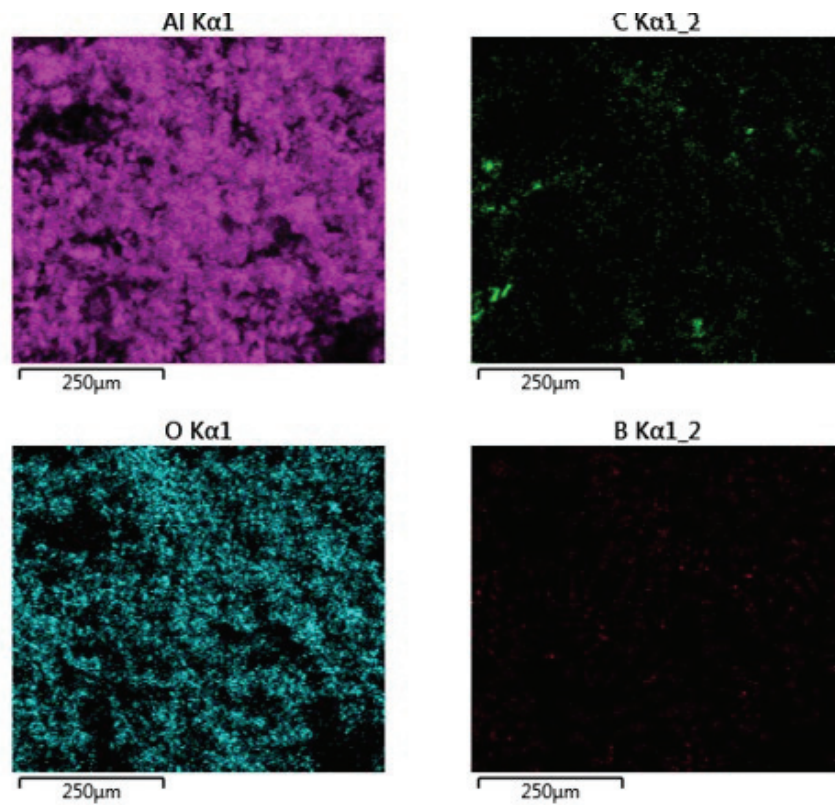


Figure 4.11. The dispersion of elements found in Al matrix composite powder reinforced 5 wt. % of B<sub>4</sub>C by EDS analysis.

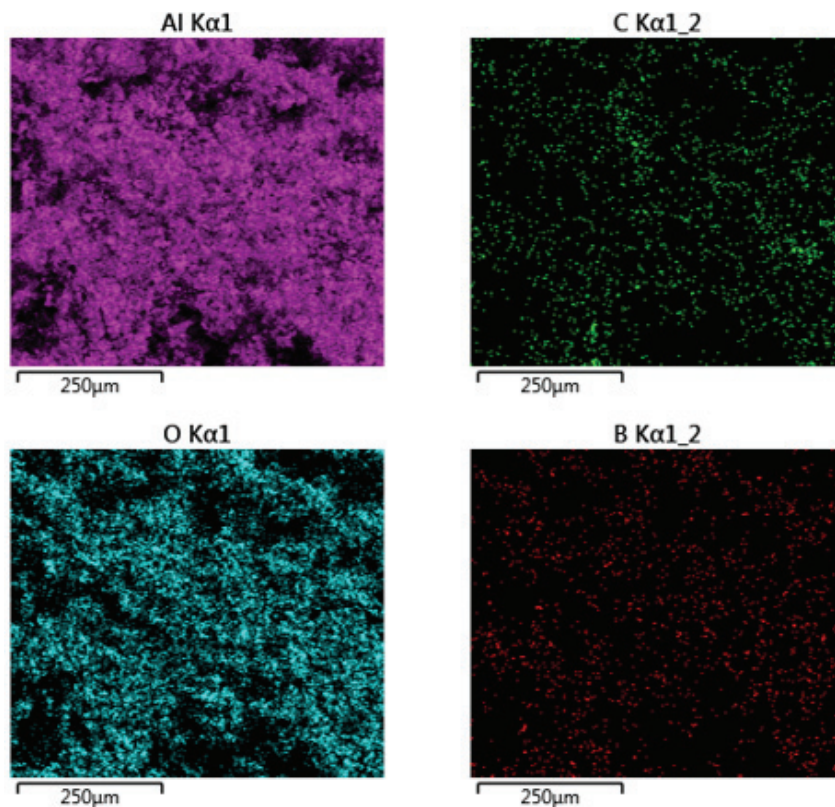


Figure 4.12 The dispersion of elements found in Al matrix composite powder reinforced 10 wt. % of B<sub>4</sub>C by EDS analysis.

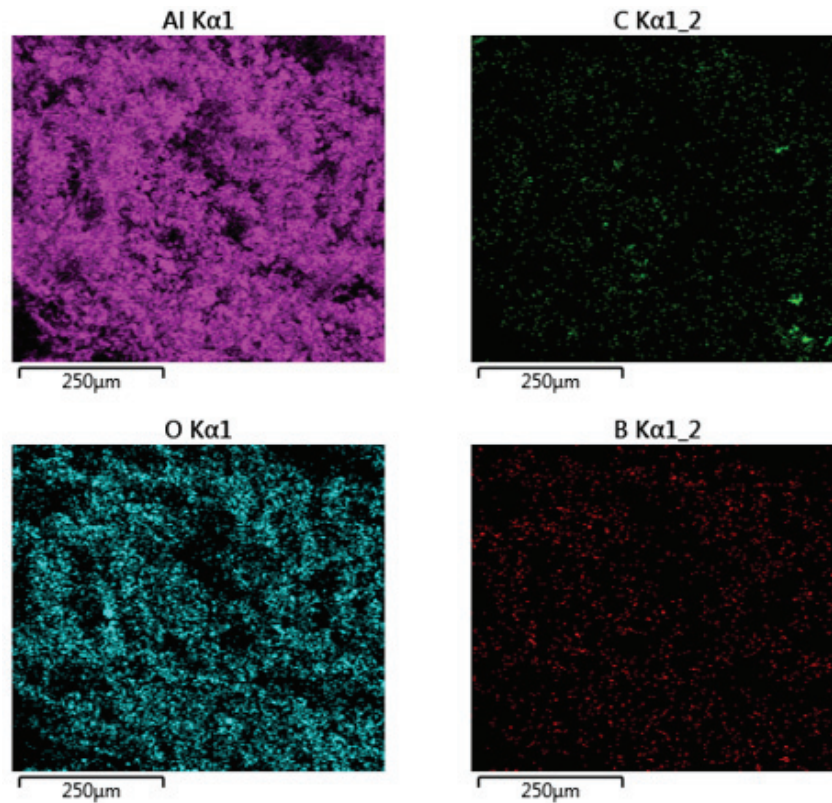


Figure 4.13. The dispersion of elements found in Al matrix composite powder reinforced 15 wt. % of B<sub>4</sub>C by EDS analysis.

## 4.2. Sintering Process

The samples sintered under different temperatures (550, 575, 600 and 625°C) were examined to investigate the effect of sintering temperature on the microstructure and mechanical behaviours of composite samples. It can be seen from Figure 4.14 and Figure 4.15 that the microstructure of samples changed with direct proportion to the sintering temperature, and these changes (increase in darker regions) are more recognizable at higher sintering temperature, which were resulted from the higher reactivity between Al and B<sub>4</sub>C with increase in processing temperature. In the literature, it was reported that various phase compositions including Al, C and B elements might occur with rising temperature.<sup>6,13,30,81</sup> The darker and greyish regions which may indicate different phases on the microstructure of sintered samples can be clearly noticed in Figure 4.14 and Figure 4.15. Figure 4.16 represents the backscattered image of 10 wt.% of B<sub>4</sub>C reinforced Al matrix composite sample sintered at 550 °C and the existence of elements in composite sample with their distributions by EDS technique.



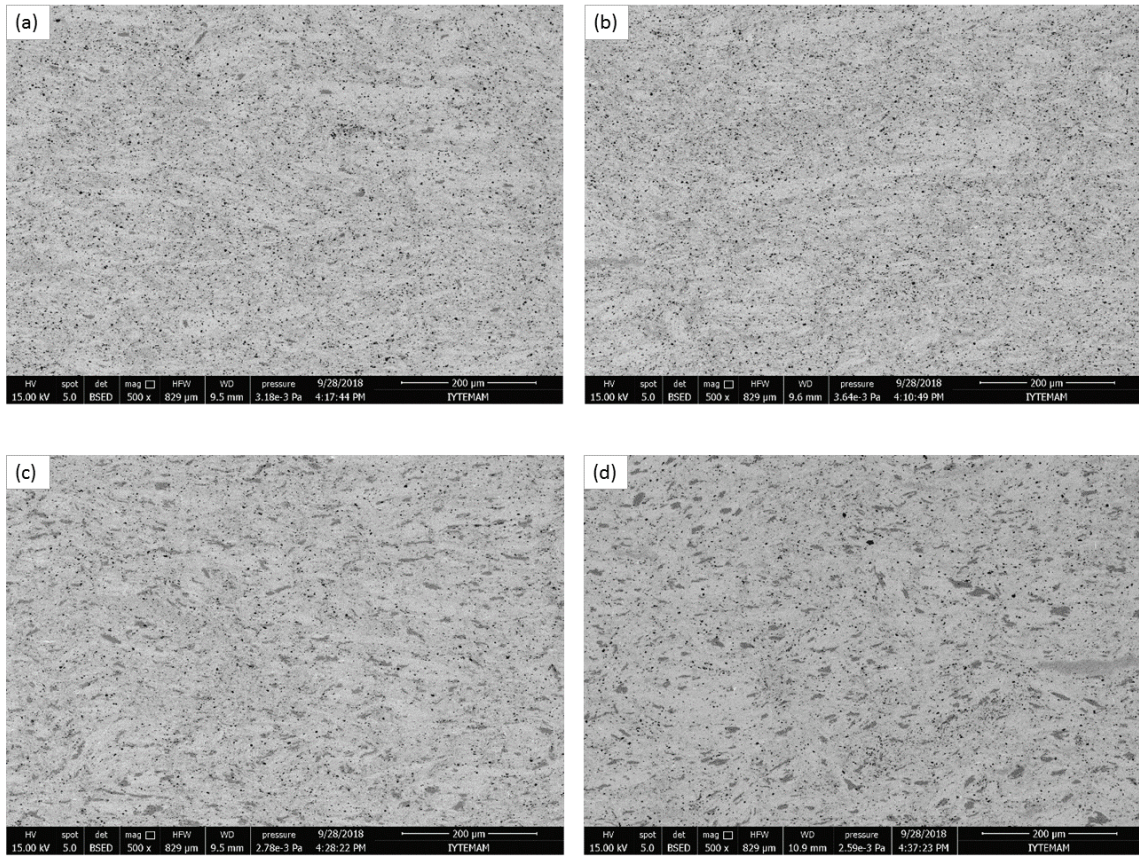


Figure 4.14. SEM images of 10 wt.% of  $B_4C$  reinforced Al matrix composite sample sintered at a) 550 °C, b) 575 °C, c) 600 °C and d) 625 °C at 500x magnification.

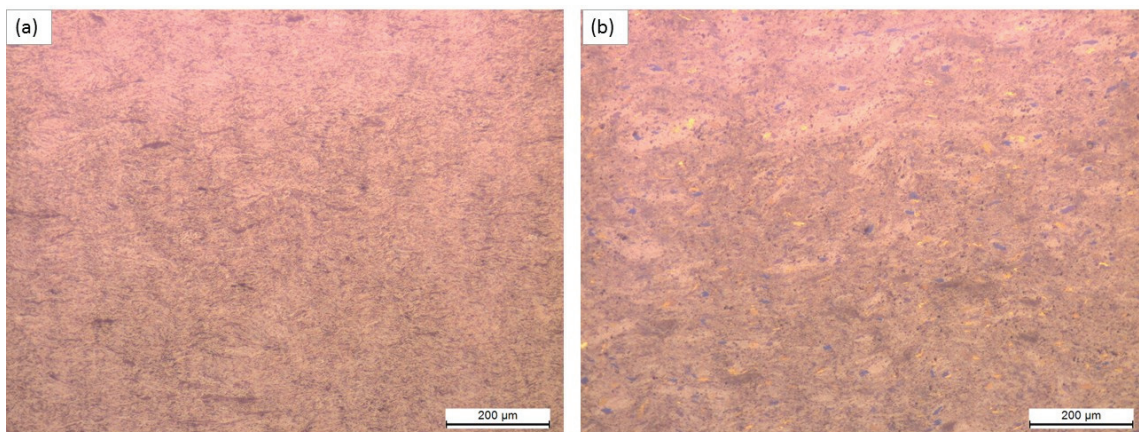


Figure 4.15. Optical microscope images of 10 wt.% of  $B_4C$  reinforced Al matrix composite sample sintered at a) 550 °C and b) 625 °C

The presence of  $B_4C$  reinforcing particles was observed from Figure 4.16 corresponding the dark region. The EDS mapping analysis was used as can be seen in



Figure 4.17, but EDS mapping analysis does not have enough sensitivity to detect the boron (B) and carbon (C) elements due to their low atomic numbers.

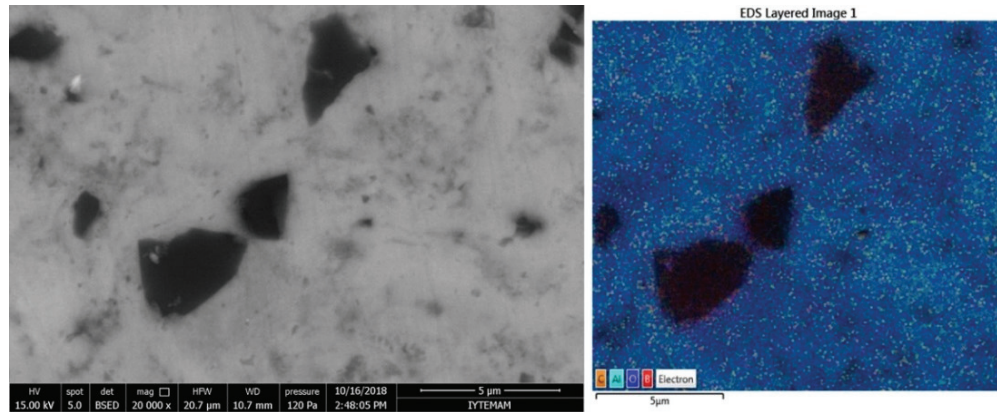


Figure 4.16. Backscattered SEM image of 10 wt.% of  $B_4C$  reinforced Al matrix composite sintered at 550 °C.

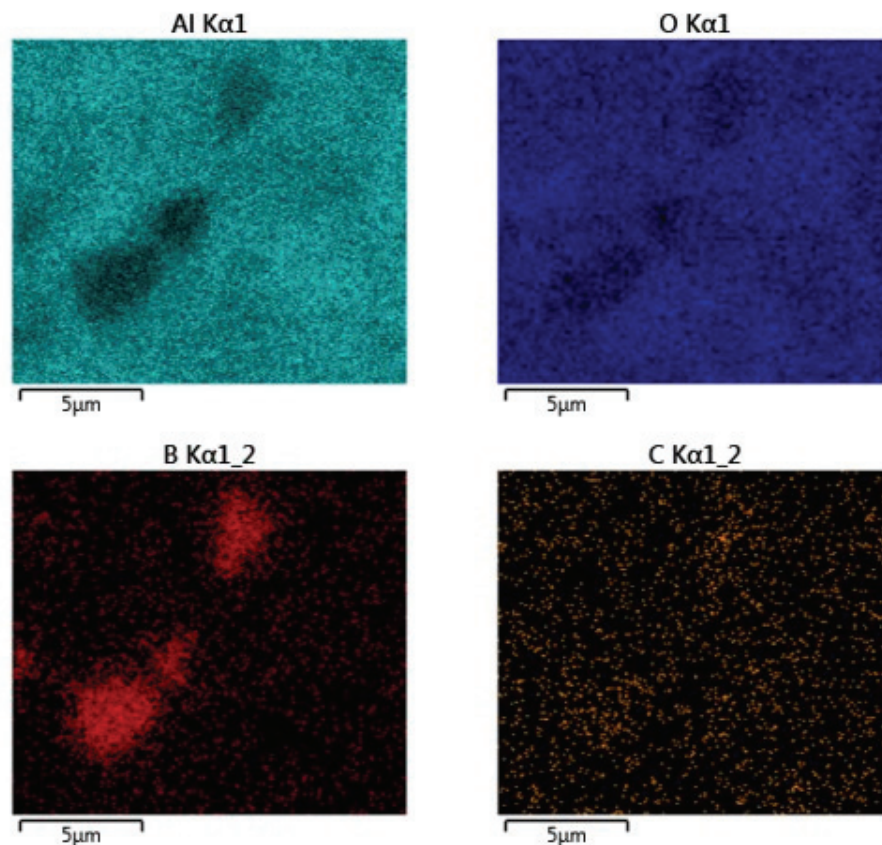


Figure 4.17. EDS element mapping of 10 wt.% of  $B_4C$  particle reinforced Al matrix composite sample sintered at 550°C.

The EDS line analysis was used along with the EDS element mapping in order to obtain more details as can be seen in Figure 4.18, which supports the presence of B<sub>4</sub>C particles.

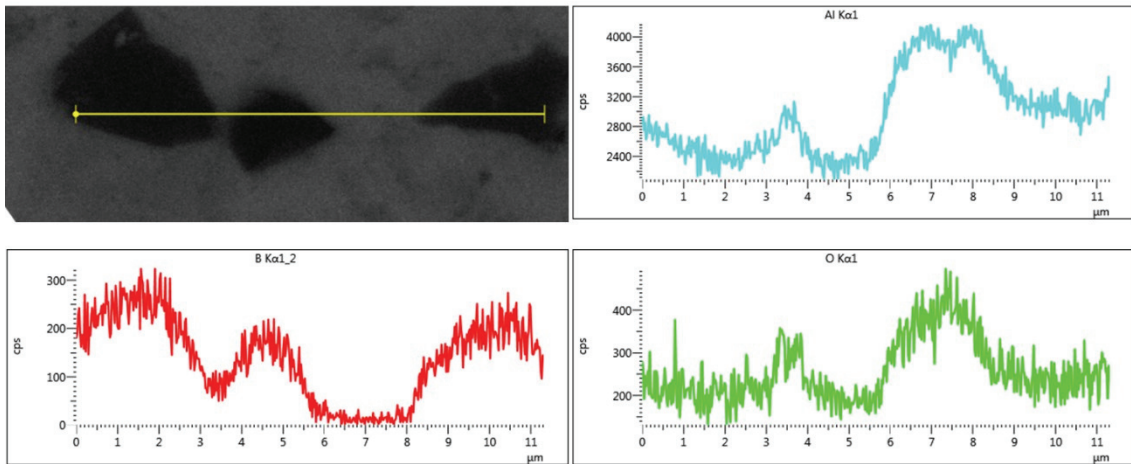


Figure 4.18. EDS line analysis of 10 wt.% of B<sub>4</sub>C particle reinforced Al matrix composite sample sintered at 550 °C.

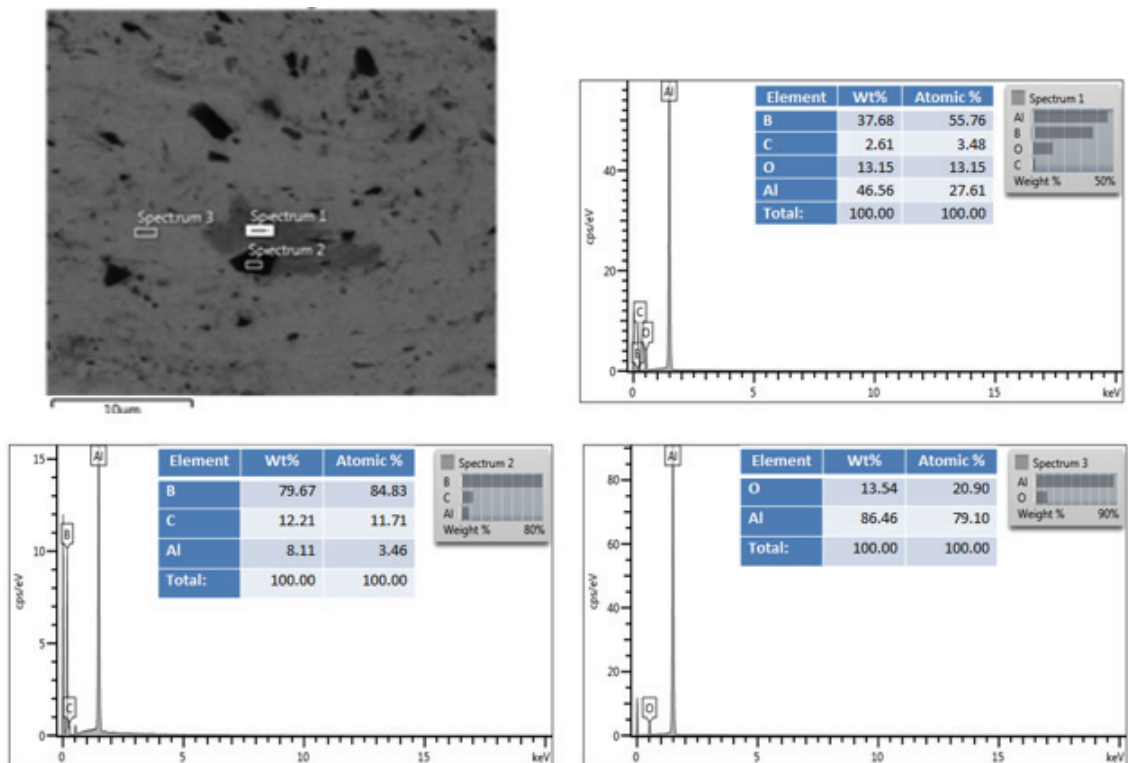


Figure 4.19. EDS analysis of 10 wt.% of B<sub>4</sub>C reinforced Al matrix composite sample sintered at 625°C.

The EDS spectrum analysis was used along with the EDS mapping and line analyses in order to obtain more details as can be seen in Figure 4.17. The results based on the EDS analysis of sintered samples indicated that these phases correspond to the presence of  $B_4C$ , Al and other possible second phases, which are represented in Figure 4.19. The spectrum 2 shows the dark region that potentially contains  $B_4C$  particles. The light gray regions may only contain Al matrix while darker gray regions can be composed of Al and  $B_4C$  phases which could be corresponding to the interfacial reaction products due to the chemical reaction between matrix and reinforcement.

The X-ray diffraction patterns of the as-received powders and sintered composite samples were also obtained to identify the presence of  $B_4C$ , Al and other phases. Figure 4.20 represents the X-ray diffraction patterns of as received Al matrix and  $B_4C$  reinforcing particles. The new interfacial reaction products for the composite sintered at 625 °C were also supported by the X-ray diffraction patterns as seen clearly in Figure 4.21. 5, 10 and 15 wt. % of  $B_4C$  reinforced Al matrix composites after sintering process at 550°C, 575°C, 600°C and 625°C and room temperature before sintering process were investigated, and the effect of sintering temperature and the content of  $B_4C$  particles on the microstructure of composites is depicted in the X-ray diffraction patterns in Figure 4.22 and Figure 4.23. It can be explicitly seen that the changes in the intensity and position of diffraction patterns depend on sintering temperature and the content of  $B_4C$  particles.

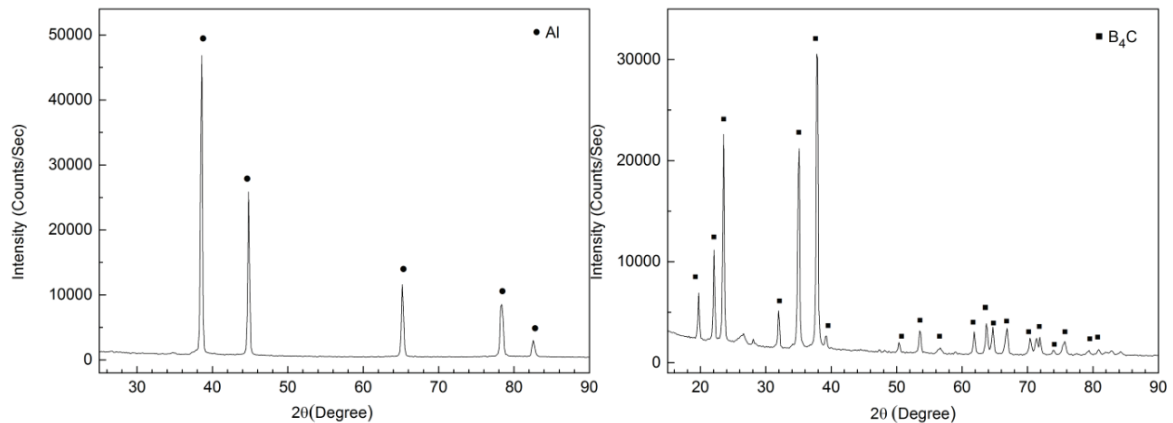


Figure 4.20. X-ray diffraction patterns of as- received Al and  $B_4C$  powders.

The X-ray diffraction patterns of composite before sintering (RT) show only the presence of the Al particles, and the diffraction peak corresponding to  $B_4C$  particles is not

detectable since the detection of  $B_4C$  is difficult due to the low content of  $B_4C$  in the Al matrix.

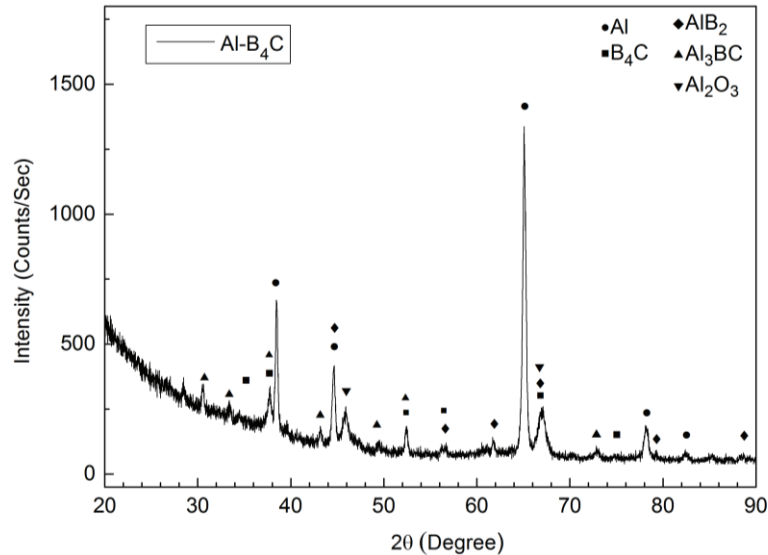


Figure 4.21. X-ray diffraction pattern of  $B_4C$  particle reinforced Al -MMC sample sintered at 625 °C.

Additionally, there is no evidence of any possible second phases, in which the chemical reaction did not occur between Al and  $B_4C$  particles during fabrication of composite powder using ball milling process. The content of  $B_4C$  particles does not have important effect on the formation of second phases at lower temperature. However, it is prominent parameter for the variety of chemical compounds and their amounts at higher processing temperature because the reactivity between Al and  $B_4C$  particles increases when subjected to high temperature.

The XRD results of sintered composites show the presence of both Al and secondary phases. It was observed the sintering temperature does not affect on the formation of chemical compound with containing low content of  $B_4C$  particles, but the decrement of the intensity of large peaks corresponding Al with an increase in sintering temperature show that elevated sintering temperature slightly leads to occur the chemical compound. The X-ray diffraction patterns of 5 wt.% of  $B_4C$  reinforced composites sintered at 550°C, 575 °C, 600°C and 625°C do not clearly show an evidence for the formation of chemical compounds. However,  $B_4C$  reinforced composites with higher contents, i.e. 10 and 15 wt.% show the presence of secondary phases. Figure 4.22 illustrates that the minor peaks represent potential secondary phases such as  $AlB_2$ ,  $Al_3BC$

and  $\text{Al}_2\text{O}_3$  detected and the largest peaks represent Al matrix, but the intensity of diffraction peaks corresponding to  $\text{B}_4\text{C}$  particles can be slightly detected at only higher content, i.e. 10 and 15 wt.% and elevated temperature at 575 °C and 625 °C by X-ray diffraction technique. Also, Figure 4.23 revealed that the intensity of some X-ray diffraction peaks corresponding second phases decreased. This can be attributed to the decreased content of  $\text{B}_4\text{C}$  particle by increasing sintering temperature.

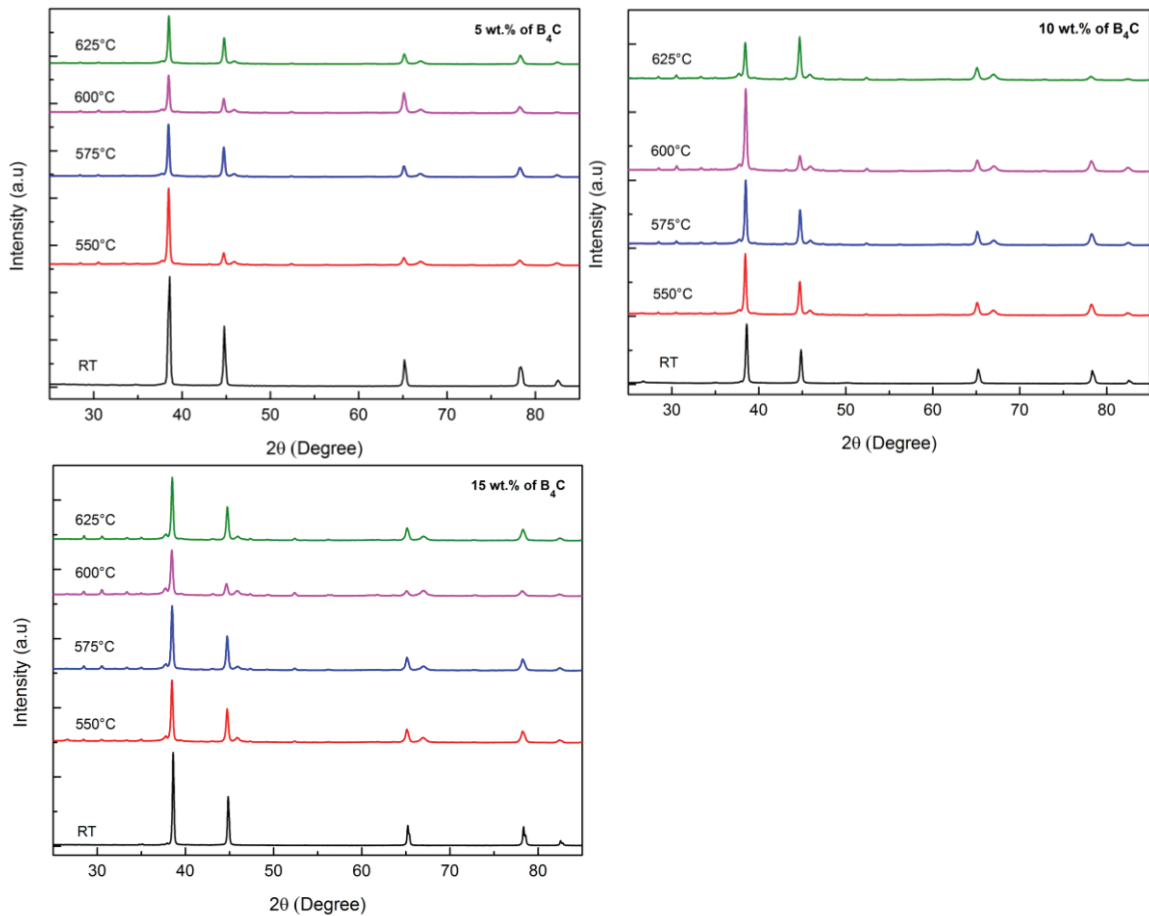


Figure 4.22. The graphs of X-ray diffraction patterns of Al matrix composites with 5, 10 and 15 wt.%  $\text{B}_4\text{C}$  contents sintered at RT, 550, 575, 600 and 625 °C.

The decrease in the intensity of the Al peaks with the increasing temperature is likely to be due to the chemical reaction between  $\text{B}_4\text{C}$  and Al particles at higher temperatures, and as introduced earlier the new phases were formed during the sintering process consuming Al. The number of peaks corresponding to the interfacial reaction products increased with an increase in the content of  $\text{B}_4\text{C}$  and the sintering temperature. It was concluded that the content of  $\text{B}_4\text{C}$  does not have significant effect at lower



temperature; however, it is an important parameter at higher temperature for the formation of interfacial reaction product.

At lower sintering temperature (550°C and 575°C), it can be clearly seen that no chemical compounds or secondary phases such as  $\text{AlB}_2$ ,  $\text{Al}_3\text{BC}$  and  $\text{Al}_2\text{O}_3$  were detected at the interface of Al and  $\text{B}_4\text{C}$  using XRD measurement as seen in Figure 4.23. At higher temperature, the interfacial reaction products were detected, and the presence of these product changed in relation to the temperature and the content of reinforcing material. The increase in the intensity of other peaks and the decrease in the intensity of Al peaks indicate the reactivity by increasing temperature. The new phases formed such as  $\text{AlB}_2$ ,  $\text{Al}_3\text{BC}$  and  $\text{Al}_2\text{O}_3$  are expected to play a role on the modification of mechanical and tribological properties of composites.

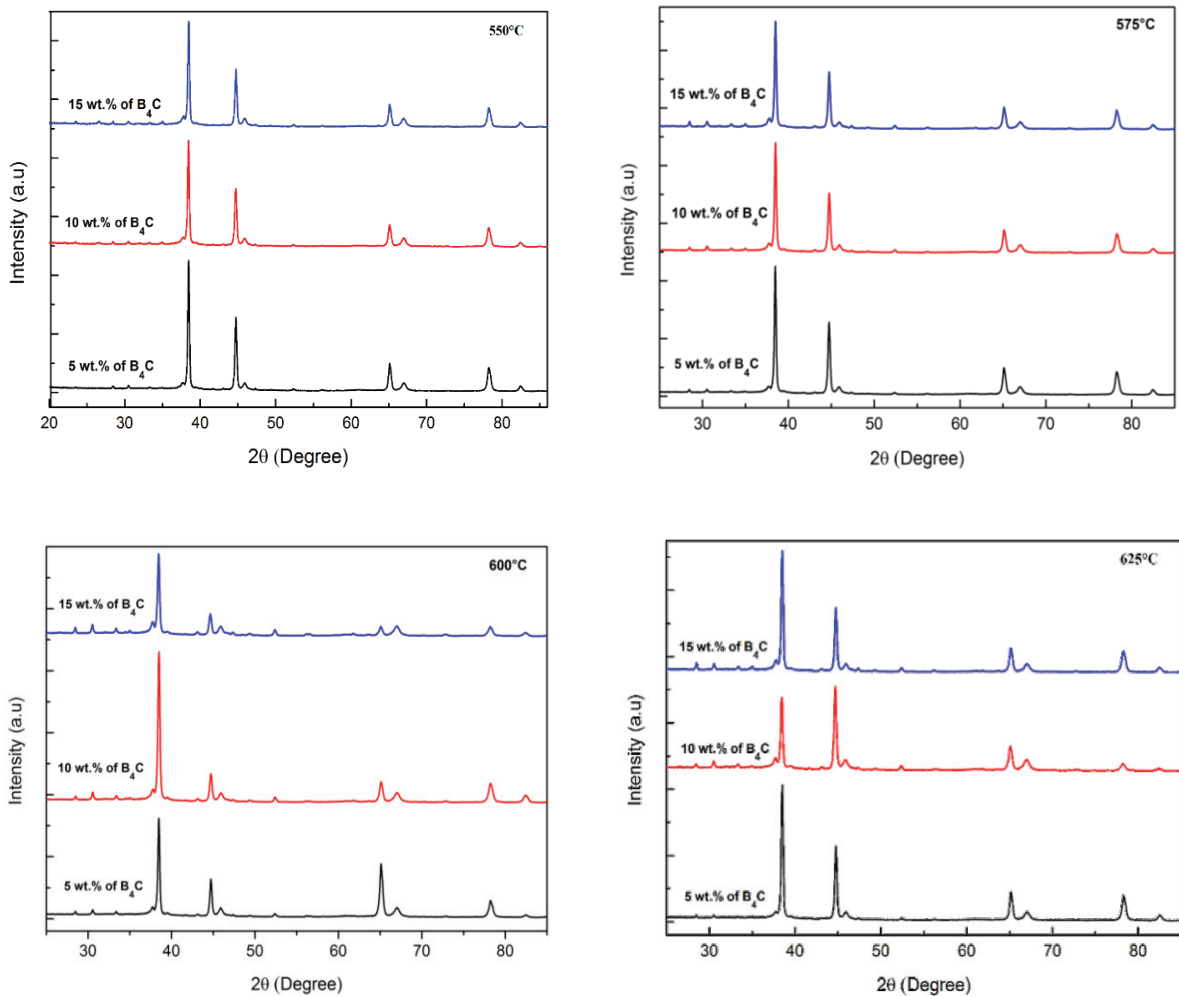


Figure 4.23. The graphs of X-ray diffraction patterns of Al matrix composites with 5, 10 and 15 wt.%  $\text{B}_4\text{C}$  contents sintered at 550, 575, 600 and 625°C

### 4.3. The Mechanical and Tribological Behaviours of AMCs

The change in the B<sub>4</sub>C content caused a moderate change in the density. Figure 4.24 shows the changes in densities of 5, 10 and 15 wt. % B<sub>4</sub>C reinforced Al matrix composites as a function of sintering temperature. The density decreased with an increase in the content of B<sub>4</sub>C. This is due to the lower density of B<sub>4</sub>C with 2.52 g/cm<sup>3</sup> compared to 2.7 g/cm<sup>3</sup> density for pure Al. The density also increased at higher sintering temperature, and this is likely to be due to the decrease in the micro-porosity<sup>36</sup>. The elevated temperature leads to increase in the reactivity between Al and B<sub>4</sub>C particles, which resulted in the formation of chemical products. These chemical products could reduce the agglomeration tendency of reinforcement.<sup>3</sup> Figure 4.25 depicts that the pore volume increases with the increase in the content of B<sub>4</sub>C, which means that the porosity is proportional to the content of reinforcement particle.<sup>32,36,52</sup> It can be understood that the higher concentration of B<sub>4</sub>C particle, especially 10 wt.% of B<sub>4</sub>C, promoted the amount of pores while reduced the pore size.

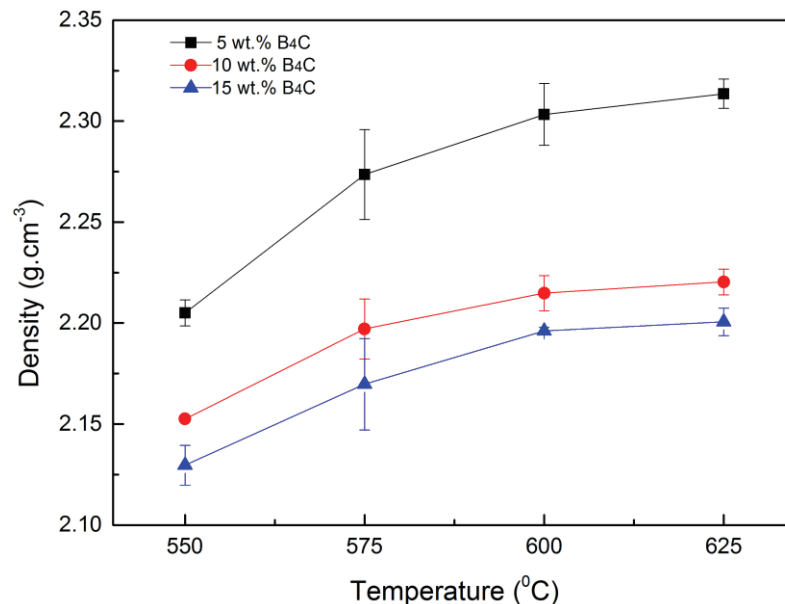


Figure 4.24. The variation of density as a function of the sintering temperature and the content of B<sub>4</sub>C.

The Vickers microhardness values of 5, 10 and 15 wt.% B<sub>4</sub>C reinforced Al composites samples as a function of the sintering temperature and the content of B<sub>4</sub>C are

presented in Figure 4.26. The hardness value is proportional to the content of  $B_4C$ . The enhancement of hardness by increasing in the weight percentage of the  $B_4C$  particles is mainly resulted from the presence of extremely harder  $B_4C$  particles into the Al matrix. These harder particles and their well distribution into the Al matrix are more likely to improve the ability of the softer matrix to resist deformation since the presence of hard ceramic particle into matrix acts as an obstacle to the motion of dislocation, resulting in enhancement in the strength of composites and higher hardness value compared to unreinforced Al matrix.

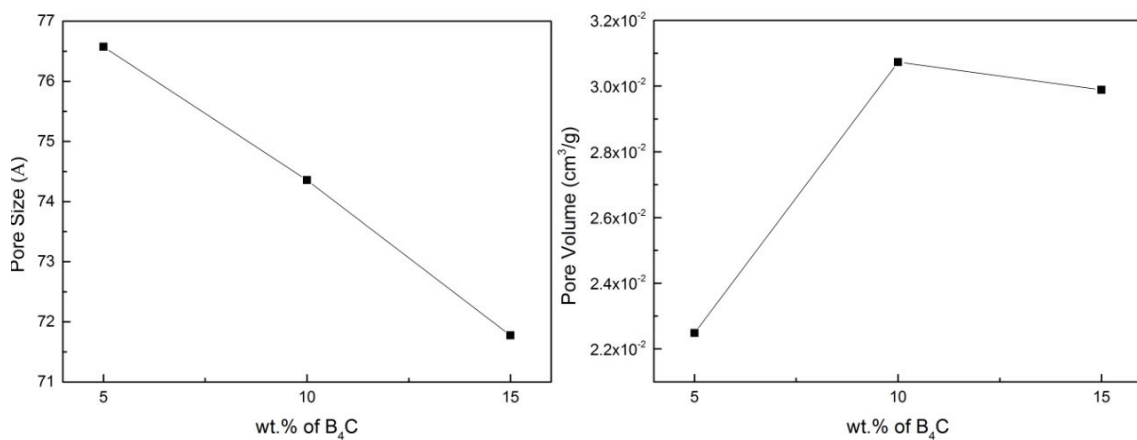


Figure 4.25. Porosity values of  $B_4C$  reinforced Al matrix composites sintered at  $575^\circ C$  as a function of  $B_4C$  content using BET (Brunaues- Emmett-Teller) density analysis.

Additionally, the hardness values irregularly changed depending on the variation of sintering temperature for each  $B_4C$  content. The sintering temperature is another important parameter, as well as the content of  $B_4C$  particles and its distribution into matrix, which influence on the hardness of the composite. The sintering temperature leads to the interfacial reaction products, the change in micro- porosity, potential particle agglomeration regions and non- uniform distribution of secondary, which has a prominent role to determine the mechanical and tribological properties of Al matrix composites. Figure 4.26 indicated the correlation of hardness value and sintering temperature. The hardness values of composites for all content  $B_4C$  sintered at  $550^\circ C$  was enhanced. This could be due to pores become smaller in amount and size by activated sintering mechanism.<sup>36</sup> Also, there is no evidence of the formation of interfacial reaction products based on XRD results, which could improve the hardness values of composites.

Other critical issue is that the reaction occurred between Al-C-B elements under the increasing temperature. The formation of secondary phases changes depending on sintering temperature.<sup>36</sup> The types and amounts of secondary phases became effective on the mechanical properties of composite sample negatively or positively since these interfacial reaction products can be intermetallic or ceramic phases. The composite sample sintered at 575°C for all content B<sub>4</sub>C had a decrease in hardness value with increased density. The reason could be due the reaction products with high density occurred at 575 °C. Also, it was observed that the hardness value does not show a regular trend at 600 °C and 625 °C. The hardness values of composite with 15 wt.% B<sub>4</sub>C sintered at 600 and with 5 wt. % of B<sub>4</sub>C at 625 °C decreased probably due to the increase in the amount of interfacial reaction products with high density and the heterogeneous distribution of the interfacial products in the composite. On the other hand, the hardness values of the composites with 5 and 10 wt. % B<sub>4</sub>C sintered at 600 °C, and 10 wt. % and 15 wt. % B<sub>4</sub>C sintered at 625 °C increased. This can be due to the fact that the formation of AlB<sub>2</sub> and Al<sub>3</sub>BC at elevated sintering temperatures improves the hardness of composites with 10 and 15 wt. % of B<sub>4</sub>C.<sup>3</sup>

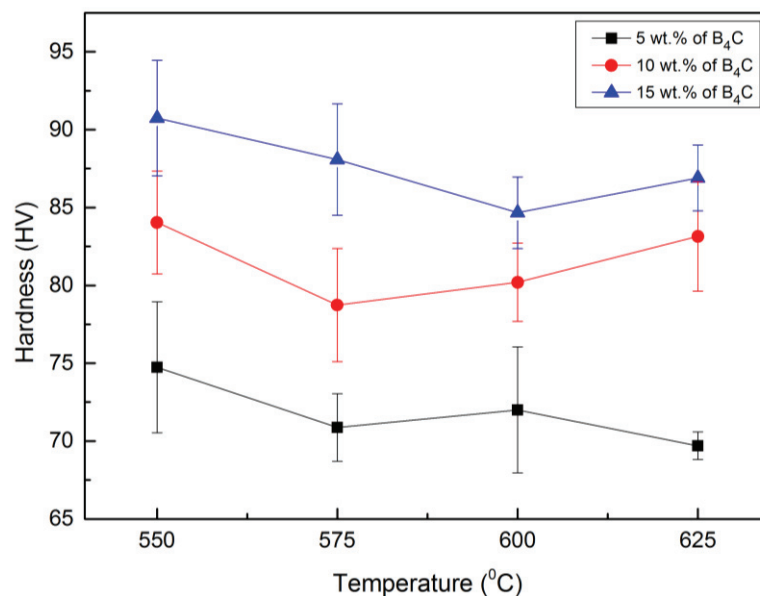


Figure 4.26. Variation of hardness with varying the content of B<sub>4</sub>C and the sintering temperature.

The coefficient of friction and the wear rate of 5, 10 and 15 wt. % of B<sub>4</sub>C reinforced Al matrix composites sintered at 575°C were determined by performing ball-

on disc dry sliding wear test. The composite samples sintered at 575°C (as adequate sintering temperature) were chosen for the tribological test since the tribological part of the study only focused on the investigation of the wear performance of B<sub>4</sub>C reinforced Al matrix composites at a fixed sintering temperature. Therefore, the effect of possible second phases and the change in porosity on the microstructure and mechanical properties of composites at elevated sintering temperatures would be minimized in order to precisely evaluate the effect of B<sub>4</sub>C content on the wear performance. Figure 4.27 shows the variation of the coefficient of friction (COF) of composites as a function of the content of B<sub>4</sub>C. The unreinforced Al matrix has a higher coefficient of friction since Al is a ductile material. The coefficient of friction values dramatically decreased with the addition of hard ceramic B<sub>4</sub>C particle with 5 wt.% followed by a sharp increase in COF value of composite with 10 wt. % of B<sub>4</sub>C whereas the COF value of composite with 15 wt.% remarkably decreased again. It can be definitely seen from Figure 4.27 that there is no steady trend between the COF values of composites with 5, 10 and 15 wt.% B<sub>4</sub>C content. When a higher amount of B<sub>4</sub>C reinforcement was added, it was observed that the coefficient of friction value remarkably increased beyond that of 5 wt. % B<sub>4</sub>C content. This can be due to the fact that the homogenous distribution could not be achieved completely as higher concentration of reinforcing particles, i.e. 10 and 15 wt.% may have led to the agglomeration problem and increase in the COF values.

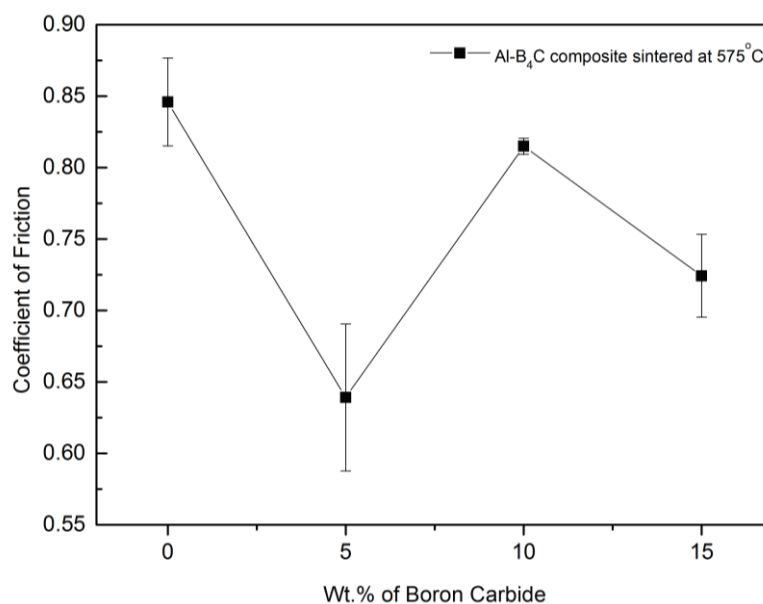


Figure 4.27. Variation of the coefficient of friction with varying content of the B<sub>4</sub>C for the Al composites sintered at 575 °C.

Moreover, the increase in the COF could be due to the oxide layer which can be formed on the surface of an oxygen-sensitive aluminium material under normal conditions (at RT).<sup>14,82</sup> An increase is seen in such oxidation tendency along with the increasing temperature. The tribology test performed was likely to create a thicker oxide layer on the aluminium surface along with the heat caused by friction under room temperature. These hard oxide particles that are broken off with wear during the test led to more wear, and the ratio of wear to be higher than expected. However, in general the presence of B<sub>4</sub>C for all content decreased the COF value when compared the unreinforced Al matrix and improved the wear performance of Al matrix.

Figure 4.28 indicates that the wear rate of B<sub>4</sub>C reinforced Al matrix composite samples reduced as compared to that of unreinforced Al matrix. The dramatic decrease in the wear rate with 5 and 10 wt. % B<sub>4</sub>C content showed that the wear rate of composite was improved by the presence of B<sub>4</sub>C. This can be due to the introducing of the hard ceramic B<sub>4</sub>C particles into the Al matrix with homogeneous distribution. However, a slight increase in the wear rate of composite with 15 wt. % B<sub>4</sub>C was observed. This can be due to the porosity and agglomeration tendency of reinforcement in the composites with the higher concentration, i.e. 15 wt. % B<sub>4</sub>C particles.

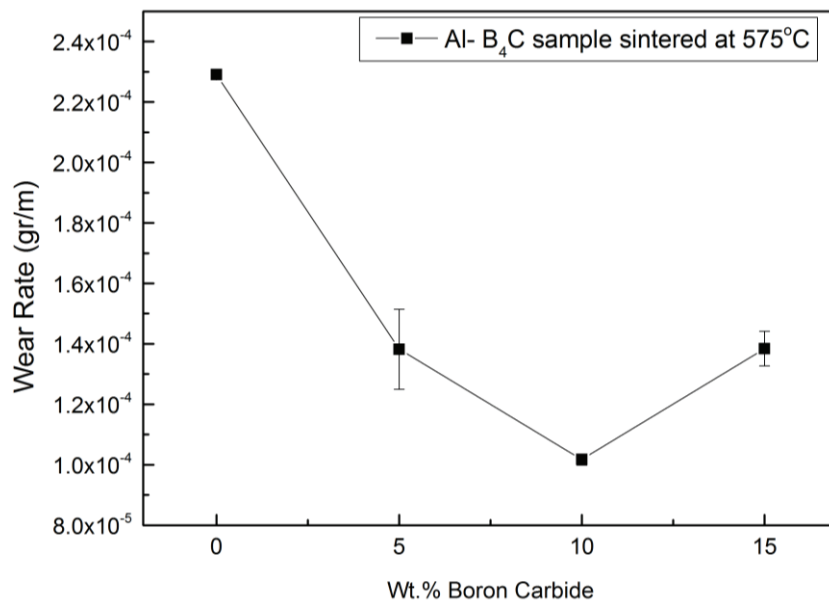


Figure 4.28. The variation of the wear rate with varying the content of B<sub>4</sub>C for the Al composites sintered at 575 °C.

Additionally, Figure 4.29 exhibits the wear tracks of 0, 5, 10 and 15 wt.% B<sub>4</sub>C reinforced Al matrix composites sintered at 575 °C and pure Al sample without sintering. The depth and diameter of wear tracks provide the information about the wear performance of composite samples. The width and depth of wear tracks of 5, 10 and 15 wt.% B<sub>4</sub>C reinforced Al matrix composites sintered at 575 °C is smaller than those of 0 wt.% B<sub>4</sub>C reinforced composite both at RT and sintered at 575 °C, because the unreinforced Al matrix is more ductile than the reinforced composites, and the ductility of composites decreased with the presence of the hard B<sub>4</sub>C particles. Thus, it can be concluded that the wear performance of aluminium was improved by the addition of B<sub>4</sub>C.

Figure 4.30 visualized the optical images of wear tracks on each B<sub>4</sub>C content. As can be observed, the track diameter becomes larger proportionally with an increase of B<sub>4</sub>C content. The higher concentrations of B<sub>4</sub>C, i.e. 10 and 15 wt.%, had wider wear tracks in diameter. This can be attributed to the more contact area between increasing number of B<sub>4</sub>C particle peaks and the tester ball, which resulted in the higher friction in the contact zone.

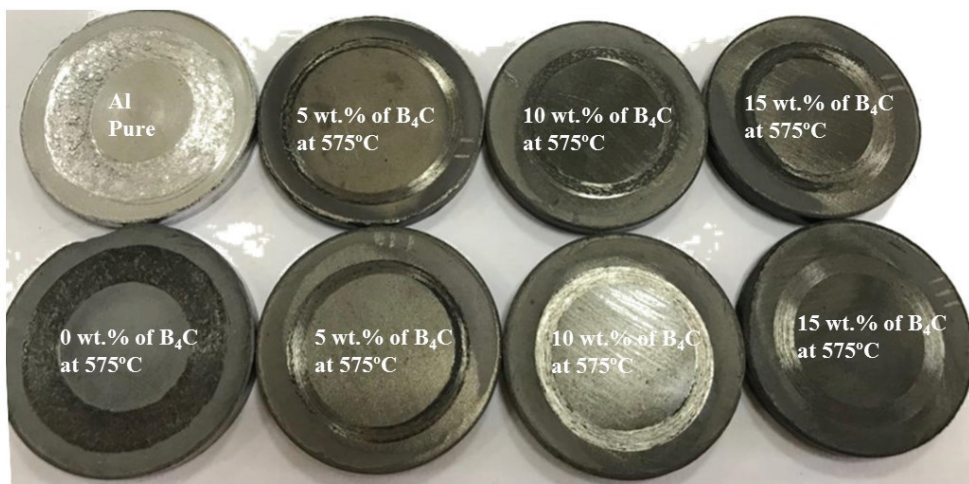


Figure 4.29. The wear tracks of 5, 10 and 15 wt.% B<sub>4</sub>C reinforced Al matrix composites sintered at 575 °C.

The information on the wear performance obtained by the wear track of composites based on optical images was accompanied by the trend of wear rate results based on the calculation from the weight loss of composite samples. However, the coefficient of friction results, which were obtained from the dry sliding test machine, did not overlap the wear rate results and the wear track analysis. The irrational trend of the



COF values of composites brought to an assumption that the wear tester could have a mechanical problem or an improper contact between the abrasive ball and the composite samples.

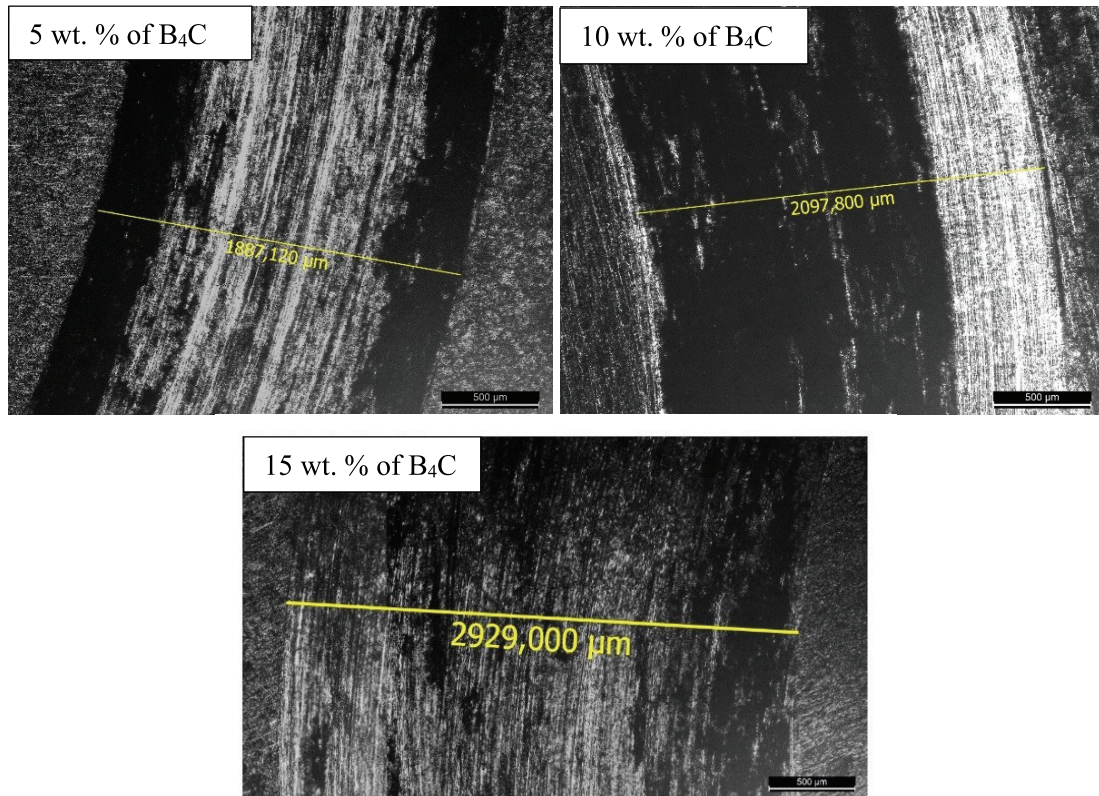


Figure 4.30. The optical microscope images of wear tracks of 5, 10 and 15 wt.% B<sub>4</sub>C reinforced Al matrix composites sintered at 575 °C.

Figure 4.31 represents the hardened steel (100Cr6) balls used for ball-on disc dry sliding wear test, and they were deformed differently due to the different B<sub>4</sub>C contents in the contact zone between the composites and ball. Also, the material removal from the surface of steel balls can be easily seen in Figure 4.31, which was resulted from the friction between the specimens and ball.



Figure 4.31. Hardened steel balls used for ball-on disc dry sliding wear test.

. Figure 4.32 shows the backscattered SEM images of worn surface of 10 wt.% B<sub>4</sub>C reinforced Al matrix composite and many scratches and grooves along the sliding direction can be observed. The reason behind these formations can be the higher level of deformation between the composite samples and the steel ball due to higher friction between them. Also, the darker and lighter tracks formed on the worn surface through the dry sliding test, may correspond B<sub>4</sub>C, Al particles and the oxidation layer on the specimen.

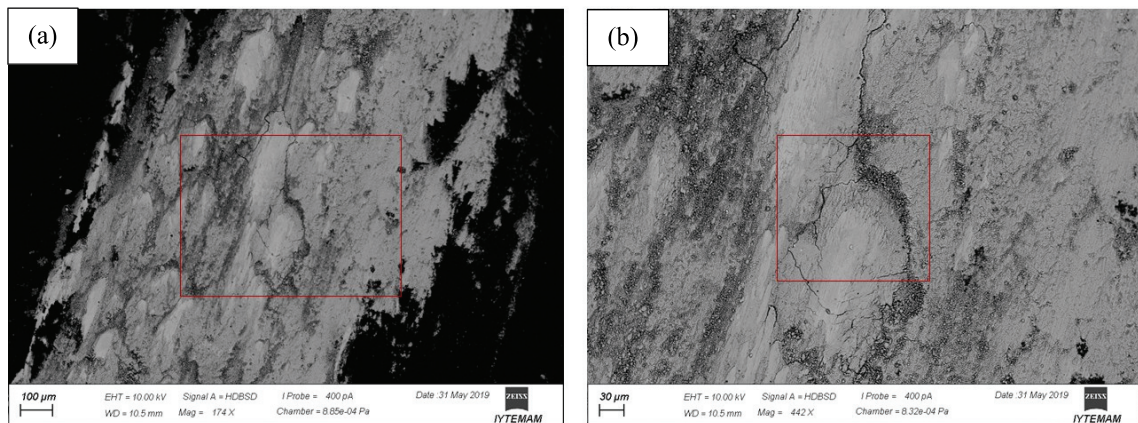


Figure 4.32. The SEM images of worn surface of 10 wt.% of B<sub>4</sub>C reinforced Al matrix composite sample sintered at 575°C a) 174x b) 442 x magnifications.

Figure 4.33 indicates the EDS analyses of the worn surface of 10 wt. of B<sub>4</sub>C reinforced Al matrix composite samples sintered at 575°C. Along with Al, a remarkable amount of presence of iron (Fe) and oxygen (O) elements were detected. Fe were considered to be transferred from the steel ball to the worn surface of the specimen, and the presence of O was attributed to the oxidation of composite surface during the ball-on-disc dry sliding wear test. The presence of the elements may have led to the formation of mechanically milling layer (MML) on the surface. The MML was reported to be able to affect the tribological performance of composite samples by acting as a solid lubricant on surface.<sup>14,65,82,83</sup>

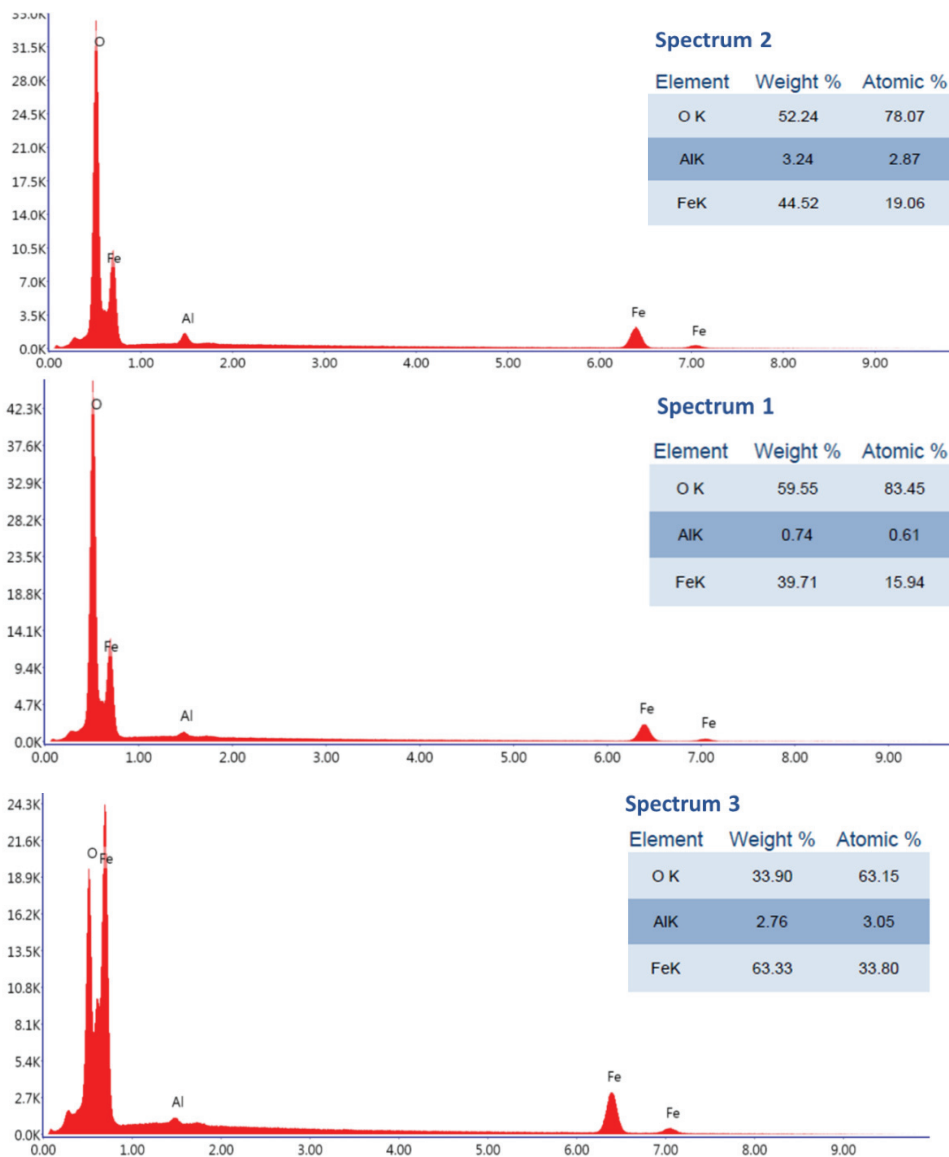
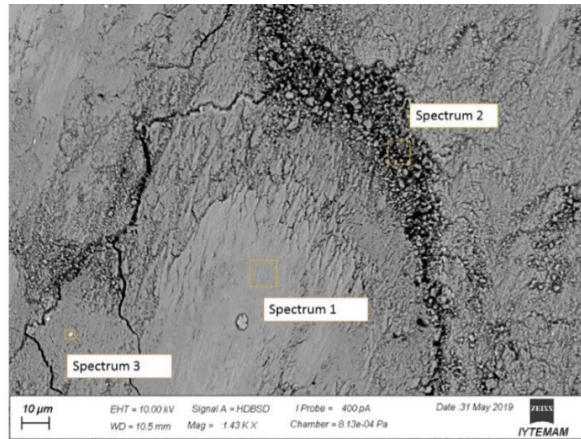


Figure 4.33. EDS analysis of worn surface of 10 wt. % B4C reinforced Al matrix composite sample sintered at 575 °C.

## CHAPTER 5

### CONCLUSION

The main objective of the study is categorized as; to evaluate a development process for the fabrication of  $B_4C$  reinforced aluminium matrix composites with optimum processing parameters, and to determine the tribological and mechanical performance of fabricated composites.

The results based on ball milling process indicate that the particle size increased up to 3 hours milling time whereas it significantly decreased with increased milling time after 3 hours. The addition of PCA enhanced the efficiency of the mechanical alloying (MA) process during the ball milling by preventing the excessive cold welding, thus the particle size growth, the agglomeration and contamination of powders were avoided. The MA process not only provided the decrease of the particle size but also allowed  $B_4C$  particles to be embedded into Al matrix with homogeneous distribution. Considering the results of the ball milling process, as a part of the study, appropriate parameters were introduced to fabricate the composite powders by the MA process.

The changes in the physical and mechanical properties of composite samples were evaluated as a function of temperature and the content of  $B_4C$  particle. It was obvious that the presence of  $B_4C$  decreased the density of composite samples due to its lower density and increased micro-porosity; however, the increase in the sintering temperature increase the density value probably due to the formation of interfacial reaction products, and also the porosity was minimized by the sintering process.

The mechanical properties of Al matrix were improved with the addition of  $B_4C$  particles since the incorporation of hard ceramic  $B_4C$  particles with uniform distribution achieve homogenous load transfer within the matrix. Also, the hardness value was improved by increasing  $B_4C$  content. However, the hardness behaviour of the composite was not clear with increasing sintering temperature. This could be due to the presence of secondary phases detected at elevated sintering temperatures.

Additionally, the dry sliding wear behaviour of composites was evaluated by a ball-on-disc test apparatus as a function of  $B_4C$  content to precisely investigate the effect of  $B_4C$  content on the wear performance. The addition of  $B_4C$  improved the wear



performance of composite compared to the unreinforced matrix. However, 15 wt.% B<sub>4</sub>C content slightly decreased the wear performance of composites. This can be due to the agglomeration of B<sub>4</sub>C particles and micro-porosity occurred in composite sample at higher ceramic particle concentration. The low B<sub>4</sub>C concentrations up to 10 wt. % was determined to give the best performance in the study. Therefore, the wear performance of AMC was improved by the presence of B<sub>4</sub>C particles in adequate amounts.

Finally, it is concluded that the addition of B<sub>4</sub>C into aluminium provides enhanced mechanical and tribological properties when compared to unreinforced Al matrices. The critical point is the amount of the B<sub>4</sub>C content since higher concentration led to the agglomeration of reinforcing particles, which resulted in the degradation of mechanical and tribological properties. The B<sub>4</sub>C reinforced Al matrix composites with improved mechanical and tribological properties can be fabricated using PM methods with an appropriate amount of B<sub>4</sub>C.

## REFERENCES

- (1) Mohammad Sharifi, E.; Karimzadeh, F.; Enayati, M. H. Fabrication and Evaluation of Mechanical and Tribological Properties of Boron Carbide Reinforced Aluminum Matrix Nanocomposites. *Mater. Des.* **2011**, *32* (6), 3263–3271. <https://doi.org/10.1016/j.matdes.2011.02.033>.
- (2) Harichandran, R.; Selvakumar, N. Effect of Nano/Micro B4C Particles on the Mechanical Properties of Aluminium Metal Matrix Composites Fabricated by Ultrasonic Cavitation-Assisted Solidification Process. *Arch. Civ. Mech. Eng.* **2016**, *16* (1), 147–158. <https://doi.org/10.1016/j.acme.2015.07.001>.
- (3) Mohanty, R. M.; Balasubramanian, K.; Seshadri, S. K. Boron Carbide-Reinforced Aluminium 1100 Matrix Composites: Fabrication and Properties. *Mater. Sci. Eng. A* **2008**, *498* (1–2), 42–52. <https://doi.org/10.1016/j.msea.2007.11.154>.
- (4) Shaw, L.; Zawrah, M.; Villegas, J.; Luo, H.; Miracle, D. Effects of Process-Control Agents on Mechanical Alloying of Nanostructured Aluminum Alloys. *Metall. Mater. Trans. A Phys. Metall. Mater. Sci.* **2003**, *34* (1), 159–170. <https://doi.org/10.1007/s11661-003-0217-7>.
- (5) Zhang, Y. F.; Lu, L.; Yap, S. M. Prediction of the Amount of PCA for Mechanical Milling. *J. Mater. Process. Technol.* **1999**, *89–90*, 260–265. [https://doi.org/10.1016/S0924-0136\(99\)00042-4](https://doi.org/10.1016/S0924-0136(99)00042-4).
- (6) Viala, J. C.; Bouix, J.; Gonzalez, G.; Esnouf, C. Chemical Reactivity of Aluminium with Boron Carbide. *J. Mater. Sci.* **1997**, *32* (17), 4559–4573. <https://doi.org/10.1023/A:1018625402103>.
- (7) Tabandeh-Khorshid, M.; Omrani, E.; Menezes, P. L.; Rohatgi, P. K. Tribological Performance of Self-Lubricating Aluminum Matrix Nanocomposites: Role of Graphene Nanoplatelets. *Eng. Sci. Technol. an Int. J.* **2016**, *19* (1), 463–469. <https://doi.org/10.1016/j.jestch.2015.09.005>.
- (8) Abenojar, J.; Velasco, F.; Martínez, M. A. Optimization of Processing Parameters for the Al + 10% B4C System Obtained by Mechanical Alloying. *J. Mater. Process. Technol.* **2007**, *184* (1–3), 441–446. <https://doi.org/10.1016/j.jmatprotec.2006.11.122>.
- (9) Introduction to Composites [https://nptel.ac.in/courses/101104010/lecture1/1\\_2.htm](https://nptel.ac.in/courses/101104010/lecture1/1_2.htm) (accessed Jun 1, 2019).
- (10) Gómez, L.; Busquets-Mataix, D.; Amigó, V.; Salvador, M. D. Analysis of Boron Carbide Aluminum Matrix Composites. *J. Compos. Mater.* **2009**, *43* (9), 987–995. <https://doi.org/10.1177/0021998308097731>.
- (11) Kumaraswamy, H. S.; Bharat, V.; Krishna Rao, T. Influence of Mechanical & Tribological Behaviour Of Al 2024 MMC Fabricated by Stir Casting Technique- A Review. *Mater. Today Proc.* **2018**, *5* (5), 11962–11970. <https://doi.org/10.1016/j.matpr.2018.02.170>.

- (12) Topcu, I.; Gulsoy, H. O.; Kadioglu, N.; Gulluoglu, A. N. Processing and Mechanical Properties of B<sub>4</sub>C Reinforced Al Matrix Composites. *J. Alloys Compd.* **2009**, *482* (1–2), 516–521. <https://doi.org/10.1016/j.jallcom.2009.04.065>.
- (13) Shorowordi, K. M.; Laoui, T.; Haseeb, A. S. M. A.; Celis, J. P.; Froyen, L. Microstructure and Interface Characteristics of B<sub>4</sub>C, SiC and Al<sub>2</sub>O<sub>3</sub>reinforced Al Matrix Composites: A Comparative Study. *J. Mater. Process. Technol.* **2003**, *142* (3), 738–743. [https://doi.org/10.1016/S0924-0136\(03\)00815-X](https://doi.org/10.1016/S0924-0136(03)00815-X).
- (14) Li, X. Y.; Tandon, K. N. Microstructural Characterization of Mechanically Mixed Layer and Wear Debris in Sliding Wear of an Al Alloy and an Al Based Composite. *Wear* **2000**, *245* (1–2), 148–161. [https://doi.org/10.1016/S0043-1648\(00\)00475-0](https://doi.org/10.1016/S0043-1648(00)00475-0).
- (15) Shorowordi, K. M.; Haseeb, A. S. M. A.; Celis, J. P. Chemical and Structural Nature of Tribo-Surface of Aluminium-SiC Composites at Nanometre and Micrometre Length Scales. *Mater. Sci. Eng. A* **2006**, *425* (1–2), 213–218. <https://doi.org/10.1016/j.msea.2006.03.058>.
- (16) Nie, C.-Z.; Gu, J.-J.; Liu, J.-L.; Zhang, D. Production of Boron Carbide Reinforced 2024 Aluminum Matrix Composites by Mechanical Alloying. *Mater. Trans.* **2007**, *48* (5), 990–995. <https://doi.org/10.2320/matertrans.48.990>.
- (17) Shirvanimoghaddam, K.; Khayyam, H.; Abdizadeh, H.; Karbalaee Akbari, M.; Pakseresht, A. H.; Ghasali, E.; Naebe, M. Boron Carbide Reinforced Aluminium Matrix Composite: Physical, Mechanical Characterization and Mathematical Modelling. *Mater. Sci. Eng. A* **2016**, *658*, 135–149. <https://doi.org/10.1016/j.msea.2016.01.114>.
- (18) Chen, C.; Guo, L.; Luo, J.; Hao, J.; Guo, Z.; Volinsky, A. A. Aluminum Powder Size and Microstructure Effects on Properties of Boron Nitride Reinforced Aluminum Matrix Composites Fabricated by Semi-Solid Powder Metallurgy. *Mater. Sci. Eng. A* **2015**, *646*, 306–314. <https://doi.org/10.1016/j.msea.2015.08.081>.
- (19) Kerti, I.; Toptan, F. Microstructural Variations in Cast B<sub>4</sub>C-Reinforced Aluminium Matrix Composites (AMCs). *Mater. Lett.* **2008**, *62* (8–9), 1215–1218. <https://doi.org/10.1016/j.matlet.2007.08.015>.
- (20) Cross, T. EFFECTS OF BALL MILLING AND SINTERING ON ALUMINA AND ALUMINA-BORON COMPOUNDS By. **2014**, No. August, 9–13.
- (21) Canute, X.; Majumder, M. C. Investigation of Tribological and Mechanical Properties of Aluminium Boron Carbide Composites Using Response Surface Methodology and Desirability Analysis. *Ind. Lubr. Tribol.* **2018**, *70* (2), 301–315. <https://doi.org/10.1108/ILT-01-2017-0010>.
- (22) Rajesh, G. .; Auradi, V.; Umashankar; Kori, S. . Processing and Evaluation of Dry Sliding Wear Behaviour of B<sub>4</sub>Cp Reinforced Aluminium Matrix Composites. *Procedia Mater. Sci.* **2014**, *5*, 289–294. <https://doi.org/10.1016/j.mspro.2014.07.269>.
- (23) Bhujanga, D. P.; Manohara, H. R. Processing and Evaluation of Mechanical



Properties and Dry Sliding Wear Behavior of AA6061-B4C Composites. *Mater. Today Proc.* **2018**, 5 (9), 19773–19782. <https://doi.org/10.1016/j.matpr.2018.06.340>.

- (24) The Wettability <https://www.masterbond.com/techtips/surface-wetting> (accessed Jun 1, 2019).
- (25) Kala, H.; Mer, K. K. S.; Kumar, S. A Review on Mechanical and Tribological Behaviors of Stir Cast Aluminum Matrix Composites. *Procedia Mater. Sci.* **2014**, 6 (Icmpc), 1951–1960. <https://doi.org/10.1016/j.mspro.2014.07.229>.
- (26) Panwar, N.; Chauhan, A. Fabrication Methods of Particulate Reinforced Aluminium Metal Matrix Composite-A Review. *Mater. Today Proc.* **2018**, 5 (2), 5933–5939. <https://doi.org/10.1016/j.matpr.2017.12.194>.
- (27) Engineering, M.; Engineering, M. Evaluation of Mechanical Behaviour of Aluminium Alloy Boron Carbide. **2016**, 32–36.
- (28) Vijaya Ramnath, B.; Elanchezhian, C.; Jaivignesh, M.; Rajesh, S.; Parswajinan, C.; Siddique Ahmed Ghias, A. Evaluation of Mechanical Properties of Aluminium Alloy-Alumina-Boron Carbide Metal Matrix Composites. *Mater. Des.* **2014**, 58, 332–338. <https://doi.org/10.1016/j.matdes.2014.01.068>.
- (29) Lashgari, H. R.; Zangeneh, S.; Shahmir, H.; Saghafi, M.; Emamy, M. Heat Treatment Effect on the Microstructure, Tensile Properties and Dry Sliding Wear Behavior of A356-10%B4C Cast Composites. *Mater. Des.* **2010**, 31 (9), 4414–4422. <https://doi.org/10.1016/j.matdes.2010.04.034>.
- (30) Rajan, T. P. D.; Pai, B. C.; Hubli, R. C.; Mahesh, V. P.; Nair, P. S. Processing of Surface-Treated Boron Carbide-Reinforced Aluminum Matrix Composites by Liquid–Metal Stir-Casting Technique. *J. Compos. Mater.* **2011**, 45 (23), 2371–2378. <https://doi.org/10.1177/0021998311401086>.
- (31) Siddhartha Prabhakar, N.; Radhika, N.; Raghu, R. Analysis of Tribological Behavior of Aluminium/B4C Composite under Dry Sliding Motion. *Procedia Eng.* **2014**, 97, 994–1003. <https://doi.org/10.1016/j.proeng.2014.12.376>.
- (32) Canakci, A.; Arslan, F.; Varol, T. Effect of Volume Fraction and Size of B<sub>4</sub>C Particles on Production and Microstructure Properties of B<sub>4</sub>C Reinforced Aluminium Alloy Composites. *Mater. Sci. Technol.* **2013**, 29 (8), 954–960. <https://doi.org/10.1179/1743284713Y.0000000232>.
- (33) Sharma, P.; Sharma, S.; Khanduja, D. On the Use of Ball Milling for the Production of Ceramic Powders. *Mater. Manuf. Process.* **2015**, 30 (11), 1370–1376. <https://doi.org/10.1080/10426914.2015.1037904>.
- (34) Ayvaz, M. PRODUCTION AND CHARACTERIZATION OF ALUMINUM BASED COMPOSITES BY POWDER METALLURGY METHOD FOR DIFFERENT MATRIX COMPOSITION AND AMOUNT OF THE. **2014**, 1, 45–53.
- (35) Machio, C.; Chikwanda, H. K.; Chikosha, S. Effect of Process Control Agent

- (PCA) on the Characteristics of Mechanically Alloyed Ti-Mg Powders. *J. South African Inst. Min. Metall.* **2011**, *111* (3), 149–153.
- (36) Rahimian, M.; Ehsani, N.; Parvin, N.; Baharvandi, H. reza. The Effect of Particle Size, Sintering Temperature and Sintering Time on the Properties of Al-Al<sub>2</sub>O<sub>3</sub> Composites, Made by Powder Metallurgy. *J. Mater. Process. Technol.* **2009**, *209* (14), 5387–5393. <https://doi.org/10.1016/j.jmatprotec.2009.04.007>.
- (37) Bhattacharya, P.; Bellon, P.; Averback, R. S.; Hales, S. J. Nanocrystalline TiAl Powders Synthesized by High-Energy Ball Milling: Effects of Milling Parameters on Yield and Contamination. *J. Alloys Compd.* **2004**, *368* (1–2), 187–196. <https://doi.org/10.1016/j.jallcom.2003.08.079>.
- (38) Wang, L.; Choi, H.; Myoung, J. M.; Lee, W. Mechanical Alloying of Multi-Walled Carbon Nanotubes and Aluminium Powders for the Preparation of Carbon/Metal Composites. *Carbon N. Y.* **2009**, *47* (15), 3427–3433. <https://doi.org/10.1016/j.carbon.2009.08.007>.
- (39) Herrera-Ramírez, J.; Pérez-Bustamante, R.; Castañeda-Balderas, R.; Ledezma-Sillas, E.; Carreño-Gallardo, C.; Estrada-Guel, I.; López-Meléndez, C. B4C Particles Reinforced Al2024 Composites via Mechanical Milling. *Metals (Basel)*. **2018**, *8* (8), 647. <https://doi.org/10.3390/met8080647>.
- (40) Khakbiz, M.; Akhlaghi, F. Synthesis and Structural Characterization of Al-B4C Nano-Composite Powders by Mechanical Alloying. *J. Alloys Compd.* **2009**, *479* (1–2), 334–341. <https://doi.org/10.1016/j.jallcom.2008.12.076>.
- (41) Nazık, C.; Tarakçioğlu, N.; Özkaya, S.; Erdemir, F.; Çanakçı, A. Determination of Effect of B 4 C Content on Density and Tensile Strength of AA7075 / B 4 C Composite Produced via Powder Technology. **2016**, *4* (4), 251–254. <https://doi.org/10.18178/ijmmm.2016.4.4.266>.
- (42) Lu, L.; Zhang, Y. F. Influence of Process Control Agent on Interdiffusion between Al and Mg during Mechanical Alloying. *J. Alloys Compd.* **1999**, *290* (1–2), 279–283. [https://doi.org/10.1016/S0925-8388\(99\)00221-2](https://doi.org/10.1016/S0925-8388(99)00221-2).
- (43) Alizadeh, A.; Taheri-Nassaj, E.; Baharvandi, H. R. Preparation and Investigation of Al-4 Wt% B4C Nanocomposite Powders Using Mechanical Milling. *Bull. Mater. Sci.* **2011**, *34* (5), 1039–1048. <https://doi.org/10.1007/s12034-011-0158-5>.
- (44) Sokhansanj, A.; Hadian, A. M. Purification of Attrition Milled Nano-Size Boron Carbide Powder. *Int. J. Mod. Phys. Conf. Ser.* **2012**, *05*, 94–101. <https://doi.org/doi:10.1142/S2010194512001894>.
- (45) Meena, K. L.; Khandelwal, M. Synthesis and Analysis of Alumina , Zirconia and Alumina- Toughened-Zirconia Composites. **2015**, *4* (10), 108–113.
- (46) Rocha, C. J.; Leal Neto, R. M.; Gonçalves, V. S.; Carvalho, L. L.; Ambrozio Filho, F. An Investigation of the Use of Stearic Acid as a Process Control Agent in High Energy Ball Milling of Nb-Al and Ni-Al Powder Mixtures. *Mater. Sci. Forum* **2003**, *416–418*, 144–149. <https://doi.org/10.4028/www.scientific.net/MSF.416-418.144>.

- (47) Kleiner, S.; Bertocco, F.; Khalid, F. A.; Beffort, O. Decomposition of Process Control Agent during Mechanical Milling and Its Influence on Displacement Reactions in the Al-TiO<sub>2</sub> System. *Mater. Chem. Phys.* **2005**, *89* (2–3), 362–366. <https://doi.org/10.1016/j.matchemphys.2004.09.014>.
- (48) Mechanical Milling [https://ninithi.wordpress.com/topdown\\_methods/](https://ninithi.wordpress.com/topdown_methods/) (accessed Jun 3, 2019).
- (49) Suryanarayana, C. Mechanical Alloying and Milling. **2001**, *46*.
- (50) Suryanarayana, C.; Al-Joubori, A. Alloyed Steels: Mechanically. *Encycl. Iron, Steel, Their Alloy.* **2016**, No. January, 159–177. <https://doi.org/10.1081/e-eisa-120053049>.
- (51) Govindachari, T. R.; Premila, M. S. The Benzofuran Norwedelic Acid from *Wedelia* Calendulaceae. *Phytochemistry* **1985**, *24* (12), 3068–3069. <https://doi.org/10.1016/j.matpr.2018.06.368>.
- (52) Rahimian, M.; Parvin, N.; Ehsani, N. Investigation of Particle Size and Amount of Alumina on Microstructure and Mechanical Properties of Al Matrix Composite Made by Powder Metallurgy. *Mater. Sci. Eng. A* **2010**, *527* (4–5), 1031–1038. <https://doi.org/10.1016/j.msea.2009.09.034>.
- (53) Habibi, M. K.; Hamouda, A. S.; Gupta, M. Hybridizing Boron Carbide (B<sub>4</sub>C) Particles with Aluminum (Al) to Enhance the Mechanical Response of Magnesium Based Nano-Composites. *J. Alloys Compd.* **2013**, *550*, 83–93. <https://doi.org/10.1016/j.jallcom.2012.09.128>.
- (54) Rahimian, M.; Parvin, N.; Ehsani, N. The Effect of Production Parameters on Microstructure and Wear Resistance of Powder Metallurgy Al-Al<sub>2</sub>O<sub>3</sub> Composite. *Mater. Des.* **2011**, *32* (2), 1031–1038. <https://doi.org/10.1016/j.matdes.2010.07.016>.
- (55) Sintering process <https://www.slideshare.net/spssil/powder-metallurgy-42203766> (accessed Jun 16, 2019).
- (56) Ghasali, E.; Alizadeh, M.; Ebadzadeh, T.; Pakseresht, A. H.; Rahbari, A. Investigation on Microstructural and Mechanical Properties of B<sub>4</sub>C-Aluminum Matrix Composites Prepared by Microwave Sintering. *J. Mater. Res. Technol.* **2015**, *4* (4), 411–415. <https://doi.org/10.1016/j.jmrt.2015.02.005>.
- (57) Turatti, A. M.; Pereira, A. S. Wear Resistant Boron Carbide Compacts Produced by Pressureless Sintering. *Ceram. Int.* **2017**, *43* (11), 7970–7977. <https://doi.org/10.1016/j.ceramint.2017.03.064>.
- (58) Rahimian, M.; Ehsani, N.; Parvin, N.; Baharvandi, H. R. The Effect of Sintering Temperature and the Amount of Reinforcement on the Properties of Al-Al<sub>2</sub>O<sub>3</sub> Composite. *Mater. Des.* **2009**, *30* (8), 3333–3337. <https://doi.org/10.1016/j.matdes.2008.11.027>.
- (59) Baradeswaran, A.; Elaya Perumal, A. Influence of B<sub>4</sub>C on the Tribological and Mechanical Properties of Al 7075-B<sub>4</sub>C Composites. *Compos. Part B Eng.* **2013**,

54 (1), 146–152. <https://doi.org/10.1016/j.compositesb.2013.05.012>.

- (60) Toptan, F.; Kerti, I.; Rocha, L. A. Reciprocal Dry Sliding Wear Behaviour of B<sub>4</sub>C p Reinforced Aluminium Alloy Matrix Composites. *Wear* **2012**, 290–291, 74–85. <https://doi.org/10.1016/j.wear.2012.05.007>.
- (61) Sonber, J. K.; Limaye, P. K.; Murthy, T. S. R. C.; Sairam, K.; Nagaraj, A.; Soni, N. L.; Patel, R. J.; Chakravartty, J. K. Tribological Properties of Boron Carbide in Sliding against WC Ball. *Int. J. Refract. Met. Hard Mater.* **2015**, 51, 110–117. <https://doi.org/10.1016/j.ijrmhm.2015.03.010>.
- (62) Moshtaghioun, B. M.; Gomez-Garcia, D.; Dominguez-Rodriguez, A.; Todd, R. I. Abrasive Wear Rate of Boron Carbide Ceramics: Influence of Microstructural and Mechanical Aspects on Their Tribological Response. *J. Eur. Ceram. Soc.* **2016**, 36 (16), 3925–3928. <https://doi.org/10.1016/j.jeurceramsoc.2016.06.029>.
- (63) García-Cordovilla, C.; Narciso, J.; Louis, E. Abrasive Wear Resistance of Aluminium Alloy/Ceramic Particulate Composites. *Wear* **1996**, 192 (1–2), 170–177. [https://doi.org/10.1016/0043-1648\(95\)06801-5](https://doi.org/10.1016/0043-1648(95)06801-5).
- (64) He, L.; Tan, Y.; Wang, X.; Xu, T.; Hong, X. Microstructure and Wear Properties of Al<sub>2</sub>O<sub>3</sub>-CeO<sub>2</sub>/Ni-Base Alloy Composite Coatings on Aluminum Alloys by Plasma Spray. *Appl. Surf. Sci.* **2014**, 314 (2), 760–767. <https://doi.org/10.1016/j.apsusc.2014.07.047>.
- (65) Wang, S. Q.; Yang, Z. R.; Zhao, Y. T.; Wei, M. X. Sliding Wear Characteristics of AZ91D Alloy at Ambient Temperatures of 25–200 °C. *Tribol. Lett.* **2010**, 38 (1), 39–45. <https://doi.org/10.1007/s11249-009-9569-5>.
- (66) Patidar, D.; Rana, R. S. Effect of B<sub>4</sub>C Particle Reinforcement on the Various Properties of Aluminium Matrix Composites: A Survey Paper. *Mater. Today Proc.* **2017**, 4 (2), 2981–2988. <https://doi.org/10.1016/j.matpr.2017.02.180>.
- (67) Ramnath, B. V.; Elanchezian, C.; Annamalai, R. M.; Aravind, S.; Atreya, T. S. A.; Vignesh, V.; Subramanian, C. Aluminium Metal Matrix Composites - A Review. *Rev. Adv. Mater. Sci.* **2014**, 38 (1), 55–60. <https://doi.org/10.1016/j.jmrt.2015.05.003>.
- (68) Shorowordi, K. M.; Haseeb, A. S. M. A.; Celis, J. P. Tribo-Surface Characteristics of Al-B<sub>4</sub>C and Al-SiC Composites Worn under Different Contact Pressures. *Wear* **2006**, 261 (5–6), 634–641. <https://doi.org/10.1016/j.wear.2006.01.023>.
- (69) Rao, R. N.; Das, S.; Mondal, D. P.; Dixit, G. Effect of Heat Treatment on the Sliding Wear Behaviour of Aluminium Alloy (Al-Zn-Mg) Hard Particle Composite. *Tribol. Int.* **2010**, 43 (1–2), 330–339. <https://doi.org/10.1016/j.triboint.2009.06.013>.
- (70) Ahn, H. S.; Cuong, P. D.; Shin, K. H.; Lee, K. S. Tribological Behavior of Sputtered Boron Carbide Coatings and the Influence of Processing Gas. *Wear* **2005**, 259 (7–12), 807–813. <https://doi.org/10.1016/j.wear.2005.02.096>.
- (71) Moshtaghioun, B. M.; Gomez-Garcia, D.; Dominguez-Rodriguez, A.; Todd, R. I.

- Grain Size Dependence of Hardness and Fracture Toughness in Pure near Fully-Dense Boron Carbide Ceramics. *J. Eur. Ceram. Soc.* **2016**, 36 (7), 1829–1834. <https://doi.org/10.1016/j.jeurceramsoc.2016.01.017>.
- (72) Bodunrin, M. O.; Alaneme, K. K.; Chown, L. H. Aluminium Matrix Hybrid Composites: A Review of Reinforcement Philosophies; Mechanical, Corrosion and Tribological Characteristics. *J. Mater. Res. Technol.* **2015**, 4 (4), 434–445. <https://doi.org/10.1016/j.jmrt.2015.05.003>.
- (73) Islam, M. A.; Bepari, M. M. A.; Shorowordi, K. M. Dry Sliding Wear in Case-Hardened Niobium Microalloyed Steels. *J. Mater. Process. Technol.* **2005**, 160 (3), 401–409. <https://doi.org/10.1016/j.jmatprotec.2004.04.424>.
- (74) Alizadeh, M.; Alizadeh, M.; Amini, R. Structural and Mechanical Properties of Al/B4C Composites Fabricated by Wet Attrition Milling and Hot Extrusion. *J. Mater. Sci. Technol.* **2013**, 29 (8), 725–730. <https://doi.org/10.1016/j.jmst.2013.04.015>.
- (75) Abdollahi, A.; Alizadeh, A.; Baharvandi, H. R. Dry Sliding Tribological Behavior and Mechanical Properties of Al2024-5wt.%B4C Nanocomposite Produced by Mechanical Milling and Hot Extrusion. *Mater. Des.* **2014**, 55, 471–481. <https://doi.org/10.1016/j.matdes.2013.09.024>.
- (76) Kumar, K. S.; Patnaik, V. S. Experimental Investigation on Aluminium Alloy Composites for Wear Behaviour. *Int. Conf. Electr. Electron. Optim. Tech. ICEEOT 2016* **2016**, 3846–3852. <https://doi.org/10.1109/ICEEOT.2016.7755433>.
- (77) Wu, Z.; Liang, Y.; Fu, E.; Du, J.; Wang, P.; Fan, Y.; Zhao, Y. Effect of Ball Milling Parameters on the Refinement. **2018**. <https://doi.org/10.3390/met8040281>.
- (78) Optical microscope <https://laboratoryinfo.com/simple-microscope-parts/> (accessed Jun 5, 2019).
- (79) Bragg Law <https://www.slideserve.com/celeste-marty/diffraction-electron-and-x-ray> (accessed Jun 11, 2019).
- (80) Dong, R.; Zhu, W.; Zhao, C.; Zhang, Y. No Title. *Metall. Mater. Trans. A* **49** (12), 6147–6160.
- (81) Halverson, D. C.; Pyzik, A. J.; Aksay, Ii. A.; Snowden, W. E. Processing of Boron Carbide-Aluminum Composites. *J. Am. Ceram. Soc.* **1989**, 72 (5), 775–780. <https://doi.org/10.1111/j.1151-2916.1989.tb06216.x>.
- (82) Rao, R. N.; Das, S. Effect of Matrix Alloy and Influence of SiC Particle on the Sliding Wear Characteristics of Aluminium Alloy Composites. *Mater. Des.* **2010**, 31 (3), 1200–1207. <https://doi.org/10.1016/j.matdes.2009.09.032>.
- (83) Lu, D.; Gu, M.; Shi, Z. Materials Transfer and Formation of Mechanically Mixed Layer in Dry Sliding Wear of Metal Matrix Composites against Steel. *Tribol. Lett.* **1999**, 6 (1), 57–61. <https://doi.org/10.1023/A:1019182817316>.